КРИСТАЛЛОГРАФИЯ

SOVIET PHYSICS

Crystallography

VOLUME 2 NUMBER 3

A Translation
of the journal
Crystallography
of the
Academy of Sciences of the USSR

(RUSSIAN ORIGINAL VOL. 2, NO. 3)

Published by the
AMERICAN INSTITUTE OF PHYSICS
INCORPORATED

SOVIET PHYSICS

Crystallography

A translation of the journal "Crystallography" of the Academy of Sciences of the USSR

A publication of the
AMERICAN INSTITUTE
OF PHYSICS

Governing Board

Frederick Seitz, *Chairman*

Members

Walter S. Baird
Jesse W. Beams
Raymond T. Birge
R. H. Bolt
J. W. Buchta
J. H. Dillon
Vernet E. Eaton
Herbert A. Erf
Irvine C. Gardner
S. A. Goudsmit
C. Kittel
Winston E. Kock
R. Bruce Lindsay
Walter C. Michels
G. E. Pake
R. Ronald Palmer
Joseph B. Platt
Ralph A. Sawyer
H. D. Smyth
John Strong
George E. Uhlenbeck

Officers and Staff

Elmer Hutchisson
Director
Henry A. Barton
Associate Director
Wallace Waterfall
Secretary and Treasurer
Edward P. Tober
Mgr., Production and Distribution
Theodore Vorburger
Advertising Manager
Ruth F. Bryans
Publication Manager
Kathryn Setze
Assistant Treasurer
Alice Mastropietro
Circulation Manager
Eugene H. Kone
Director of Public Relations
William C. Kelly
Director of Education Projects

American Institute of Physics Advisory Board on Russian Translations

Robert T. Beyer, *Chairman*

Freeman Dyson, Dwight Gray, Morton Hamermesh,
David Harker, Vladimir Rojansky, Harrold F. Weaver

Advisory Editor, Soviet Physics – Crystallography: David Harker, Protein Structure Project, Polytechnic Institute of Brooklyn, Brooklyn 2, New York.

"Soviet Physics – Crystallography" is published by the American Institute of Physics, with the cooperation of the American Crystallographic Association, for the purpose of making available in English reports of current Soviet research in crystallography as contained in the journal "Crystallography" of the Academy of Sciences of the USSR. The translation begins with the 1957 issues.

Transliteration of the names of Russian authors follows the system employed by the Library of Congress.

This translating and publishing project was undertaken by the Institute in the conviction that dissemination of the results of research everywhere in the world is invaluable to the advancement of science. The National Science Foundation of the United States encouraged the project initially and is supporting it in large part by a grant. Translation and printing are being handled by Consultants Bureau, Inc.

The American Institute of Physics and its translators propose to translate faithfully all of the scientific material in the "Crystallographic Journal of the Academy of Sciences of the USSR" appearing after January 1, 1957. The views expressed in the translated material, therefore, are intended to be those expressed by the original authors, and not those of the translators nor of the American Institute of Physics.

One volume is published annually. The volume numbering coincides with that of the original Russian journal.

Subscription Prices:

Per year (6 issues), starting with Vol. 2, No. 1

General:	*United States and Canada*	$25.00
	Elsewhere	27.00
Libraries of non-profit academic institutions:		
	United States and Canada	10.00
	Elsewhere	12.00
Back numbers, all issues		5.00

Subscriptions should be addressed to the American Institute of Physics, 335 East 45th Street, New York 17, New York.

Copyright American Institute of Physics Incorporated, 1958

SOVIET PHYSICS

Crystallography

VOLUME 2, NUMBER 3 MAY-JUNE, 1957

SHUBNIKOV GROUPS

N.V. Belov, N.N. Neronova and T.S. Smirnova

1651 Shubnikov groups are presented in the new international notation, prefaced by a few fundamental theorems which govern their derivation.

The 1651 Shubnikov groups (symmetrical and antisymmetrical space groups) can be easily derived from the 230 Fedorov groups if their derivation is based on the corresponding bicolored (plus-minus) translation lattices, 36 of which are shown in Table 1. Actually there are 22 lattices which are colored, the 14 others are common single-colored Bravais lattices.

On the basis of an almost obvious theorem, in the case of a bicolored translation lattice any bicolored symmetry element will either coincide geometrically with the same kind of uncolored symmetry element (a plane with a different translational component, an axis or a center) or will alternate with it. In the symbol of the corresponding Shubnikov group, following the first sign of the translation group, it is sufficient to show (according to the international principle of arrangement) only the uncolored elements of symmetry, i.e., one of the Fedorov groups.

In the case of the 14 uncolored or common Bravais lattices, the colored symmetry elements enter into the symbols of the actual Shubnikov bicolored groups. Their introduction is regulated by two very simple theorems. According to the first, the symmetry elements of odd order may be only uncolored or grey [1], i.e., proper Shubnikov groups with such elements of symmetry (axis 3) cannot exist. According to the second theorem, if in a finite or infinite three-dimensional bicolored pattern (with black-white symmetry), the black half of the figures be changed to white, one of the Fedorov groups will be obtained, precisely the one in which the former colored elements have been replaced by analogous uncolored ones. This means that in the case of uncolored lattices we will arrive at black-white groups, by replacing one, two or three independent elements, which define any one of the Fedorov groups, by corresponding colored elements in all possible combinations. One must take into consideration the possibility of unequal orientation of the lattice in relation to the group of symmetry elements. The complete list of 1651 Shubnikov groups is given below, including the 230 common Fedorov groups and the 230 grey groups. Bicolored (plus-minus) symmetry elements are shown by a dash over the symbol. Grey groups are shown by the addition, at the end of the symbol, of 1' which is the symmetry element responsible for the change of color of all the components of the pattern [1]. This sign is absent in the grey groups of the cubic system where it seemed more convenient to add the apostrophe to the corresponding (odd) axes of the 3rd order.

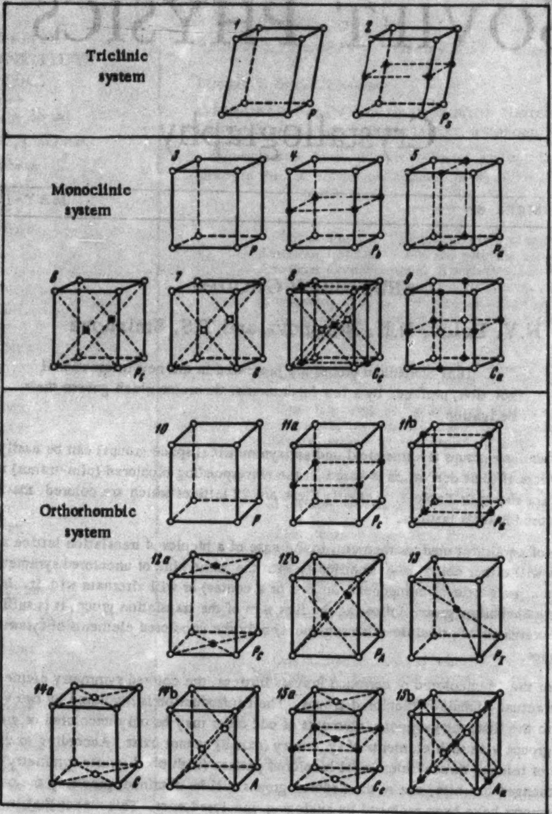
Triclinic system
1
P
2
P_s
Monoclinic system
3
P
4
P_b
5
P_a
6
P_c
7
C
8
C_c
9
C_a
Orthorhombic system
10
P
11a
P_c
11b
P_B
12a
P_C
12b
P_A
13
P_I
14a
C
14b
A
15a
C_c
15b
A_a

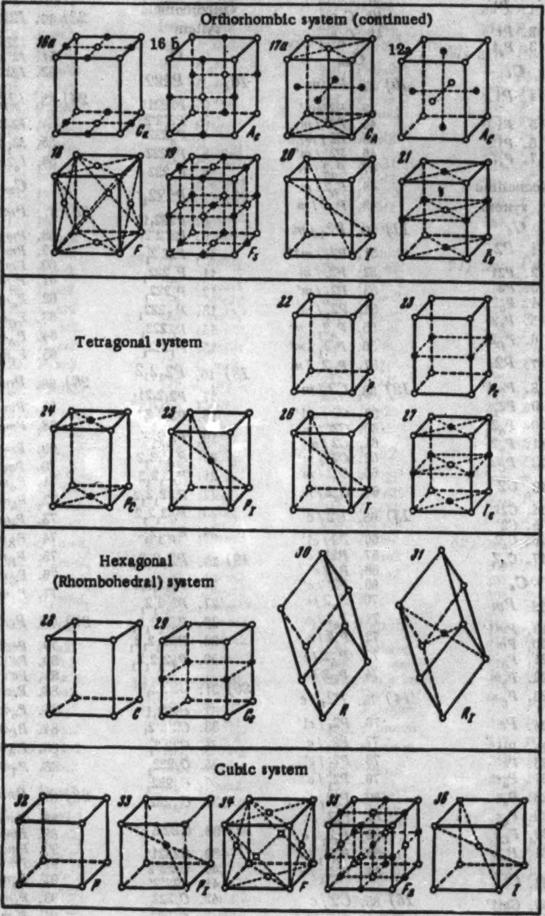
Orthorhombic system (continued)
16a
C_a
16 b
A_c
17a
C_A
12a
A_C
18
F
19
F_s
20
I
21
I_a
Tetragonal system
22
P
23
P_c
24
P_C
25
P_I
26
I
27
I_c
Hexagonal
(Rhombohedral) system
28
C
29
C_c
30
R
31
R_I
Cubic system
32
P
33
P_I
34
F
35
F_S
36
I

LIST OF SHUBNIKOV SPACE GROUPS

Triclinic system

C_1

1) 1. $P1$
2. $P1'$
3. P_s1

C_i

2) 4. $P\bar{1}$
5. $P\bar{1}1'$
6. $P\bar{1}'$
7. $P_s\bar{1}$

Monoclinic system

C_2

3) 1. $P2$
2. $P21'$
3. $P2'$
4. P_a2
5. P_b2
6. P_C2

4) 7. $P2_1$
8. $P2_11'$
9. $P2_1'$
10. P_a2_1
11. P_b2_1
12. P_C2_1

5) 13. $C2$
14. $C21'$
15. $C2'$
16. C_c2
17. C_a2

C_s

6) 18. Pm
19. $Pm1'$
20. Pm'
21. P_am
22. P_bm
23. P_Cm

7) 24. Pc
25. $Pc1'$
26. Pc'
27. P_ac
28. P_cc
29. P_bc
30. P_Cc
31. P_Ac

8) 32. Cm
33. $Cm1'$
34. Cm'
35. C_cm
36. C_am

9) 37. Cc
38. $Cc1'$
39. Cc'
40. C_cc
41. C_ac

C_{2h}

10) 42. $P2/m$
43. $P2/m1'$
44. $P2'/m$
45. $P2/m'$
46. $P2'/m'$
47. P_a2/m
48. P_b2/m
49. P_C2/m

11) 50. $P2_1/m$
51. $P2_1/m1'$
52. $P2_1'/m$
53. $P2_1/m'$
54. $P2_1'/m'$
55. P_a2_1/m
56. P_b2_1/m
57. P_C2_1/m

12) 58. $C2/m$
59. $C2/m1'$
60. $C2'/m$
61. $C2/m'$
62. $C2'/m'$
63. C_c2/m
64. C_a2/m

13) 65. $P2/c$
66. $P2/c1'$
67. $P2'/c$
68. $P2/c'$
69. $P2'/c'$
70. P_a2/c
71. P_b2/c
72. P_c2/c
73. P_A2/c
74. P_C2/c

14) 75. $P2_1/c$
76. $P2_1/c1'$
77. $P2_1'/c$
78. $P2_1/c'$
79. $P2_1'/c'$
80. P_a2_1/c
81. P_b2_1/c
82. P_c2_1/c
83. P_A2_1/c
84. P_C2_1/c

15) 85. $C2/c$
86. $C2/c1'$
87. $C2'/c$
88. $C2/c'$
89. $C2'/c'$
90. C_c2/c
91. C_a2/c

Orthorhombic system

D_2

16) 1. $P222$
2. $P2221'$
3. $P2'2'2$
4. P_a222
5. P_C222
6. P_I222

17) 7. $P222_1$
8. $P222_11'$
9. $P2'2'2_1$
10. $P22'2_1'$
11. P_a222_1
12. P_c222_1
13. P_A222_1
14. P_C222_1
15. P_I222_1

18) 16. $P2_12_12$
17. $P2_12_121'$
18. $P2_1'2_1'2$
19. $P2_12_1'2'$
20. $P_a2_12_12$
21. $P_c2_12_12$
22. $P_A2_12_12$
23. $P_C2_12_12$
24. $P_I2_12_12$

19) 25. $P2_12_12_1$
26. $P2_12_12_11'$
27. $P2_1'2_1'2_1$
28. $P_a2_12_12_1$
29. $P_C2_12_12_1$
30. $P_I2_12_12_1$

20) 31. $C222_1$
32. $C222_11'$
33. $C2'2'2_1$
34. $C22'2_1'$
35. C_c222_1
36. C_a222_1
37. C_A222_1

21) 38. $C222$
39. $C2221'$
40. $C2'2'2$
41. $C22'2'$
42. C_c222
43. C_a222
44. C_A222

22) 45. $F222$
46. $F2221'$
47. $F2'2'2$
48. F_s222

23) 49. $I222$
50. $I2221'$
51. $I2'2'2$
52. I_c222

24) 53. $I2_12_12_1$
54. $I2_12_12_11'$
55. $I2_1'2_1'2_1$
56. $I_c2_12_12_1$

C_{2v}

25) 57. $Pmm2$
58. $Pmm21'$
59. $Pm'm2'$
60. $Pm'm'2$
61. P_cmm2
62. P_amm2
63. P_Cmm2
64. P_Amm2
65. P_Imm2

26) 66. $Pmc2_1$
67. $Pmc2_11'$
68. $Pm'c2_1'$
69. $Pmc'2_1'$
70. $Pm'c'2_1$
71. P_amc2_1
72. P_bmc2_1
73. P_cmc2_1
74. P_Amc2_1
75. P_Bmc2_1
76. P_Cmc2_1
77. P_Imc2_1

27) 78. $Pcc2$
79. $Pcc21'$
80. $Pc'c2$
81. $Pc'c'2$
82. P_ccc2
83. P_acc2
84. P_Ccc2
85. P_Acc2
86. P_Icc2

28) 87. $Pma2$
88. $Pma21'$
89. $Pm'a2'$
90. $Pma'2'$
91. $Pm'a'2$
92. P_ama2
93. P_bma2
94. P_cma2
95. P_Ama2

96. P_Bma2
97. P_Cma2
98. P_Ima2
29) 99. $Pca2_1$
100. $Pca2_11'$
101. $Pc'a2'_1$
102. $Pca'2'_1$
103. $Pc'a'2_1$
104. P_aca2_1
105. P_bca2_1
106. P_cca2_1
107. P_Aca2_1
108. P_Bca2_1
109. P_Cca2_1
110. P_Ica2_1
30) 111. $Pnc2$
112. $Pnc21'$
113. $Pn'c2'$
114. $Pnc'2'$
115. $Pn'c'2$
116. P_anc2
117. P_bnc2
118. P_cnc2
119. P_Anc2
120. P_Bnc2
121. P_Cnc2
122. P_Inc2
31) 123. $Pmn2_1$
124. $Pmn2_11'$
125. $Pm'n2'_1$
126. $Pmn'2'_1$
127. $Pm'n'2_1$
128. P_amn2_1
129. P_bmn2_1
130. P_cmn2_1
131. P_Amn2_1
132. P_Bmn2_1
133. P_Cmn2_1
134. P_Imn2_1
32) 135. $Pba2$
136. $Pba21'$
137. $Pb'a2'$
138. $Pb'a'2$
139. P_cba2
140. P_aba2
141. P_Cba2
142. P_Aba2
143. P_Iba2
33) 144. $Pna2_1$
145. $Pna2_11'$
146. $Pn'a2'_1$
147. $Pna'2'_1$
148. $Pn'a'2_1$
149. P_ana2_1
150. P_bna2_1
151. P_cna2_1
152. P_Ana2_1
153. P_Bna2_1
154. P_Cna2_1
155. P_Cna2_1
34) 156. $Pnn2$
157. $Pnn21'$
158. $Pn'n2'$
159. $Pn'n'2$
160. P_ann2
161. P_cnn2
162. P_Ann2
163. P_Cnn2
164. P_Inn2
35) 165. $Cmm2$
166. $Cmm21'$
167. $Cm'm2'$
168. $Cm'm'2$
169. C_cmm2
170. C_amm2
171. C_Amm2
36) 172. $Cmc2_1$
173. $Cmc2_11'$
174. $Cm'c2'_1$
175. $Cmc'2'_1$
176. $Cm'c'2_1$
177. C_cmc2_1
178. C_amc2_1
179. C_Amc2_1
37) 180. $Ccc2$
181. $Ccc21'$
182. $Cc'c2'$
183. $Cc'c'2$
184. C_ccc2
185. C_acc2
186. C_Acc2
38) 187. $Amm2$
188. $Amm21'$
189. $Am'm2'$
190. $Amm'2'$
191. $Am'm'2$
192. A_amm2
193. A_cmm2
194. A_Cmm2
39) 195. $Abm2$
196. $Abm21'$
197. $Ab'm2'$
198. $Abm'2'$
199. $Ab'm'2$
200. A_abm2
201. A_cbm2
202. A_Cbm2
40) 203. $Ama2$
204. $Ama21'$
205. $Am'a2'$
206. $Ama'2'$
207. $Am'a'2$
208. A_ama2
209. A_cma2
210. A_Cma2
41) 211. $Aba2$
212. $Aba21'$
213. $Ab'a2'$
214. $Aba'2'$
215. $Ab'a'2$
216. A_aba2
217. A_cba2
218. A_Cba2
42) 219. $Fmm2$
220. $Fmm21'$
221. $Fm'm2'$
222. $Fm'm'2$
223. F_smm2
43) 224. $Fdd2$
225. $Fdd21'$
226. $Fd'd2'$
227. $Fd'd'2$
228. F_sdd2
44) 229. $Imm2$
230. $Imm21'$
231. $Im'm2'$
232. $Im'm'2$
233. I_cmm2
234. I_amm2
45) 235. $Iba2$
236. $Iba21'$
237. $Ib'a2'$
238. $Ib'a'2$
239. I_cba2
240. I_aba2
46) 241. $Ima2$
242. $Ima21'$
243. $Im'a2'$
244. $Ima'2'$
245. $Im'a'2$
246. I_cma2
247. I_ama2
248. I_bma2

$\mathbf{D}_{2h}$

47) 249 $Pmmm$
250. $Pmmm1'$
251. $Pm'mm$
252. $Pm'm'm$
253. $Pm'm'm'$
254. P_ammm
255. P_Cmmm
256. P_Immm
48) 257. $Pnnn$
258. $Pnnn1'$
259. $Pn'nn$
260. $Pn'n'n$
261. $Pn'n'n'$
262. P_annn
263. P_Cnnn
264. P_Innn
49) 265. $Pccm$
266. $Pccm1'$
267. $Pc'cm$
268. $Pccm'$
269. $Pc'c'm$
270. $Pc'cm'$
271. $Pc'c'm'$
272. P_accm
273. P_cccm
274. P_Accm
275. P_Cccm
276. P_Iccm
50) 277. $Pban$
278. $Pban1'$
279. $Pb'an$
280. $Pban'$
281. $Pb'a'n$
282. $Pb'an'$
283. $Pb'a'n'$
284. P_aban
285. P_cban
286. P_Aban
287. P_Cban
288. P_Iban
51) 289. $Pmma$
290. $Pmma1'$
291. $Pm'ma$
292. $Pmm'a$
293. $Pmma'$
294. $Pm'm'a$
295. $Pmm'a'$
296. $Pm'ma'$
297. $Pm'm'a'$
298. P_amma
299. P_bmma
300. P_cmma
301. P_Amma
302. P_Bmma
303. P_Cmma
304. P_Imma
52) 305. $Pnna$
306. $Pnna1'$
307. $Pn'na$
308. $Pnn'a$
309. $Pnna'$
310. $Pn'n'a$
311. $Pnn'a'$
312. $Pn'na'$
313. $Pn'n'a'$
314. P_anna
315. P_bnna
316. P_cnna
317. P_Anna
318. P_Bnna
319. P_Cnna
320. P_Inna
53) 321. $Pmna$
322. $Pmna1'$
323. $Pm'na$
324. $Pmn'a$
325. $Pmna'$
326. $Pm'n'a$
327. $Pmn'a'$
328. $Pm'na'$

329. Pm'n'a'
330. $P_{a}mna$
331. $P_{b}mna$
332. $P_{c}mna$
333. $P_{A}mna$
334. $P_{B}mna$
335. $P_{C}mna$
336. $P_{I}mna$

54) 337. Pcca

338. Pcca1'
339. Pc'ca
340. Pcc'a
341. Pcca'
342. Pc'c'a
343. Pcc'a'
344. Pc'ca'
345. Pc'c'a'
346. $P_{a}cca$
347. $P_{b}cca$
348. $P_{c}cca$
349. $P_{A}cca$
350. $P_{B}cca$
351. $P_{C}cca$
352. $P_{I}cca$

55) 353. Pbam

354. Pbam1'
355. Pb'am
356. Pbam'
357. Pb'a'm
358. Pb'am'
359. Pb'a'm'
360. $P_{a}bam$
361. $P_{c}bam$
362. $P_{A}bam$
363. $P_{C}bam$
364. $P_{I}bam$

56) 365. Pccn

366. Pccn1'
367. Pc'cn
368. Pccn'
369. Pc'c'n
370. Pc'cn'
371. Pc'c'n'
372. $P_{a}ccn$
373. $P_{c}ccn$
374. $P_{A}ccn$
375. $P_{C}ccn$
376. $P_{I}ccn$

57) 377. Pbcm

378. Pbcm1'
379. Pb'cm
380. Pbc'm
381. Pbcm'
382. Pb'c'm
383. Pbc'm'
384. Pb'cm'
385. Pb'c'm'
386. $P_{a}bcm$
387. $P_{b}bcm$
388. $P_{c}bcm$
389. $P_{A}bcm$
390. $P_{B}bcm$
391. $P_{C}bcm$
392. $P_{I}bcm$

58) 393. Pnnm

394. Pnnm1'
395. Pn'nm
396. Pnnm'
397. Pn'n'm
398. Pnn'm'
399. Pn'n'm'
400. $P_{a}nnm$
401. $P_{c}nnm$
402. $P_{A}nnm$
403. $P_{C}nnm$
404. $P_{I}nnm$

59) 405. Pmmn

406. Pmmn1'
407. Pm'mn
408. Pmmn'
409. Pm'm'n
410. Pmm'n'
411. Pm'm'n'
412. $P_{a}mmn$
413. $P_{c}mmn$
414. $P_{A}mmn$
415. $P_{C}mmn$
416. $P_{I}mmn$

60) 417. Pbcn

418. Pbcn1'
419. Pb'cn
420. Pbc'n
421. Pbcn'
422. Pb'c'n
423. Pbc'n'
424. Pb'cn'
425. Pb'c'n'
426. $P_{a}bcn$
427. $P_{b}bcn$
428. $P_{c}bcn$
429. $P_{A}bcn$
430. $P_{B}bcn$
431. $P_{C}bcn$
432. $P_{I}bcn$

61) 433. Pbca

434. Pbca1'
435. Pb'ca
436. Pb'c'a
437. Pb'c'a'
438. $P_{a}bca$
439. $P_{C}bca$
440. $P_{I}bca$

62) 441. Pnma

442. Pnma1'
443. Pn'ma
444. Pnm'a
445. Pnma'
446. Pn'm'a
447. Pnm'a'
448. Pn'ma'
449. Pn'm'a'
450. $P_{a}nma$
451. $P_{b}nma$
452. $P_{c}nma$
453. $P_{A}nma$
454. $P_{B}nma$
455. $P_{C}nma$
456. $P_{I}nma$

63) 457. Cmcm

458. Cmcm1'
459. Cm'cm
460. Cmc'm
461. Cmcm'
462. Cm'c'm
463. Cmc'm'
464. Cm'cm'
465. Cm'c'm'
466. $C_{c}mcm$
467. $C_{a}mcm$
468. $C_{A}mcm$

64) 469. Cmca

470. Cmca1'
471. Cm'ca
472. Cmc'a
473. Cmca'
474. Cm'c'a
475. Cmc'a'
476. Cm'ca'
477. Cm'c'a'
478. $C_{c}mca$
479. $C_{a}mca$
480. $C_{A}mca$

65) 481. Cmmm

482. Cmmm1'
483. Cm'mm
484. Cmmm'
485. Cm'm'm
486. Cmm'm'
487. Cm'm'm'
488. $C_{c}mmm$
489. $C_{a}mmm$
490. $C_{A}mmm$

66) 491. Cccm

492. Cccm1'
493. Cc'cm
494. Cccm'
495. Cc'c'm
496. Ccc'm'
497. Cc'c'm'
498. $C_{c}ccm$
499. $C_{a}ccm$
500. $C_{A}ccm$

67) 501. Cmma

502. Cmma1'
503. Cm'ma
504. Cmma'
505. Cm'm'a
506. Cmm'a'
507. Cm'm'a'
508. $C_{c}mma$
509. $C_{a}mma$
510. $C_{A}mma$

68) 511. Ccca

512. Ccca1'
513. Cc'ca
514. Ccca'
515. Cc'c'a
516. Ccc'a'
517. Cc'c'a'
518. $C_{c}cca$
519. $C_{a}cca$
520. $C_{A}cca$

69) 521. Fmmm

522. Fmmm1'
523. Fm'mm
524. Fm'm'm
525. Fm'm'm'
526. $F_{s}mmm$

70) 527. Fddd

528. Fddd1'
529. Fd'dd
530. Fd'd'd
531. Fd'd'd'
532. $F_{s}ddd$

71) 533. Immm

534. Immm1
535. Im'mm'
536. Im'm'm
537. Im'm'm'
538. $I_{c}mmm$

72) 539. Ibam

540. Ibam1'
541. Ib'am
542. Ibam'
543. Ib'a'm
544. Iba'm'
545. Ib'a'm'
546. $I_{c}bam$
547. $I_{a}bam$

73) 548. Ibca

549. Ibca1'
550. Ib'ca
551. Ib'c'a
552. Ib'c'a'
553. $I_{c}bca$

74) 554. Imma

555. Imma1'
556. Im'ma
557. Imma'
558. Im'm'a
559. Imm'a'
560. Im'm'a'
561. $I_{c}mma$
562. $I_{a}mma$

Tetragonal
system
C_4

75) 1. P4

2. P41'
3. P4'

4. P_c4
5. P_C4
6. P_I4
76) 7. $P4_1$
8. $P4_11'$
9. $P4_1'$
10. P_c4_1
11. P_C4_1
12. P_I4_1
77) 13. $P4_2$
14. $P4_21'$
15. $P4_2'$
16. P_c4_2
17. P_C4_2
18. P_I4_2
78) 19. $P4_3$
20. $P4_31'$
21. $P4_3'$
22. P_c4_3
23. P_C4_3
24. P_I4_3
79) 25. $I4$
26. $I41'$
27. $I4'$
28 I_c4
80) 29. $I4_1$
30. $I4_11'$
31. $I4_1'$
32. I_c4_1

S_4

81) 33. $P\bar{4}$
34. $P\bar{4}1'$
35. $P\bar{4}'$
36. $P_c\bar{4}$
37. $P_C\bar{4}$
38. $P_I\bar{4}$
82) 39. $I\bar{4}$
40. $I\bar{4}1'$
41. $I\bar{4}'$
42. $I_c\bar{4}$

C_{4h}

83) 43. $P4/m$
44. $P4/m1'$
45. $P4'/m$
46. $P4/m'$
47. $P4'/m'$
48. P_c4/m
49. P_C4/m
50. P_I4/m
84) 51. $P4_2/m$
52. $P4_2/m1'$
53. $P4_2'/m$
54. $P4_2/m'$
55. $P4_2'/m'$
56. P_c4_2/m
57. P_C4_2/m
58. P_I4_2/m
85) 59. $P4/n$
60. $P4/n1'$
61. $P4'/n$
62. $P4/n'$
63. $P4'/n'$
64. P_c4/n
65. P_C4/n
66. P_I4/n
86) 67. $P4_2/n$
68. $P4_2/n1'$
69. $P4_2'/n$
70. $P4_2/n'$
71. $P4_2'/n'$
72. P_c4_2/n
73. P_C4_2/n
74. P_I4_2/n
87) 75. $I4/m$
76. $I4/m1'$
77. $I4'/m$
78. $I4/m'$
79. $I4'/m'$
80. I_c4/m
88) 81. $I4_1/a$
82. $I4_1/a1'$
83. $I4_1'/a$
84. $I4_1/a'$
85. $I4_1'/a'$
86. I_c4_1/a

D_4

89) 87. $P422$
88. $P4221'$
89. $P4'22'$
90. $P42'2'$
91. $P4'2'2$
92. P_c422
93. P_C422
94. P_I422
90) 95. $P42_12'$
96. $P42_121'$
97. $P4'2_12'$
98. $P42_1'2'$
99. $P4'2_1'2$
100. P_c42_12
101. P_C42_12
102. P_I42_12
91) 103. $P4_122$
104. $P4_1221'$
105. $P4_1'22'$
106. $P4_12'2'$
107. $P4_1'2'2$
108. P_c4_122
109. P_C4_122
110. P_I4_122
92) 111. $P4_12_12$
112. $P4_12_121'$
113. $P4_1'2_12'$
114. $P4_12_1'2'$
115. $P4_1'2_1'2$
116. $P_c4_12_12$
117. $P_C4_12_12$
118. $P_I4_12_12$
93) 119. $P4_222$
120. $P4_2221'$
121. $P4_2'22'$
122. $P4_22'2'$
123. $P4_2'2'2$
124. P_c4_222
125. P_C4_222
126. P_I4_222
94) 127. $P4_22_12$
128. $P4_22_121'$
129. $P4_2'2_12'$
130. $P4_22_1'2'$
131. $P4_2'2_1'2$
132. $P_c4_22_12$
133. $P_C4_22_12$
134. $P_I4_22_12$
95) 135. $P4_322$
136. $P4_3221'$
137. $P4_3'22'$
138. $P4_32'2'$
139. $P4_3'2'2$
140. P_c4_322
141. P_C4_322
142. P_I4_322
96) 143. $P4_32_12$
144. $P4_32_121'$
145. $P4_3'2_12'$
146. $P4_32_1'2'$
147. $P4_3'2_1'2$
148. $P_c4_32_12$
149. $P_C4_32_12$
150. $P_I4_32_12$
97) 151. $I422$
152. $I4221'$
153. $I4'22'$
154. $I42'2'$
155. $I4'2'2$
156. I_c422
98) 157. $I4_122$
158. $I4_1221'$
159. $I4_1'22'$
160. $I4_12'2'$
161. $I4_1'2'2$
162. I_c4_122

C_{4v}

99) 163. $P4mm$
164. $P4mm1'$
165. $P4'm'm$
166. $P4'mm'$
167. $P4m'm'$
168. P_c4mm
169. P_C4mm
170. P_I4mm
100) 171. $P4bm$
172. $P4bm1'$
173. $P4'b'm$
174. $P4'bm'$
175. $P4b'm'$
176. P_c4bm
177. P_C4bm
178. P_I4bm
101) 179. $P4_2cm$
180. $P4_2cm1'$
181. $P4_2'c'm$
182. $P4_2'cm'$
183. $P4_2c'm'$
184. P_c4_2cm
185. P_C4_2cm
186. P_I4_2cm
102) 187. $P4_2nm$
188. $P4_2nm1'$
189. $P4_2'n'm$
190. $P4_2'nm'$
191. $P4_2n'm'$
192. P_c4_2nm
193. P_C4_2nm
194. P_I4_2nm
103) 195. $P4cc$
196. $P4cc1'$
197. $P4'c'c$
198. $P4'cc'$
199. $P4c'c'$
200. P_c4cc
201. P_C4cc
202. P_I4cc
104) 203. $P4nc$
204. $P4nc1'$
205. $P4'n'c$
206. $P4'nc'$
207. $P4n'c'$
208. P_c4nc
209. P_C4nc
210. P_I4nc
105) 211. $P4_2mc$
212. $P4_2mc1'$
213. $P4_2'm'c$
214. $P4_2'mc'$

215. $P4_2m'c'$
216. P_c4_2mc
217. P_C4_2mc
218. P_I4_2mc

106) 219. $P4_2bc$
220. $P4_2bc1'$
221. $P4_2'b'c$
222. $P4_2'bc'$
223. $P4_2b'c'$
224. P_c4_2bc
225. P_C4_2bc
226. P_I4_2bc

107) 227. $I4mm$
228. $I4mm1'$
229. $I4'm'm$
230. $I4'mm'$
231. $I4m'm'$
232. I_c4mm

108) 233. $I4cm$
234. $I4cm1'$
235. $I4'c'm$
236. $I4'cm'$
237. $I4c'm'$
238. I_c4cm

109) 239. $I4_1md$
240. $I4_1md1'$
241. $I4_1'm'd$
242. $I4_1'md'$
243. $I4_1m'd'$
244. I_cmd

110) 245. $I4_1cd$
246. $I4_1cd1'$
247. $I4_1'c'd$
248. $I4_1'cd'$
249. $I4_1c'd'$
250. I_c4_1cd

D_{2d}

111) 251. $P\bar{4}2m$
252. $P\bar{4}2m1'$
253. $P\bar{4}'2'm$
254. $P\bar{4}'2m'$
255. $P\bar{4}2'm'$
256. $P_c\bar{4}2m$
257. $P_C\bar{4}2m$
258. $P_I\bar{4}2m$

112) 259. $P\bar{4}2c$
260. $P\bar{4}2c1'$
261. $P\bar{4}'2'c$
262. $P\bar{4}'2c'$
263. $P\bar{4}2'c'$
264. $P_c\bar{4}2c$
265. $P_C\bar{4}2c$
266. $P_I\bar{4}2c$

113) 267. $P\bar{4}2_1m$
268. $P\bar{4}2_1m1'$
269. $P\bar{4}'2_1'm$
270. $P\bar{4}'2_1m'$
271. $P\bar{4}2_1'm'$
272. $P_c\bar{4}2_1m$
273. $P_C\bar{4}2_1m$
274. $P_I\bar{4}2_1m$

114) 275. $P\bar{4}2_1c$
276. $P\bar{4}2_1c$
277. $P\bar{4}'2_1'c$
278. $P\bar{4}'2_1c$
279. $P\bar{4}2_1'c'$
280. $P_c\bar{4}2_1c$
281. $P_C\bar{4}2_1c$
282. $P_I\bar{4}2_1c$

115) 283. $P\bar{4}m2$
284. $P\bar{4}m21'$
285. $P\bar{4}'m'2$
286. $P\bar{4}'m2'$
287. $P\bar{4}m'2'$
288. $P_c\bar{4}m2$
289. $P_C\bar{4}m2$
290. $P_I\bar{4}m2$

116) 291. $P\bar{4}c2$
292. $P\bar{4}c21'$
293. $P\bar{4}'c'2$
294. $P\bar{4}'c2'$
295. $P\bar{4}c'2'$
296. $P_c\bar{4}c2$
297. $P_C\bar{4}c2$
298. $P_I\bar{4}c2$

117) 299. $P\bar{4}b2$
300. $P\bar{4}b21'$
301. $P\bar{4}'b'2$
302. $P\bar{4}'b2'$
303. $P\bar{4}b'2'$
304. $P_c\bar{4}b2$
305. $P_C\bar{4}b2$
306. $P_I\bar{4}b2$

118) 307. $P\bar{4}n2$
308. $P\bar{4}n21'$
309. $P\bar{4}'n'2$
310. $P\bar{4}'n2'$
311. $P\bar{4}n'2'$
312. $P_c\bar{4}n2$
313. $P_C\bar{4}n2$
314. $P_I\bar{4}n2$

119) 315. $I\bar{4}m2$
316. $I\bar{4}m21'$
317. $I\bar{4}'m'2$
318. $I\bar{4}'m2'$
319. $I\bar{4}m'2'$
320. $I_c\bar{4}m2$

120) 321. $I\bar{4}c2$
322. $I\bar{4}c21'$
323. $I\bar{4}'c'2$
324. $I\bar{4}'c2'$
325. $I\bar{4}c'2'$
326. $I_c\bar{4}c2$

121) 327. $I\bar{4}2m$
328. $I\bar{4}2m1'$
329. $I\bar{4}'2'm$
330. $I\bar{4}'2m'$
331. $I\bar{4}2'm'$
332. $I_c\bar{4}2m$

122) 333. $I\bar{4}2d$
334. $I\bar{4}2d1'$
335. $I\bar{4}'2'd$
336. $I\bar{4}'2d'$
337. $I\bar{4}2'd'$
338. $I_c\bar{4}2d$

D_{4h}

123) 339. $P4/mmm$
340. $P4/mmm1'$
341. $P4/m'mm$
342. $P4'/mm'm$
343. $P4'/mmm'$
344. $P4'/m'm'm$
345. $P4/mm'm'$
346. $P4'/m'mm'$
347. $P4/m'm'm'$
348. P_c4/mmm
349. P_C4/mmm
350. P_I4/mmm

124) 351. $P4/mcc$
352. $P4/mcc1'$
353. $P4/m'cc$
354. $P4'/mc'c$
355. $P4'/mcc'$
356. $P4'/m'c'c$
357. $P4/mc'c'$
358. $P4'/m'cc'$
359. $P4/m'c'c'$
360. P_c4/mcc
361. P_C4/mcc
362. P_I4/mcc

125) 363. $P4/nbm$
364. $P4/nbm1'$
365. $P4/n'bm$
366. $P4'/nb'm$
367. $P4'/nbm'$
368. $P4'/n'b'm$
369. $P4/nb'm'$
370. $P4'/n'bm'$
371. $P4/n'b'm'$
372. P_c4/nbm
373. P_C4/nbm
374. P_I4/nbm

126) 375. $P4/nnc$
376. $P4/nnc1'$
377. $P4/n'nc$
378. $P4'/nn'c$
379. $P4'/nnc'$
380. $P4'/n'n'c$
381. $P4/nn'c'$
382. $P4'/n'nc'$
383. $P4/n'n'c'$
384. P_c4/nnc
385. P_C4/nnc
386. P_I4/nnc

127) 387. $P4/mbm$
388. $P4mbm1'$
389. $P4/m'bm$
390. $P4'/mb'm$
391. $P4'/mbm'$
392. $P4'/m'b'm$
393. $P4/mb'm'$
394. $P4'/m'bm'$
395. $P4/m'b'm'$
396. P_c4/mbm
397. P_C4/mbm
398. P_I4/mbm

128) 399. $P4/mnc$
400. $P4/mnc1'$
401. $P4/m'nc$
402. $P4'/mn'c$
403. $P4'/mnc'$
404. $P4'/m'n'c$
405. $P4/mn'c'$
406. $P4'/m'nc'$
407. $P4/m'n'c'$
408. P_c4/mnc
409. P_C4/mnc
410. P_I4/mnc

129) 411. $P4nmm$
412. $P4/nmm1'$
413. $P4/n'mm$
414. $P4'/nm'm$
415. $P4'/nmm'$
416. $P4'/n'm'm$
417. $P4/nm'm'$
418. $P4'/n'mm'$
419. $P4/n'm'm'$
420. P_c4/nmm
421. P_C4/nmm
422. P_I4/nmm

130) 423. $P4/ncc$
424. $P4/ncc1'$
425. $P4/n'cc$
426. $P4'/nc'c$
427. $P4'/ncc'$
428. $P4'/n'cc'$
429. $P4/nc'c'$
430. $P4'/n'cc'$
431. $P4/n'c'c'$
432. P_c4/ncc

433. P_C4/ncc
434. P_I4/ncc

131) 435. $P4_2/mmc$
436. $P4_2/mmc1'$
437. $P4_2/m'mc$
438. $P4'_2/mm'c$
439. $P4'_2/mmc'$
440. $P4'_2/m'm'c$
441. $P4_2/mm'c'$
442. $P4'_2/m'mc'$
443. $P4_2/m'm'c'$
444. P_c4_2/mmc
445. P_C4_2/mmc
446. P_I4_2/mmc

132) 447. $P4_2/mcm$
448. $P4_2/mcm1'$
449. $P4_2/m'cm$
450. $P4'_2/mc'm$
451. $P4'_2/mcm'$
452. $P4'_2/m'c'm$
453. $P4_2/mc'm'$
454. $P4'_2/m'cm'$
455. $P4_2/m'c'm'$
456. P_c4_2/mcm
457. P_C4_2/mcm
458. P_I4_2/mcm

133) 459. $P4_2/nbc$
460. $P4_2/nbc1'$
461. $P4_2/n'bc$
462. $P4'_2/nb'c$
463. $P4'_2/nbc'$
464. $P4'_2/n'b'c$
465. $P4_2/nb'c'$
466. $P4'_2/n'bc'$
467. $P4_2/n'b'c'$
468. P_c4_2/nbc
469. P_C4_2/nbc
470. P_I4_2/nbc

134) 471. $P4_2/nnm$
472. $P4_2/nnm1'$
473. $P4_2/n'nm$
474. $P4'_2/nn'm$
475. $P4'_2/nnm'$
476. $P4'_2/n'n'm$
477. $P4_2/nn'm'$
478. $P4'_2/n'nm'$
479. $P4_2/n'n'm'$
480. P_c4_2/nnm
481. P_C4_2/nnm
482. P_I4_2/nnm

135) 483. $P4_2/mbc$
484. $P4_2/mbc1'$
485. $P4_2/m'bc$
486. $P4'_2/mb'c$
487. $P4'_2/mbc'$
488. $P4'_2/m'b'c$
489. $P4_2/mb'c'$
490. $P4'_2/m'bc'$
491. $P4_2/m'b'c'$
492. P_c4_2/mbc
493. P_C4_2/mbc
494. P_I4_2/mbc

136) 495. $P4_2/mnm$
496. $P4_2/mnm1$,
497. $P4_2/m'nm$
498. $P4'_2/mn'm$
499. $P4'_2/mnm'$
500. $P4'_2/m'n'm$
501. $P4_2/mn'm'$
502. $P4'_2/m'nm'$
503. $P4_2/m'n'm'$
504. P_c4_2/mnm
505. P_C4_2/mnm
506. P_I4_2/mnm

137) 507. $P4_2/nmc$
508. $P4_2/nmc1'$
509. $P4_2/n'mc$
510. $P4'_2/nm'c$
511. $P4'_2/nmc'$
512. $P4'_2/n'm'c$
513. $P4_2/nm'c'$
514. $P4'_2/n'mc'$
515. $P4_2/n'm'c'$
516. P_c4_2/nmc
517. P_C4_2/nmc
518. P_I4_2/nmc

138) 519. $P4_2/ncm$
520. $P4_2/ncm1'$
521. $P4_2/n'cm$
522. $P4'_2/nc'm$
523. $P4'_2/ncm'$
524. $P4'_2/n'c'm$
525. $P4_2/nc'm'$
526. $P4'_2/n'cm'$
527. $P4_2/n'c'm'$
528. P_c4_2/ncm
529. P_C4_2/ncm
530. P_I4_2/ncm

139) 531. $I4/mmm$
532. $I4/mmm1'$
533. $I4/m'mm$
534. $I4'/mm'm$
535. $I4'/mmm'$
536. $I4'/m'm'm$
537. $I4/mm'm'$
538. $I4'/m'mm'$
539. $I4/m'm'm'$
540. I_c4/mmm

140) 541. $I4/mcm$
542. $I4/mcm1'$
543. $I4/m'cm$
544. $I4'/mc'm$
545. $I4'/mcm'$
546. $I4'/m'c'm$
547. $I4/mc'm'$
548. $I4'/m'cm'$
549. $I4/m'c'm'$
550. I_c4/mcm

141) 551. $I4_1/amd$
552. $I4_1/amd1'$
553. $I4_1/a'md$
554. $I4'_1/am'd$
555. $I4'_1/amd'$
556. $I4'_1/a'm'd$
557. $I4_1/am'd'$
558. $I4'_1/a'md'$
559. $I4_1/a'm'd'$
560. I_c4_1/amd

142) 561. $I4_1/acd$
562. $I4_1/acd1'$
563. $I4_1/a'cd$
564. $I4'_1/ac'd$
565. $I4'_1/acd'$
566. $I4'_1/a'c'd$
567. $I4_1/ac'd'$
568. $I4'_1/a'cd'$
569. $I4_1/a'c'd'$
570. I_c4_1/acd

Hexagonal system

A. Rhombohedral sub-system

C_3

143) 1. $P3$
2. $P31'$
3. P_c3

144) 4. $P3_1$
5. $P3_11'$
6. P_c3_1

145) 7. $P3_2$
8. $P3_21'$
9. P_c3_2

146) 10. $R3$
11. $R31'$
12. R_I3

C_{3i}

147) 13. $P\bar{3}$
14. $P\bar{3}1'$
15. $P\bar{3}'$
16. $P_c\bar{3}$

148) 17. $R\bar{3}$
18. $R\bar{3}1'$
19. $R\bar{3}'$
20. $R_I\bar{3}$

D_3

149) 21. $P312$
22. $P31'2$
23. $P312'$
24. P_c312

150) 25. $P321$
26. $P321'$
27. $P32'1$
28. P_c321

151) 29. $P3_112$
30. $P3_11'2$
31. $P3_112'$
32. P_c3_112

152) 33. $P3_121$
34. $P3_121'$
35. $P3_12'1$
36. P_c3_121

153) 37. $P3_212$
38. $P3_21'2$
39. $P3_212'$
40. P_c3_212

154) 41. $P3_221$
42. $P3_221'$
43. $P3_22'1$
44. P_c3_221

155) 45. $R32$
46. $R321'$
47. $R32'$
48. R_I32

C_{3v}

156) 49. $P3m1$
50. $P3m1'$
51. $P3m'1$
52. P_c3m1

157) 53. $P31m$
54. $P31'm$
55. $P31m'$
56. P_c31m

158) 57. $P3c1$
58. $P3c1'$
59. $P3c'1$
60. P_c3c1

159) 61. $P31c$
62. $P31'c$
63. $P31c'$
64. P_c31c

160) 65. $R3m$
66. $R3m1'$
67. $R3m'$
68. R_I3m

161) 69. $R3c$
70. $R3c1'$
71. $R3c'$
72. R_I3c

D_{3d}

162) 73. $P\bar{3}1m$
74. $P\bar{3}1'm$
75. $P\bar{3}'1m$
76. $P\bar{3}'1m'$
77. $P\bar{3}1m'$
78. $P_c\bar{3}1m$

163) 79. $P\bar{3}1c$
80. $P\bar{3}1'c$
81. $P\bar{3}'1c$
82. $P\bar{3}'1c'$
83. $P\bar{3}1c'$
84. $P_c\bar{3}1c$

164) 85. $P\bar{3}m1$
86. $P\bar{3}m1'$
87. $P\bar{3}'m1$
88. $P\bar{3}'m'1$
89. $P\bar{3}m'1$
90. $P_c\bar{3}m1$

165) 91. $P\bar{3}c1$
92. $P\bar{3}c1'$
93. $P\bar{3}'c1$
94. $P\bar{3}'c'1$
95. $P\bar{3}c'1$
96. $P_c\bar{3}c1$

166) 97. $R\bar{3}m$
98. $R\bar{3}m1'$
99. $R\bar{3}'m$
100. $R\bar{3}'m'$
101. $R\bar{3}m'$
102. $R_I\bar{3}m$

167) 103. $R\bar{3}c$
104. $R\bar{3}c1'$
105. $R\bar{3}'c$
106. $R\bar{3}'c'$
107. $R\bar{3}c'$
108. $R_I\bar{3}c$

B. Hexagonal sub-system

C_6

168) 109. $P6$
110. $P61'$
111. $P6'$
112. P_c6

169) 113. $P6_1$
114. $P6_11'$
115. $P6_1'$
116. P_c6_1

170) 117. $P6_5$
118. $P6_51'$
119. $P6_5'$
120. P_c6_5

171) 121. $P6_2$
122. $P6_21'$
123. $P6_2'$
124. P_c6_2

172) 125. $P6_4$
126. $P6_41'$
127. $P6_4'$
128. P_c6_4

173) 129. $P6_3$
130. $P6_31'$
131. $P6_3'$
132. P_c6_3

C_{3h}

174) 133. $P\bar{6}$
134. $P\bar{6}1'$
135. $P\bar{6}'$
136. $P_c\bar{6}$

C_{6h}

175) 137. $P6/m$
138. $P6/m1'$
139. $P6'/m$
140. $P6/m'$
141. $P6'/m'$
142. P_c6/m

176) 143. $P6_3/m$
144. $P6_3/m1'$
145. $P6_3'/m$
146. $P6_3/m'$
147. $P6_3'/m'$
148. P_c6_3/m

D_6

177) 149. $P622$
150. $P6221'$
151. $P6'2'2$
152. $P6'22'$
153. $P62'2'$
154. P_c622

178) 155. $P6_122$
156. $P6_1221'$
157. $P6_1'2'2$
158. $P6_1'22'$
159. $P6_12'2'$
160. P_c6_122

179) 161. $P6_522$
162. $P6_5221'$
163. $P6_5'2'2$
164. $P6_5'22'$
165. $P6_52'2'$
166. P_c6_522

180) 167. $P6_222$
168. $P6_2221'$
169. $P6_2'2'2$
170. $P6_2'22'$
171. $P6_22'2'$
172. P_c6_222

181) 173. $P6_422$
174. $P6_4221'$
175. $P6_4'2'2$
176. $P6_4'22'$
177. $P6_42'2'$
178. P_c6_422

182) 179. $P6_322$
180. $P6_3221'$
181. $P6_3'2'2$
182. $P6_3'22'$
183. $P6_32'2'$
184. P_c6_322

C_{6v}

183) 185. $P6mm$
186. $P6mm1'$
187. $P6'm'm$
188. $P6'mm'$
189. $P6m'm'$
190. P_c6mm

184) 191. $P6cc$
192. $P6cc1'$
193. $P6'c'c$
194. $P6'cc'$
195. $P6c'c'$
196. P_c6cc

185) 197. $P6_3cm$
198. $P6_3cm1'$
199. $P6_3'c'm$
200. $P6_3'cm'$
201. $P6_3c'm'$
202. P_c6_3cm

186) 203. $P6_3mc$
204. $P6_3mc1'$
205. $P6_3'm'c$
206. $P6_3'mc'$
207. $P6_3m'c'$
208. P_c6_3mc

D_{3h}

187) 209. $P\bar{6}m2$
210. $P\bar{6}m21'$
211. $P\bar{6}'m'2$
212. $P\bar{6}'m2'$
213. $P\bar{6}m'2'$
214. $P_c\bar{6}m2$

188) 215. $\bar{P}6c2$
216. $P\bar{6}c21'$
217. $P\bar{6}'c'2$
218. $P\bar{6}'c2'$
219. $P\bar{6}c'2'$
220. $P_c\bar{6}c2$

189) 221. $P\bar{6}2m$
222. $P\bar{6}2m1'$
223. $P\bar{6}'2'm$
224. $P\bar{6}'2m'$
225. $P\bar{6}2'm'$
226. $P_c\bar{6}2m$

190) 227. $P\bar{6}2c$
228. $P\bar{6}2c1'$
229. $P\bar{6}'2'c$
230. $P\bar{6}'2c'$
231. $P\bar{6}2'c'$
232. $P_c\bar{6}2c$

D_{6h}

191) 233. $P6/mmm$
234. $P/6mmm1'$
235. $P6/m'mm$
236. $P6'/mm'm$
237. $P6'/mmm'$
238. $P6'/m'm'm$
239. $P6'/m'mm'$
240. $P6/mm'm'$
241. $P6/m'm'm'$
242. P_c6/mmm

192) 243. $P/6mcc$
244. $P6/mcc1'$
245. $P6/m'cc$
246. $P6'/mc'c$
247. $P6'/mcc'$
248. $P6'/m'c'c$
249. $P6'/m'cc'$
250. $P6/mc'c'$
251. $P6/m'c'c'$
252. P_c6/mcc

193) 253. $P6_3/mcm$
254. $P6_3/mcm1'$
255. $P6_3/m'cm$
256. $P6_3'/mc'm$
257. $P6_3'/mcm'$
258. $P6_3'/m'c'm$
259. $P6_3'/m'cm'$
260. $P6_3/mc'm'$
261. $P6_3/m'c'm'$
262. P_c6_3/mcm

194) 263. $P6_3mmc$
264. $P6_3/mmc1'$
265. $P6_3/m'mc$
266. $P6_3'/mm'c$
267. $P6_3'/mmc'$
268. $P6_3'/m'm'c$

269. $P6_3'/m'mc'$
270. $P6_3/mm'c'$
271. $P6_3/m'm'c'$
272. P_c6_3/mmc

Cubic system

T

195) 1. $P23$
2. $P23'$
3. P_I23

196) 4. $F23$
5. $F23'$
6. F_s23

197) 7. $I23$
8. $I23'$

198) 9. $P2_13$
10. $P2_13'$
11. P_I2_13

199) 12. $I2_13$
13. $I2_13'$

T_h

200) 14. $Pm3$
15. $Pm3'$
16. $Pm'3$
17. P_Im3

201) 18. $Pn3$
19. $Pn3'$
20. $Pn'3$
21. P_In3

202) 22. $Fm3$
23. $Fm3'$
24. $Fm'3$
25. F_sm3

203) 26. $Fd3$
27. $Fd3'$
28. $Fd'3$
29. F_sd3

204) 30. $Im3$
31. $Im3'$
32. $Im'3$

205) 33. $Pa3$
34. $Pa3'$
35. $Pa'3$
36. P_Ia3

206) 37. $Ia3$
38. $Ia3'$
39. $Ia'3$

O

207) 40. $P432$
41. $P43'2$
42. $P4'32'$
43. P_I432

208) 44. $P4_232$
45. $P4_23'2$
46. $P4_2'32'$
47. P_I4_232

209) 48. $F432$
49. $F43'2$
50. $F4'32'$
51. F_s432

210) 52. $F4_132$
53. $F4_13'2$
54. $F4_1'32'$
55. F_s4_132

211) 56. $I432$
57. $I43'2$
58. $I4'32'$

212) 59. $P4_332$
60. $P4_33'2$
61. $P4_3'32'$
62. P_I4_332

213) 63. $P4_132$
64. $P4_13'2$
65. $P4_1'32'$
66. P_I4_132

214) 67. $I4_132$
68. $I4_13'2$
69. $I4_1'32'$

T_d

215) 70. $P\bar{4}3m$
71. $P\bar{4}3'm$
72. $P\bar{4}'3m'$
73. $P_I\bar{4}3m$

216) 74. $F\bar{4}3m$
75. $F\bar{4}3'm$
76. $F\bar{4}'3m'$
77. $F_s\bar{4}3m$

217) 78. $I\bar{4}3m$
79 $I\bar{4}3'm$
80. $I\bar{4}'3m'$

218) 81. $P\bar{4}3n$
82. $P\bar{4}3'n$
83. $P\bar{4}'3n'$
84. $P_I\bar{4}3n$

219) 85. $F\bar{4}3c$
86. $F\bar{4}3'c$
87. $F\bar{4}'3c'$
88. $F_s\bar{4}3c$

220) 89. $I\bar{4}3d$
90. $I\bar{4}'3'd$
91. $I\bar{4}3d$

O_h

221) 92. $Pm3m$
93. $Pm3'm$
94. $Pm'3m$
95. $Pm3m'$
96. $Pm'3m'$
97. P_Im3m

222) 98. $Pn3n$
99. $Pn3'n$
100. $Pn'3n$
101. $Pn3n'$
102. $Pn'3n'$
103. P_In3n

223) 104. $Pm3n$
105. $Pm3'n$
106. $Pm'3n$
107. $Pm3n'$
108. $Pm'3n'$
109. P_Im3n

224) 110. $Pn3m$
111. $Pn3'm$
112. $Pn'3m$
113 $Pn3m'$
114. $Pn'3m'$
115. P_In3m

225) 116. $Fm3m$
117. $Fm3'm$
118. $Fm'3m$
119. $Fm3m'$
120. $Fm'3m'$
121. F_sm3m

226) 122. $Fm3c$
123. $Fm3'c$
124. $Fm'3c$
125. $Fm3c'$
126. $Fm'3c'$
127. F_sm3c

227) 128. $Fd3m$
129. $Fd3'm$
130. $Fd'3m$
131. $Fd3m'$
132. $Fd'3m'$
133. F_sd3m

228) 134. $Fd3c$
135. $Fd3'c$
136. $Fd'3c$
137. $Fd3c'$
138. $Fd'3c'$
139. F_sd3c

229) 140. $Im3m$
141. $Im3'm$
142. $Im'3m$
143. $Im3m'$
144. $Im'3m'$

230) 145. $Ia3d$
146. $Ia3'd$
147. $Ia'3d$
148. $Ia3d'$
149. $Ia'3d'$

A. M. Zamorzaev [2-4] was the first to derive the Shubnikov groups. In 1954 the authors of this paper [5] derived these groups by a method which was used as the basis for a short course on Fedorov groups given by one of the authors [6]. In these papers it is also possible to find the proof for the more important theorems relating to this subject.

LITERATURE CITED

[1] A. V. Shubnikov, Symmetry and Antisymmetry of Finite Bodies [in Russian] (1951).

[2] A. M. Zamorzaev, Dissertation: Generalization of Fedorov Groups [in Russian] (Leningrad, 1953).

[3] A. M. Zamorzaev, "Generalization of Fedorov groups," Kristallografiia, 2, 1, 15-20 (1957) [Soviet Physics—Crystallography p. 10].

[4] A. M. Zamorzaev and E. I. Sokolov, "Symmetry and Various Kinds of Antisymmetry of Finite Bodies," Kristallograffia, 2, 1, 9-14 (1957). [Soviet Physics—Crystallography, p. 6].

[5] N. V. Belov, N. N. Neronova and T. S. Smirnova, "1651 Shubnikov Groups," Trudy Inst. Krist. 11, 33-67 (1955).

[6] N. V. Belov, "Class method for deriving space point groups," Trudy Inst. Krist. 6, 25-68 (1951).

Institute of Crystallography
Academy of Sciences USSR

Received March 9, 1957

DEVELOPMENT OF THE STUDY OF CRYSTAL FORMS

I.I. Shafranovskii

Different varieties of forms: crystallographic, structural, edge forms, vertex forms and their occurrence in real crystals.

Nonideal forms of real crystals serving as indicators of the symmetry of a crystal forming media.

The brilliant success of the study of fine sculpture on the faces of crystals and of the internal structure of crystals require broadening and refinement of the concepts of crystal forms. This is necessary in order to interpret the phenomena of crystal morphology in the light of discoveries of modem structural crystallography.

A number of works by Soviet authors devoted to this subject appeared in crystallographic literature during the past two decades.

The present paper is a review of these studies.

Impetus to these investigations was given by A. V. Shubnikov, who showed all possible striations on the faces of five cubes of different symmetry and stated succinctly that "crystallography distinguishes five cubes, while geometry deals with only one." [1, 2].

Developing this idea, G. B. Bokii derived 146 crystallographic varieties of the 47 simple forms familiar from courses in elementary crystallography. It should be recalled that two simple forms are distinct if they differ in the number of faces, in their shape, or in their relative position [3]. This purely geometric approach does not allow distinction between simple forms of real crystals having the same name but differing in symmetry. According to Bokii, two like simple forms are crystallographically (physically) distinct if they have different symmetry elements, or if the symmetry elements have different positions with respect to the faces [4]. In describing surfaces of real crystals, their plane symmetry, i.e., the symmetry elements normal to the surfaces, are of especial importance. It is the plane symmetry that dominates the geometry of striations, vicinal faces, etch figures, etc. Figure 1 shows different possible etch figures (or vicinal faces) for three dihedral forms with the following symmetry: $\underline{2}$ ("sphenoid"), $\underline{m}$ ("dome"), $\underline{mm}$ ("dome-sphenoid").

Consideration of crystallographic varieties makes it possible to foresee the geometric regularity which determines the sculpture of crystal faces. In describing real crystals, it is necessary to assign their forms to this or that crystallographic variety. Every deviation of the surface sculpture from plane symmetry must be noted carefully as a sign of imperfect structure of the crystal or as a peculiarity due to external causes.

In order to bring together the data of modern crystal morphology with the concepts of structural crystallography, the results of derivation of 1403 structural-crystallographic varieties of the simple crystal forms were published in 1948 [5]. Two crystallographic varieties of a simple form are structurally distinct if they have space groups differing in symmetry, or if the symmetry elements differ in their position with respect to the faces. For example, there are 36 structural-crystallographic varieties of the cube. From the point of view of crystal morphology, it is important to take into account the plane symmetry of these varieties, considering their faces as infinitely extended one-faced planes. For this purpose the elements of symmetry of the appropriate space group which are normal to the face and common to all mutually parallel plane lattices equivalent to it must be taken into consideration. There is no doubt that it is this symmetry that should give the most exact idea of the actual character of the face. Its effect on the fine sculpture of the face is the next problem. Figure 2 represents eight plane groups of infinite symmetry which occur on the faces of the cube. It can be seen that sometimes the plane symmetry of the 100 lattices is characterized by the absence of symmetry elements while the finite symmetry of their edges is 2 and 4. It would be extremely interesting to grasp the peculiarities of detail of the fine relief of such faces with the aid of the most precise methods of investigation.

It has been proved that variations in structure are reflected in relative development of different faces in real crystals. According to the Donnay-Harker principle, the morphological importance of faces, their size and frequency of occurrence depend on the elements of symmetry which are normal to them [6]. The faces perpendicular to simple axes and planes of symmetry are more important morphologically than those perpendicular to screw axes of the same order or to glide planes. This explains the absence of the pinacoid on natural quartz crystals, its rare occurrence on zircon, etc. And from this follows the significance of the structural varieties of simple forms which permit, even if only approximately, relating of the development of faces to the structural symmetry elements. The concept of these varieties points up the relationship between morphological observations and the findings of structural crystallography.

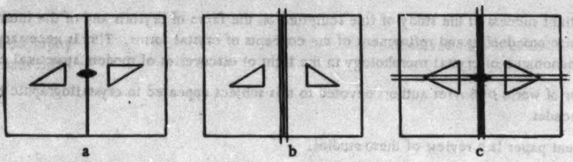

Fig. 1. Types of etch figures or vicinal faces on the faces of dihedral forms of three types.

Lately, in crystallographic literature devoted to the study of this relationship, the role of intersection edges has been much emphasized [7, 8]. The significance of the edges has often been noted also in studies of the growth of crystals [9, 10]. In connection with this, it seems useful to give the derivation of the simple edge forms by analogy with the derivation of the common simple faces. The simple edge form corresponds to the totality of equal edges of a crystal derived by the use of the symmetry elements [11]. For the lower crystal systems there are 18 such forms; for the tetragonal system, 54; for the trigonal and hexagonal, 90. Figure 3 represents edge forms for the tetragonal-pyramidal class of symmetry.

Edge forms largely determine the behavior of a crystal during growth and solution. G. G. Lemmlein described a secondary overgrowth of quartz on acicular quartz crystals which formed on the three negative prismatic edges [9]. The intermediate positive edges played a passive role in this. It is well known that sharp differences in the ease of solution are observed on the alternate prismatic edges of quartz crystals. This indicates that the six prismatic edges in quartz are formed by a combination of "two trigonal edge prisms." The significance of edge forms follows also fromthe fact that oscillatory striations on crystal faces are nothing but edge forms. Therefore, derivation of edge forms permits at the same time the derivation of possible types of striations. The latter are interesting because, on the one hand, they reveal the most important directions of crystal structure and, on the other, being very sensitive to external conditions, they serve as indicators of the physicochemical environment of crystal growth [12].

Edge forms can also be used successfully in classification of forms of skeleton crystals [13]. Figure 4 shows a skeleton crystal of dolomite encrusted on the rhombohedral edges of rhodocrosite, forming a combination of two simple edge forms [14].

Edge forms include plane and three-dimensional systems of rays, closed frames and three-dimensional frameworks. The latter are combinations of the above-mentioned two-dimensional edge forms. For classification of plane ray systems and frames so often found in skeleton crystals, it is appropriate to use the concept of edge forms. Their derivation on the basis of ten crystallographic types of plane symmetry is very simple. The plane frames are simple forms of the following shapes: single edge, two parallel edges, two intersecting edges, trigon, tetragon, hexagon, rhombus, double trigon, double tetragon, double hexagon. Simple ray systems are obtained by substituting for these frames, perpendiculars dropped from a central point on their sides.

The existence of structures in the form of interrupted skeletons and also of certain epitaxitic overgrowths makes it necessary to consider vertex forms. (A simple vertex form is a combination of vertices derived from one another by a symmetry operation.) Figure 5 shows an encrustation of dolomite on the vertices of a rhombohedron of rhodocrosite, corresponding to a combination of two vertex forms [14]. It is easy to see that the number of three-dimensional forms is 47 (recall point projections of faces on a sphere), while the number of plane vertex forms is 10. Geometrically plane vertex forms correspond to a point pattern [15, 16].

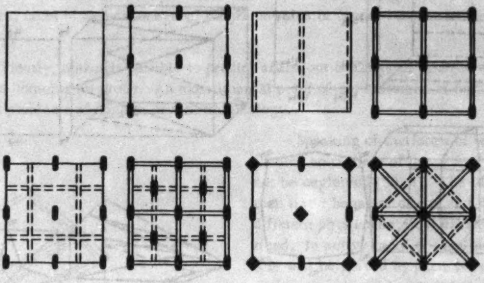

Fig. 2. Eight groups of infinite plane symmetry found on the faces of the cube.

Up to now we have been considering crystal forms from the point of view of classical study of symmetry.

Lately, A. V. Shubnikov has been developing the concepts of antisymmetry, which considerably broadens the concept of symmetry. "Just as a right-handed figure may be equal to a left-handed figure," writes A. V. Shubnikov, "so according to our hypothesis a positive figure may be equal to a negative figure. This type of equality may be called opposite equality or antiequality" [17]. As examples of antiequal figures the following may be given: a medal and its mold, a photographic positive and its negative, forms produced by growth and solution of crystals, positron and electron, etc. By analogy with symmetrical figures there appear antisymmetrical figures with appropriate elements of symmetry, simple and complex antiaxes of symmetry. In the monograph already cited, "Symmetry and antisymmetry of finite figures," A. V. Shubnikov gives a complete derivation of antisymmetry groups of finite figures.

Investigation of induced surfaces on artifical intergrowths of potash alum crystals with definite orientation show convincingly the importance of considering antisymmetry in describing these surfaces [18]. It is easily understood that the induced surfaces of two crystals give excellent examples of antiequality (of the type of the medal and its mold). Clearly this is true not only of artificial crystals but also of natural ones and in particular of twins and crystals in parallel intergrowth. Induced surfaces on crystals are much more common than freely formed faces. We need only to recall the forms of crystal grains in rocks, salt deposits, metals, etc. All such grains, as a rule, have induced surfaces. It is evident, then, that in descriptions of crystal grains the new concepts of antisymmetry must be considered.

In the above presentation of the concepts of crystallographic and structural varieties of simple forms, the latter have been subdivided into subvarieties. It is possible, however, to do the reverse and combine different but structurally related geometric species of simple forms into one. This was intuitively foreshadowed by the old crystallographers. Not for nothing did the old crystallographic form nomenclature include such names as "monoclinic and triclinic (di) pyramids (combination of rhombic prisms, dihedrons, pinacoids and pedions), "triclinic prisms" (combinations of pinacoids and pedions), etc. Not for nothing were simple forms from different systems given the same name (the tetragonal dipyramid was called the "quadratic octahedron"; the rhombic dipyramid, the "rhombic octahedron," etc.).

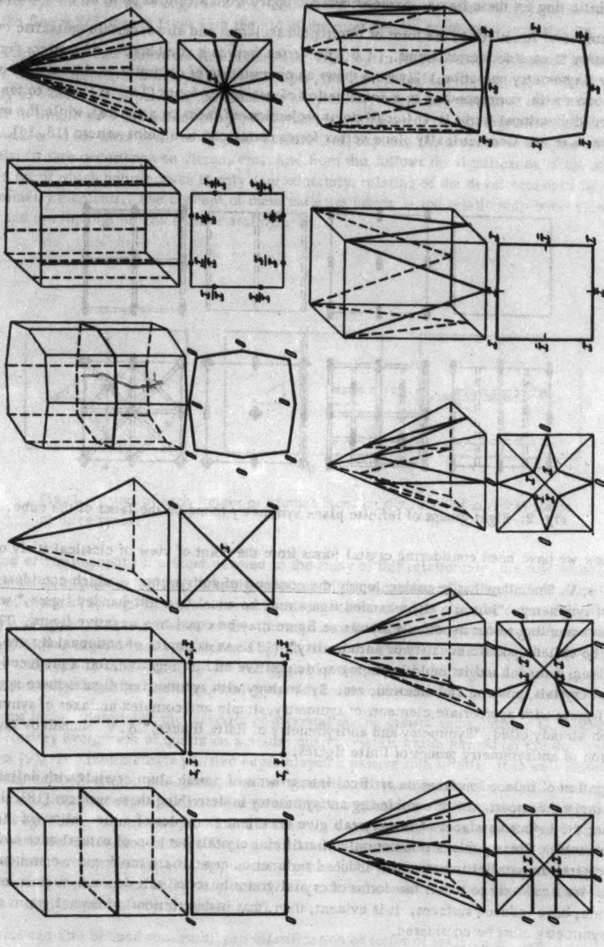

Fig. 3. Edge forms for symmetry class 4.

As an illustration, the pseudorhombohedral crystal of monoclinic azurite may be cited, in which one of the pinacoids and a rhombic prism form, as it were, a complete "rhombohedron" (Fig. 6).

A similar approach to forms was widely used by E. S. Fedorov in disclosing analogies between ideal cubic and hexagonal crystals and the pseudocubic and pseudohexagonal crystals near to them in angles but belonging to other systems [19]. The development of the concepts of pseudosymmetric forms was given in a series of works by the late Professor of Crystallography of the Leningrad Mining Institute, V. I. Mikheev (d. 1956) [20, 21].

Besides the usual symmetry elements, V. I. Mikheev introduced also planes, axes and inversion axes of homology. A homologous plane is a plane of oblique reflection. If in reflection in a plane of symmetry the projecting rays are directed normal to it then the projecting rays of a homologous plane are at a certain angle to it. An axis of homology is a line about which an oblique circular or elliptical turn is made. Any point of a system then moves along a circle or an ellipse in a plane which in general makes an angle with the axis.

It is clear that symmetry elements are special cases of elements of homology and that "homology is a more general property of figures as compared with symmetry." V. I. Mikheev gave a complete derivation of 218 types of homology (combinations of homologous elements analogous with symmetry classes). With their aid it is possible to derive homologous simple forms whose faces may belong to different crystallographic simple forms as, for example, faces of pseudohexagonal prisms on mica or faces of a pseudorhombohedron on azurite (Fig. 6).

Homology, evidently, makes it possible to predict analogous behavior of faces of different simple forms belonging to a single homologous group. An experimental proof of the existence of homology in real crystals is one of the current problems of modern crystal morphology.

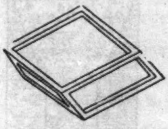

Fig. 4. A skeleton crystal of dolomite on the edges of a rhombohedron of rhodocrosite (Frondel, 1934).

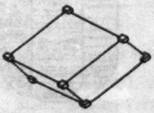

Fig. 5. A torn skeleton of dolomite encrusted on the vertices of a rhombohedron of rhodocrosite (Frondel, 1934).

Speaking of the forms of real crystals, the influence upon them of the crystal-forming medium cannot be neglected [22, 7]. The idea of dynamic rather than static behavior of one and the same structure in different physicochemical environments must be emphasized. In active (acid or alkaline) media the primary role will be played by particles of one kind, either cations or anions. In neutral media both will be equally important. This is the reason for formation of either cubic or octahedral crystals of rock salt [23]. In aqueous solutions ions of sodium and chlorine form a simple cubic lattice with the densest packing parallel to $\{100\}$; in an active medium ions of one kind act like a face-centered lattice advancing the faces $\{111\}$ corresponding to the densest planes of this type of lattice. In addition to halite, the crystal habits of sphalerite, fluorite and corundum have been examined from this point of view [24, 25]. In this connection the conclusion of N. V. Belov concerning the leading role of cations in silicate structures is especially significant [26]. The principle of intimate connection between the structure and the medium from which it formed must be considered also in determining the bonds between particles in a structure, according to the new views of Kleber, Hartman and Perdok [7, 8].

The question of relation of crystal form to structure and to the crystal-forming medium can be discussed only by always considering the two together. In discussing the dependence of the form of a real crystal on structure, its dependence on the medium is also clarified. There are as many crystal habits for a given substance as there are different modes of formation which can influence the structure of the crystal.

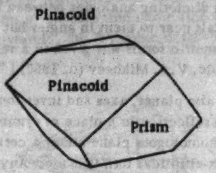

Fig. 6. A pseudorhombohedral crystal of monoclinic azurite (after V. V. Dolivo-Dobrovol'skii).

In conclusion, let us look at malformed real (nonideal) crystals which reflect the symmetry of the medium of formation. On quartz crystals, as an example, G. G. Lemmlein showed that they obey the same law as flowers: when they point up or down during growth, they have symmetry $\underline{n.m}$; when placed sidewise, they have symmetry $\underline{m}$ [27]. As has been noted by Curie the point symmetry of the gravitational field $\infty\cdot\underline{m}$ is impressed on all nature and on natural crystals also, whose outward symmetry preserves only those elements which coincide with the symmetry of the nourishing medium [2, 28, 29].

In nature the symmetry of the most common crystal forming media can be characterized by a few types (or groups) of symmetry [30].

The most common point groups are the groups $\infty\cdot\underline{m}$ (ascending or descending feeding solutions directed normal to the floor on which crystals are growing), and $\underline{m}$ (ascending or descending solutions directed parallel to the vertical wall on which crystals are growing). In the first case the highest external symmetry of a crystal is $\underline{n.m}$ (Fig. 7); in the second, $\underline{m}$ (Fig. 8). Clearly in the first case crystal forms will be characterized by he presence of "pseudopyramids" and in the second by "pseudodihedrons" and "pseudomonohedrons" (Figs. 7 and 8).

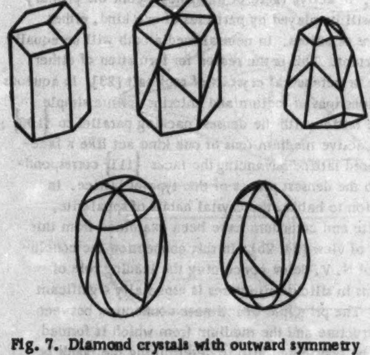

Fig. 7. Diamond crystals with outward symmetry $\underline{3\cdot m}$ (after J. L. Bournon).

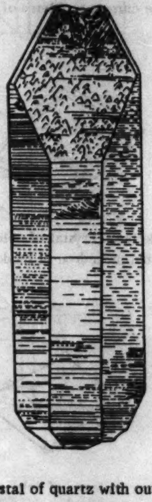

Fig. 8. A crystal of quartz with outward symmetry $\underline{m}$ (after A. E. Kariakin).

These false "simple forms" most frequently found on natural crystals serve as reliable indicators of the symmetry of the medium which had nourished them.

LITERATURE CITED

[1] A. V. Shubnikov, Crystallography (lectures) [in Russian], (1923-1925).

[2] A. V. Shubnikov, How Crystals Grow [in Russian] (1935).

[3] A. Boldyrew, "Are there 47 or 48 simple forms possible on crystals ?," Am. Mineralogist 21 (1936).

[4] G. B. Bokii, "The number of distinct simple crystal forms," Trudy Lab. Krist. Akad. Nauk SSSR 2 (1940).

[5] I. I. Shafranovskii, "Crystals forms," Trudy Inst. Akad. Nauk. SSSR 4 (1948).

[6] J. D. H. Donnay and D. Harker, "A new law of crystalmorphology extending the law of Bravais. Am. Mineralogist," 22 (1937).

[7] W. Kleber, "Kristallwachstum, Morphologie und Struktur," Acta Cryst. 8 (1955).

[8] P. Hartman and W. Perdok, "On the relation between crystal structure and crystal morphology," Acta Cryst. 8 (1955).

[9] G. G. Lemmlein, Observations on Twisted Quartz Crystals [in Russian], (1937).

[10] V. V. Vitovskii (Author's abstract of dissertation) [in Russian] (1949).

[11] V. I. Mikheev and I. I. Shafranovskii, "Edge forms of crystals, I," Min. sb. L'vov, geol. ob-va. 9 (1955).

[12] V. I. Mikheev and I. I. Shafranovskii, "Striations and the edge forms of crystals, Kristallografiia 2, 1, 166-171 (1957) [Soviet Physics - Crystallography, p. 158].

[13] I. I. Shafranovskii and V. A. Mokievskii, "Conditions of growth, geometry and symmetry of skeletal crystals," Zapiski Vsesoyuzn. Mineral Obshchestva 85, 2 (1956).

[14] C. Frondel, "Mineral incrustation upon the edges and corners of crystals," Am. Mus. 759 (1934).

[15] P. Niggli, Lehrbuch der Mineralogie (Berlin, 1926).

[16] P. Niggli, Grundlagen der Stereochemie (Basel, 1945).

[17] A. V. Shubnikov, Symmetry and Antisymmetry of Finite Figures [in Russian] (1951).

[18] V. A. Mokievskii and I. I. Shafranovskii, "Symmetry, antisymmetry and pseudosymmetry of induced surfaces, Kristallografiia 2, 1, 23-28 (1957) [Soviet Physics - Crystallography, p. 19].

[19] E. Fedorow, Das Kristallreich (1920).

[20] V. I. Mikheev, "The number of types of homology in crystals," Doklady Akad. Nauk SSSR, 71, 4 (1950).

[21] V. I. Mikheev, "New ideas in the study of symmetry (elements of homology of self-homologous systems)," Collection, Crystallography" [in Russian], 1 (1951).

[22] A. V. and O. M. Shubnikov, The Statistical Method Applied to the Study of the External Form of Crystals [in Russian] (1926).

[23] A. F. Wells, "Crystal habit and internal structure," Phil. Mag. 37 (1946).

[24] V. I. Mikheev and I. I. Shafranovskii, "The correspondence between theoretical and genetic types of sphalerite crystals," Zapiski Vsesoyuzn. Mineral Obshchestva 77, 4 (1948).

[25] N. V. Belov, "Crystal chemistry of mineralizers," Doklady Akad. Nauk SSSR 71, 1 (1950).

[26] N. V. Belov, "Essays in structural mineralogy," [in Russian] Min. sb. L'vov. geol. ob-va (1955).

[27] G. G. Lemmlein, "Distortion of form in quartz crystals due to their position during growth," Doklady Akad. Nauk SSSR, 33, 6 (1945).

[28] A. V. Shubnikov, "P. Curie's work in the field of symmetry," Uspekhi Fiz. Nauk 59, 4 (1956).

[29] G. G. Lemmlein, Sectorial Structure of Crystals [in Russian] (1948).

[30] I. I. Shafranovskii, "External symmetry of real crystals and the symmetry of the nourishing medium," Zap. Vsesoyuzn. Mineral Obshchestva 83, 3 (1954).

Leningrad School of Mines

Received February 22, 1957

SYMMETRY OF HOMOGENEOUS, CONTINUOUS ISOTROPIC MEDIA IN TENSOR, VECTOR AND SCALAR FIELDS

I. S. Zheludev

Seventeen point groups of symmetry of homogeneous, continuous isotropic media are obtained for the case when they are in fields described by polar and axial tensors of the second order.

When physical phenomena in crystals are described, it is not necessary to take into consideration their crystal lattice structure. In such cases a crystal may be studied as a homogeneous, continuous medium. Crystal physics has successfully used the concept of a crystal as a homogeneous continuous medium in describing thermal, elastic, piezoelectric and other properties.

There exist in nature not only crystalline media but also a large class of amorphous media which do not show a lattice structure. Wax, paraffin, various resins, glass etc., for example, belong to these media. Although these media show many variations, we will study only those, which, in the absence of external action, are macroscopically isotropic.

By point groups of symmetry of homogeneous, continuous isotropic media in the absence of external action we mean symmetry groups of these media at a point. A definition of this concept of point symmetry groups for such media in tensor, vector, and scalar fields (whose derivation is taken up in this paper) is given below.

Note that by homogeneous, continuous media we may mean solid, as well as liquid and gaseous, media.

1. Symmetry of Homogeneous, Continuous Isotropic Media in the Absence of External Action

As we have already indicated, we shall study only such media which are homogeneous, continuous and isotropic in the absence of external action. Isotropy of homogeneous continuous media makes it possible to classify them in two point groups of symmetry, the $\infty/\infty \cdot m$ and the ∞/∞ groups (a sphere with symmetry planes and a sphere without symmetry planes; for example, a sphere all of whose diameters are twisted at an equal angle in one direction).

A real medium will show $\infty/\infty \cdot m$ symmetry in the case where the particles of which it is composed have either symmetry elements of the first kind (simple axes) and of the second kind (reflection axes) or only symmetry elements of the first kind when the number of left and right hand particles is equal and their distribution in space is completely equivalent. A medium will belong to the ∞/∞ symmetry group in the case when only simple axes will constitute the symmetry elements of the medium's particles, and the medium will be made up of only right handed or only left handed particles. Melted paraffin is an example of a medium having $\infty/\infty \cdot m$ symmetry, and a solution of sugar in water is an example of a medium having ∞/∞ symmetry.

2. Symmetry of the External Action (symmetry of tensor, vector and scalar fields)

External action may, in the general case, change the symmetry of the media studied and make them anisotropic. In order to determine the symmetry of a medium in the presence of external action we must know just what the action is and what its symmetry is. Generally speaking the action may be of quite different kinds: mechanical, electrical, magnetic and so forth. Simultaneously with one kind of action (for example, mechanical) other kinds of actions may also take place (for example, electrical). The symmetry of these actions and the mutual distribution of their symmetry elements may also be quite different. Our problem, however, is not to describe the variety of actions, but to find a method for determining only their symmetry.

The method we suggest consists in examining the action as a sum of a series of elementary actions of which it is composed; the symmetry of the external action as a whole is determined by the superposition of the symmetry elements of these elementary actions. When deriving point groups of symmetry for homogeneous continuous media we will consider only the case in which the action on the medium, as a whole, may be reduced either to scalar, vector or tensor (described by tensors of the second order) actions, or their sum. This means, for example, that in the case of purely mechanical action we will only take cases in which the entire sum of the forces acting on the medium may be reduced either to a polar vector-force (volume displacement) or to an axial vector couple (volume rotation) or to a polar symmetric tensor-sum of two forces directed toward each other (expansion, compression) or to an axial symmetric tensor-aggregate of two equal couples whose moments of rotation are directed toward each other (twisting of the medium). In cases when the expansion-compression is hydrostatic, the action will be scalar, and in those cases when the twisting is hydrostatic the action will be pseudoscalar.

Study of external action as a composite of the six indicated elementary actions was made assuming that each one of them qualitatively characterizes a different action on the medium (for example rotation, expansion, twisting, etc.) although any one of these six elementary actions may also be represented, in its turn, as a combination of polar vectors (forces).

The symmetry of the elementary actions will be defined as the symmetry of corresponding scalars, vectors and tensors [1, 2]. The form of the tensors describing the elementary actions is shown in Table 1 and the tensors describing the elementary actions is shown in Table 1 and the action symmetry (tensor) is indicated by taking into account the fact that the scalars and vectors may be studied as individual cases of second order tensors and that the actions, described by polar and axial tensors, may differ as to symmetry (there are two symmetry groups of the symmetric polar tensor and three symmetry groups of the symmetric axial tensor). The total number of elementary action symmetry groups is therefore nine.

The tensor components $\{a_{ik}\}$ and $\{A_{ik}\}$ shown in Table 1 are transformed according to formulas

$$a'_{ik} = c_{ei} c_{mk} a_{em},$$

$$A'_{ik} = \pm c_{ei} c_{mk} A_{em},$$

where c_{ei}, c_{mk} are the cosines of the angles between corresponding old and new axes. In the formula for the transformation of the axial tensor component the plus sign is used in the case when both the coordinate systems are either right or left, and the minus sign is used in the case when the coordinate system changes sign when transformed.

Generally the action is a combination of the elementary actions given in Table 1. The total number of action symmetry groups will be determined by the number of scalar, vector and tensor combinations which are different as to symmetry and which describe the elementary actions. It is not necessary to find specifically the various possible symmetry combinations of the elementary actions, as the symmetry of these combinations and their number are determined by the symmetry and the number of symmetry groups of polar and axial tensors of the second order (taking into account the possibility of a combination of polar and axial tensors). An enumeration of these groups is given in our paper [2]. Let us only indicate that the combinations of polar tensor and axial tensor are described by a nonsymmetric polar tensor which may belong to the ∞ : m; 2 : m and $\bar{2}$ symmetry groups (the last two are new). In its turn the combinations of the axial tensor and the polar vector are described by five groups of nonsymmetric axial tensors: ∞; 2; 1; 2 · m; m (all five groups are new). Moreover the combination of an axial tensor having a $\bar{4}$ · m symmetry and an axial vector having a ∞ : m symmetry leads to one more new symmetry group, $\bar{4}$.

Thus when studying external action symmetry, limiting ourselves to the case where the actions are described by scalars, vectors, tensors of the second order and their combination, we obtain 17 different point groups of symmetry, corresponding to the 17 symmetry groups of polar and axial tensors and their combinations. These are the following groups: ∞/∞ · m; m · ∞ : m; m · 2 : m; ∞ : m; 2 : m; $\bar{2}$; ∞/∞; ∞ : 2; 2 : 2; $\bar{4}$ · m; ∞ · m; 2 · m; m; ∞; 2; 1; $\bar{4}$.

It is evident that these external action symmetry groups described in a general case by polar and axial tensors of the second order and their combinations are also symmetry groups of corresponding scalar, vector and tensor fields.

3. Symmetry of Homogeneous, Continuous Isotropic Media in Tensor, Vector and Scalar Fields

It is usually considered that the groups of crystal symmetry, introduced by P. Curie, and which contain, among other symmetry elements, axes of infinite order, also describe the symmetry of homogeneous, anisotropic media [3]. There are seven such groups: ∞/∞ · m (symmetry of a sphere with planes of symmetry), ∞/∞ (symmetry of a sphere all of whose diameters are twisted at an equal angle in the one direction) m · ∞ : m (symmetry of a stationary cylinder), ∞ : 2 (symmetry of a twisted cylinder)∞ : m (symmetry of a rotating cylinder ∞ · m (symmetry of a stationary cone) and ∞ (symmetry of a rotating cone). As far as we know there is no literature dealing with the question of whether or not this number of groups is sufficient to describe the symmetry of homogeneous, continuous media.

According to the Curie symmetry principle it is easy to find from the known symmetry of the external action and the known symmetry of the homogeneous, continuous isotropic media with no outside action all the possible point symmetry groups of such media in tensor, vector and scalar fields. The finding of these groups consists of finding the mutual elements of symmetry of the medium and the external action (superposition principle).

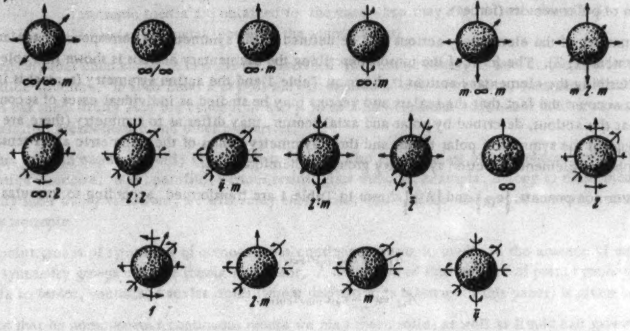

Fig. 1. Geometric forms of point groups of symmetry of homogeneous, continuous isotropic media in tensor, vector and scalar fields.

We have already defined the point symmetry of homogeneous, continuous isotropic media as symmetry at a point. In the case when external action occurs, the symmetry of the medium at a point will be determined by taking into account the symmetry of the tensor, vector and scalar fields which we have given above.

In the case where the medium, before the action, belonged to the ∞/∞ · m symmetry group, the external action can not show higher symmetry than the original symmetry of the medium. For example with hydrostatic compression (∞/∞ · m symmetry) the symmetry of the medium will be retained, but in all other cases of lower action symmetry the symmetry of the medium will coincide with the symmetry group of that action, i.e., will be entirely determined by it. In the case where the medium had an original ∞/∞ symmetry, the actions, which had ∞/∞ · m and ∞/∞ symmetry preserve the symmetry of the medium and the actions having the lowest symmetry will lower it. However, the medium will not necessarily take on the action symmetry, but the new symmetry group will have to be one of the above symmetry groups of the external action.

The above statement may be easily checked by means of the Curie symmetry principle. Thus, for example, the superposition of the ∞/∞ · m and ∞ · m symmetry groups will lead to the ∞ · m group; superpositions of groups ∞/∞ · m and 2 : m leads to the 2 : m group; superpositions of groups ∞/ ∞ and m · 2 : m to the 2 : 2 group; superpositions of groups ∞/ ∞ and ∞ : m to the ∞ group etc. Real physical processes may be compared to the examples studied. Thus a medium having ∞/ ∞ · m symmetry acquires, in an electric field, ∞ · m symmetry (electret production); a medium with the same kind of symmetry will acquire, in a magnetic field ∞ : m symmetry (magnetization of the medium and production of constant magnets); two dimensional compression (the symmetry of such compression is m · ∞ : m) of a medium having a symmetry of ∞/∞ lowers its symmetry to a ∞ : 2 symmetry etc.

TABLE 1

Form and Symmetry of Elementary Action Tensors

Series No.	Action type	Action described by	Tensor form of the elementary actions	Symmetry of the tensor and the action (Shubnikov notation	Orientation of the tensor symmetry axes
1	2	3	4	5	6
1	Scalar	A scalar	$\begin{matrix} a_{11} & 0 & 0 \\ 0 & a_{11} & 0 \\ 0 & 0 & a_{11} \end{matrix}$	$\infty/\infty \cdot m$	Axes are arbitrarily oriented
2	»	A pseudoscalar	$\begin{matrix} A_{11} & 0 & 0 \\ 0 & A_{11} & 0 \\ 0 & 0 & A_{11} \end{matrix}$	∞/∞	Axes are arbitrarily oriented
3	Vector	An axial vector	$\begin{matrix} 0 & -a_{12} & 0 \\ a_{12} & 0 & 0 \\ 0 & 0 & 0 \end{matrix}$	$\infty : m$	∞ axis coincides with X_3 axis
4	»	A polar vector	$\begin{matrix} 0 & -A_{11} & 0 \\ A_{11} & 0 & 0 \\ 0 & 0 & 0 \end{matrix}$	$\infty \cdot m$	∞ axis coincides with X_3 axis
5	Tensor	A symmetric polar tensor	$\begin{matrix} a_{11} & 0 & 0 \\ 0 & a_{11} & 0 \\ 0 & 0 & a_{33} \end{matrix}$	$m \cdot \infty : m$	∞ axis coincides with X_3 axis
6	»	»	$\begin{matrix} a_{11} & 0 & 0 \\ 0 & a_{22} & 0 \\ 0 & 0 & a_{33} \end{matrix}$	$m \cdot 2 : m$	The 2 axes coincide with the X_1,X_2,X_3 axes
7	»	A symmetric axial tensor	$\begin{matrix} A_{11} & 0 & 0 \\ 0 & A_{11} & 0 \\ 0 & 0 & A_{33} \end{matrix}$	$\infty : 2$	∞ axis coincides with X_3 axis
8	»	»	$\begin{matrix} A_{11} & 0 & 0 \\ 0 & A_{22} & 0 \\ 0 & 0 & A_{33} \end{matrix}$	$2 : 2$	The 2 axes coincides with X_1,X_2,X_3 axes
9	»	»	$\begin{matrix} A_{11} & 0 & 0 \\ 0 & -A_{11} & 0 \\ 0 & 0 & 0 \end{matrix}$	$\bar{4} \cdot m$	The $\bar{4}$ axis coincides with the X_3 axis, the 2 axes coincide with X_1 and X_2 axes

Generalizing the above, we conclude that point symmetry groups of homogeneous; continuous isotropic media in tensor, vector and scalar fields are exhausted by the following 17 groups: $\infty/\infty \cdot m$; ∞/∞; $m \cdot \infty : m$; $\infty : 2$; $\infty \cdot m$; ∞; $\bar{4} \cdot m$; $\bar{4}$; $m \cdot 2 \cdot m$; m; $2 : 2$; $2 : m$; 2; $\bar{2}$; 1.

Geometric forms corresponding in symmetry to the 17 point groups are shown in Fig. 1. It is interesting to note that the seven point symmetry groups (Curie groups having ∞ symmetry axes) the two groups coinciding with the symmetry groups of a tetragonal crystal system and all the symmetry groups of orthorhombic, monoclinic and triclinic structure are included in these groups.

As we have limited ourselves to a study of external actions, reduced to scalars, vectors and tensors (i.e., to actions described by polar and axial tensors of the second order) we have not touched on the question of whether or not any type of action on a medium may be described in this manner, and therefore we have also left open the question of how general is the case which we have studied.

The author is grateful to Academician A.V. Shubnikov for helpful discussions of problems encountered in this work.

LITERATURE CITED

[1] A.V. Shubnikov, "On the symmetry of vectors and tensors," Izv. AN SSSR, Ser. Fiz. 13, 3, 347-375 (1949).

[2] I.S. Zheludev, "Scalar, vector and tensor symmetry," Kristallografiia 2, 2, 207-216 (1957).*

[3] A.V. Shubnikov, Piezoelectric Textures [in Russian] (1946).

Institute of Crystallography, Academy of Sciences, USSR

Received March 18, 1957

---

* Soviet Physics — Crystallography, p. 202.

INTENSITY OF ELECTRON DIFFRACTION PATTERN REFLECTIONS (GENERAL CASE)

B.K. Vainshtein

The specimens to be used for structure analysis by electron diffraction are aggregates of a very large number of single small crystals (blocks), in general having any thickness. The structure of the specimen is described by introducing $f(\alpha)$, the function of crystal distribution over the angles, as well as, $p(A)$, the function of their distribution according to their dimensions. The first function gives the L-factor in the final formulas, analogous to the Lorentz factor in x-ray analysis. These formulas include also the function $p(A)$. All cases — kinematic, intermediate and dynamic scattering — are described by concrete consideration of the form of $p(A)$.

For the sake of comparison with experience, precise data of Lennander, a Swedish author, have been used. The calculated intensities are in good agreement with the experimental ones.

In order to analyze the atomic structure of crystals by means of electron diffraction, we must know the laws of distribution which govern the calculation of structural amplitudes from observed reflection intensities. The great majority of electron diffraction structure studies are carried out with specimens which are either mosaic monocrystalline films, textures* or polycrystals, i.e., aggregates of a very large number of monocrystals. Consequently the problem of calculating the intensity may be divided into two parts: a) finding the intensity scattered by a single small crystal and b) calculation of the specimen structure from the small component crystals (blocks).

In papers [1, 2, 3] and in the monograph [4] this problem had been studied by the author in a kinematic approximation, accurate for small crystals, in the case of electron diffraction structure studies. The kinematic theory may be used in the majority of cases. However the scattering may sometimes be dynamic or intermediate. In this paper, which is a sequel to papers [1-3], the general case of scattering is studied with specimens consisting of crystalline blocks of any size. This eliminates the limitations associated with the kinematic formulas for intensity and makes it possible to extend electron diffraction structure analysis.

1. Scattering by an Individual Ideal Crystal

The integral reflection intensity may be calculated in a kinematic approximation by means of the integration of the interference function in the screen plane [1-4]. Such a calculation produces formula

$$I_{hkl}(h_3) = J_0 \lambda^2 \left|\frac{\Phi_{hkl}}{\Omega}\right|^2 A_1 A_2 \frac{\sin^2 \pi A_3 h_3}{(\pi h_3)^2}. \tag{1}$$

---

* Texture (tekstur) — "a homogeneous body with nonlattice structure, composed of many particles of any physical nature definitely oriented in space according to the laws of symmetry" (A. V. Shubnikov, Piezoelectric Textures [in Russian] (1946)) — Publisher's note.

Here I_{hkl} is the integral intensity of the reflection which is a function of the distance h_3 (in reciprocal space) from the center of the crystal site hkl of the reciprocal lattice to the reflection sphere; J_0 is the original intensity, $\Phi_{hkl} = \Sigma f_{el} \exp[2\pi i (rH)]$ – is the structural amplitude, Ω is the volume of the cell and A_1, A_2, A_3 are the linear dimensions of the crystal.

Relating the scattered intensity to the original intensity which falls on a crystal with $S = A_1A_2$ area, we shall find (omitting the indexes of the h_3 and A_3 magnitudes) that the integral coefficient of reflection R_{hkl} (h) equals

$$\frac{I_{hkl}(h)}{J_0S} = R_{hkl}(h) = Q^2D_{\text{к}}, \tag{2}$$

where

$$Q_{hkl} = \lambda\,|\Phi_{hkl}|/\Omega \text{ и } D_{\text{к}}(A,\ h) = \sin^2 \pi Ah/(\pi h)^2. \tag{3}$$

It can be seen from here that when h = 0 (that is for the normal reflection)

$$R_{hkl}^{\max} = Q_{hkl}^2A^2. \tag{4}$$

Scattering may be considered kinematic only when $I_{hkl} < J_0S$, i.e., when $R_{hkl} < 1$. The R = 1 equality will indicate a transition into the region of dynamic scattering, when the basic conditions of the kinematic approximation (weakness of the scattered electron beam) is not satisfied. Therefore the condition R = 1 defines the limits of applicability of the kinematic theory and the critical thickness A'

$$QA' = \lambda\frac{|\Phi_{hkl}|}{\Omega}A' \approx 1. \tag{5}$$

In order to evaluate A' we should take an average value $|\bar{\Phi}|$ for the neighboring values of $\sin\vartheta/\lambda$ (around $0.2 \cdot 10^8$ cm). The analysis, carried out in papers [1, 4] shows that the magnitude A' increases as the structure becomes more complex; this expands the area of applicability of the kinematic theory.

Solution of the problem of dynamic scattering by approximation for two strong electron beams was given by Bethe in [5]. Using our notation the solution can be written as

$$R_{hkl}(h) = \frac{I_{hkl}(h)}{J_0S} = Q_{hkl}^2\frac{\sin^2[A\sqrt{(\pi h)^2 + Q^2}]}{(\pi h)^2 + Q^2} = Q^2D_{\text{d}}(h,\ Q,\ A). \tag{6}$$

When QA < 1, i.e., with small thicknesses A, $D_d \to D_k$ and (6) becomes, as one would expect, formula (2) of the kinematic theory. If D_d is written as $\sin^2(a\sqrt{1 + w^2})/(1 + w^2)$ as was done by Blackman [6] it will be apparent that the solution of the problem of dynamic scattering of electrons in an ideal crystal is identical with the solution of the same problem in the case of x-rays (see for example [7]). The same is true of the kinematic theory. This is not accidental, inasmuch as, despite natural differences in the nature of the interaction of these rays with a substance, the mathematical framework is identical – in both cases the diffraction of short waves by a three dimensional lattice is studied.

Both position and form of the maxima for functions D_k and D_d coincide when QA < 1; however, as was first shown by McGillavry [8] correlation is also observed in the case of greater thicknesses. From (3) and (6) it is possible to show that the zero position (even n ≥ 2) and secondary maxima (odd n ≥ 3) of these functions can be determined respectively by the values

$$h_{\text{к}}(n) = n/2A;\ h_{\text{d}} = \sqrt{\left(\frac{n}{2A}\right)^2 + \frac{Q^2}{\pi^2}}, \tag{7}$$

and, as should be expected, with $QA < 1 h_d \rightarrow h_k$. The magnitude of the maxima (odd $n \geq 3$) is the same in both cases and equals

$$R(n) = Q^2\left(\frac{2A}{n\pi}\right)^2. \qquad (8)$$

In the case of greater than critical thicknesses, when at the principal maximum (when h = 0), the kinematic theory leads to the physically absurd values $R > 1$, secondary kinematic theory maxima are found in correlation with the real maxima of the dynamic theory. However, according to [8] they are somewhat shifted. Figure 1 shows an example for the (200) Al reflection.

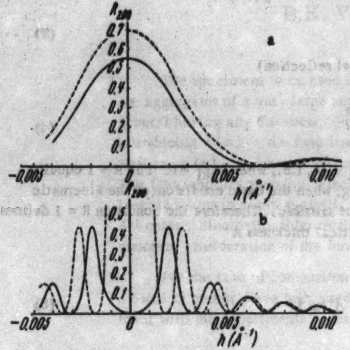

Fig. 1. R_{200}Al curves calculated according to the dynamic theory (solid lines) and according to the kinematic theory (dashed lines) (λ = 0.05 Å, Q_{200} = 0.0056 Å^{-1}). a) With thickness A = 150 Å, less than the critical $A' = Q^{-1}$ = 180 Å but close to it; b) with thickness $A = \pi A$ = 570 Å, considerably above critical.

2. Reflection Intensity of Real Specimens

Real specimens used in electron diffraction studies are composed of a large number of small crystals. It can be shown (see [9, 4]) that when point electron diffractionpatterns (due solely to the spread in angle of the crystals) are obtained, that the simultaneous appearance of all reflections (belonging to either of the planes of the reciprocal lattice) is possible.

In this part of the paper we shall show that factors, previously found [2, 3] for various specimen types (mosaic monocrystalline films, textures, polycrystals) from which the spread in angle of crystals is calculated, do not change in the case of specimens consisting of crystalline blocks of arbitrary thickness. We shall also take into account the distribution of the blocks according to thickness, whereas before only the case of kinematic scattering on thin crystals was considered.

The angular spread of the crystals may be described by means of a distribution function of the normals to a given reflecting plane. In order to calculate the total intensity one must sum expression (2), or the more general (6), taking into account the distribution function $f(\alpha)$. Here only those crystal deflections are important which produce changes in the magnitude of h (= h_3) in (2) and (6). The corresponding angle measure α is associated with the distance h in the reciprocal space by the ratio

$$h = H_{hkl} \cdot \alpha,$$

so that

$$dh = H_{hkl} d\alpha = \frac{d\alpha}{d_{hkl}}, \qquad (9)$$

where H_{hkl} is the magnitude of the reciprocal lattice vector, d_{hkl} is the interplanar distance for the given reflection (Fig. 2). The function $f(\alpha)$ differs from zero over a certain angular interval $\alpha = \alpha_1 - \alpha_2$, its normalizing condition being

$$\int_{\alpha_1}^{\alpha_2} f(\alpha)\, d\alpha = S'/S, \tag{10}$$

where S is the middle plane of one crystal, S' is a general plane of the film. (In the case of crystals of equal thickness it is possible to use, as has been previously done [2, 3], a volume ratio V'/V instead of a surface ratio. The portion of the crystals falling in the angle interval α, $\alpha + d\alpha$ will be $f(\alpha)\, d\alpha$ so that the total intensity when the specimen is rotated at a certain angle β will be equal (Fig. 2) to

$$I'_{hkl}(\beta) = \int I_{hkl}(h) f(\alpha)\, d\alpha = \int I_{hkl}(\beta - \alpha) f(\alpha)\, d\alpha. \tag{11}$$

This expression is made up of functions I and f. Let us note that inasmuch as function I is even, $I(\alpha - \beta) = I(\beta - \alpha)$. Let us now calculate the distribution of crystals according to thickness. Let this distribution be described by function $p(A)$ normalized in such a way that

$$\int p(A)\, dA = 1. \tag{12}$$

Introducing this function also into (11) we find that the intensity of scattering by a specimen, whose structure is described by functions $f(\alpha)$ and $p(A)$ is defined by the formula

$$I'_{hkl}(\beta) = \iint I_{hkl}[(\alpha - \beta),\ A]\, f(\alpha)\, p(A)\, d\alpha\, dA. \tag{13}$$

This most general expression may be made more specific only if the form of $f(\alpha)$ and $p(A)$ is assigned for any one specimen.

Let us now consider this. In the case of a mosaic monocrystalline film, $f(\alpha)$ usually exists over an effective angle interval α of the order of 3-4° (i.e., ≈ 1/15 radian) and may be replaced with sufficient accuracy by its average value, equal, according to (10) to $S'/S\ \alpha$. From expressions (2) and (6) it can be seen that for an individual crystal, I_{hkl} is proportional to J_0S: now the supplementary factor S'/S which enters in makes it possible to assign the scattered intensity not to the plane S of the individual crystal, but to the whole (electron irradiated) plane S' of the specimen and to write down the integral reflection coefficient (with its maximum value, when $\beta = 0$) as

$$R'_{hkl} = \frac{I'_{hkl}}{J_0 S'} = \frac{1}{\alpha}\int R_{hkl}(\alpha)\, p(A)\, d\alpha\, dA \tag{14}$$

or, by taking into account (2), (6) and (9) as

$$R'_{hkl} = Q^2_{hkl} L \iint D(h,\ Q,\ A)\, p(A)\, dA\, dh. \tag{15}$$

In this case (mosaic monocrystal) according to (9)

$$L = d_{hkl}/\alpha.$$

For other specimen types the appearance of this factor, which does not depend, as can now be seen from (15) on D, i.e., on the size of the crystals, has been found in [3]. A summary of the values of L is given below in Table 1.

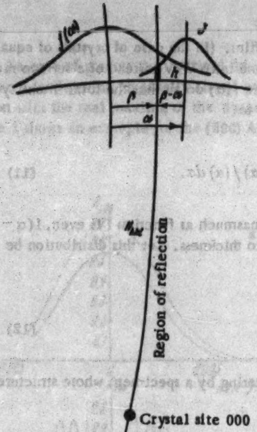

Fig. 2. Mutual arrangement of the f(α) and J(h) functions and the region of reflection.

For the kinematic case

$$\int_{-\infty}^{+\infty} D_{\text{K}}(h,\ A)\,dh = r_{\text{K}}(A) = A. \qquad (16)$$

In the dynamic theory an analogous integral was studied by Blackman [6], and its behavior also discussed in [7]. It is equal to

$$r_{\rm d}(A,\ Q) = \int_{-\infty}^{+\infty} D_{\rm d}(h,\ Q,\ A)\,dh =$$

$$= \frac{1}{Q}\int_{0}^{AQ} J_0(2x)\,dx;\ r_{\rm d} \xrightarrow[A\to\infty]{} \frac{1}{2Q}. \qquad (17)$$

Graphs of r_k and r_d are shown in Fig. 3. In the case of small thicknesses $A < A^* = Q^{-1}$ (5) these functions show close correspondence. Thus, as a result

$$R'_{hkl} = Q^2 L \int r(A,\ Q)\,p(A)\,dA. \qquad (18)$$

This is a general formula for a polydisperse specimen.* If the specimen consists of crystals of equal size A, then the integral in this expression is simply equal to r(A,Q). Then for thin crystals (case of purely kinematic scattering) from (16)

$$R'_{hkl} = Q^2_{hkl} LA \qquad (19)$$

and for thick crystals ($A > Q^{-1}$, the case of purely dynamic scattering) from (17)

$$R'_{hkl} = \frac{1}{2} Q_{hkl} L. \qquad (20)$$

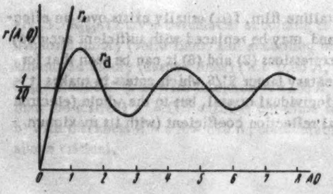

Fig. 3. Graph of the functions $r_k(A) = A$ (16) and $r_d(A,Q)$ (17).

Using these formulas and dividing the crystals into those that scatter kinematically and those that scatter dynamically one can describe scattering with sufficient approximation even for a polydispersive specimen. Let us write (18) using (16) and (17) in the form

---

* In this formula the specific form of r(A,Q) has not yet been assigned. For further calculations the Bethe approximation for two strong electron beams and expression (17) based on it, will be used. The case of two strong electron beams is a basic one in the case of crystal diffraction; the case of three electron beams is possible but considerably less probable. A greater number of electron beams may occur only accidentally, inasmuch as the reflection range in general may touch only three (including the initial) crystal sites of the reciprocal lattice. It may be assumed that the Bethe approximation is satisfactory for the solution of the problem of scattering for the majority of crystals. However in principle greater accuracy is possible as the form of function r becomes more precise.

$$R'_{hkl} = Q^2 L\left[\int_0^{A'} A p(A)\, dA + \frac{1}{2Q}\int_{A'}^{\infty} p(A)\, dA\right], \qquad (21)$$

i.e.,

$$R'_{hkl} = L\left(Q^2\overline{A}_k p_k + \frac{1}{2} Q p_d\right);\ p_k + p_d = 1. \qquad (22)$$

Here $\overline{A}_k$ is the average thickness of the crystals which scatter kinematically, p_k and p_d [these values are obtained by comparing (21) and (22)] are those crystal portions scattering kinematically and dynamically respectively.* Taking into consideration the fact that $R'_{hkl} = I'_{hkl}/J_0 S'$; that $S'\overline{A}_k p_k = V_k$ the total volume of kinematically scattering crystals and that $S'p_d = S_d$ the total area of dynamically scattering crystals, one may rewrite (22) as follows:

$$I'_{hkl} = J_0\left(Q^2 V_k + \frac{1}{2} Q S_d\right) L. \qquad (23)$$

In practical calculations one generally uses the relative values I, Φ etc. Then one can write (23) in the form

$$I^{\mathrm{rel.}}_{hkl} = \left(k_k |\Phi_{hkl}|^2 + k_d |\Phi_{hkl}|\right) L^{\mathrm{rel.}}; \qquad (24)$$

where k_k and k_d are certain coefficients which can be found directly from experiment from the decrease in the averaged intensity [4]. It is obvious that the purely kinematic scattering (18) and purely dynamic scattering (20) formulas will be particular cases of formulas (21)-(24). If the scattering has an intermediate character, when both coefficients k_k and k_d are not equal to zero, finding the values of $|\Phi|$ and $|\Phi|^2$ from experiment requires the solution of the quadratic equation (24). L factor values are given below in Table 1.

3. Analysis of Certain Experimental Data

A decrease in observed intensities according to the law $I \sim f_{el}^2$ (f_{el} is the atomic amplitude) denotes kinematic scattering, and according to law $I \sim f$ dynamic scattering. Thermal motion augments the decrease in both cases (Fig. 4). In the majority of electron diffraction pattern studies (see [4, 9]) a good correspondence between experimental and calculated amplitudes $|\Phi|$ has been found when the kinematic theory formulas were used, and in some studies for a more accurate comparison of $|\Phi_{exp}|$ and $|\Phi_{cal}|$ the temperature factor was also used, which corresponds to a greater decrease in I (Fig. 4). At the same time in individual cases [10, 11] it has been proved that the intensities better satisfy the dynamic theory formulas. This was observed in the case of point electron diffraction patterns, which is quite natural, inasmuch as the formation of large crystals is more probable in mosaic monocrystalline films. Cases of intermediate scattering were also observed (see [12]).

Many investigators, Mark and Virl' [13], Tol and Ornstein [14], Iamzin and Pinsker [15], Lennander [16] and others carried out precise measurements of the intensity of electron scattering from polycrystalline films of metals in order to check the formulas for atomic scattering in the Born approximation. The Born approximation (which is a kinematic study of atomic scattering as well as a strict solution taking the phases into consideration), is, in this case, the solution of the dynamic problem for the atom. The physical sense of the dynamic

---

*The value of A', according to (5), whose evaluation is necessary, for such a division, is itself dependent on Q, i.e., on Φ_{hkl}. Therefore p_k and p_d (and hence k_k and k_d) are, strictly speaking, variable magnitudes. However to the first approximation one does not need take this into account, taking A' for average Q.

TABLE 1

Values of L Factor

Specimen and method of measuring intensity	L	L^{rel}	Remarks
Mosaic, integral spot intensity	d_{hkl}/a	d_{hkl}	
Texture, integral intensity of the arc	$\frac{L\lambda p}{2\pi r' \sin\varphi}$	p/r'	r' is the horizontal reflection coordinate
Texture, local intensity in the arc region of length Δ	$\frac{d_{hk0}\, d_{hkl}\, p\, \Delta}{2\pi L\lambda a}$	$d_{hk0}\, d_{hkl}\, p$	p is the frequency factor, φ is the angle of inclination of the specimen to the electron beam
Polycrystal, integral intensity of the ring	$d_{hkl}\, P/2$	$d_{hkl}\, P$	$L\lambda$ — is the apparatus constant
Polycrystal, local intensity on a section of the ring of length Δ	$\frac{d^2_{hkl}\, p\Delta}{4\pi L\lambda}$	$d^2_{hkl}\, P$	

study consists in a complete calculation of the interaction between the incident and scattered waves over the entire volume of the object. Therefore the dynamic effects accumulating throughout the volume of the whole crystal, must be considerably larger than the dynamic effects for an individual atom which can be calculated within the framework of the kinematic theory of crystal scattering (see for example [17, 18]). In this connection the papers [13-16] must be considered not only as a verification of atomic scattering theory but also as a verification of the applicability of the kinematic theory. At the same time fulfillment of the f^2 law indicates the carrying out of the Born approximation; divergence toward the f law shows first of all that the kinematic theory is not applicable.

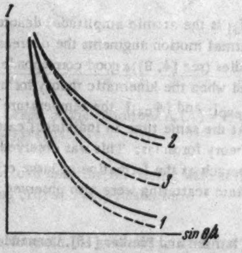

Fig. 4. 1) Decrease in intensity according to the f^2 law of kinematic scattering; 2) according to the f law of dynamic scattering; 3) case of intermediate scattering. Dashed lines show the effect of thermal motion.

In papers [13, 15, 16] the decrease in intensities basically satisfies the f^2 law, in [15, 16] divergences toward the f law were found in the case of the heaviest elements studied, Au (and partially Ag). The data obtained in paper [14] closely followed the f law, as indicated in [6], although with considerable spread in the results which is apparently due to the fact that texturization of the samples was not taken into account (see [9, 16].

A comparison of the results of such experiments with theory may be carried out only when the dimensions of the scattering crystals can be accounted for.

Let us analyze the Lennander [16] data in this light. This author carried out precision measurements of the intensity of scattering of 18 and 30-kv electrons (λ = 0.07 Å) by means of Geiger counters on polycrystalline samples of Al, Ag and Au. The result of measurements on Au is shown in Fig. 5.

If the sample consists of crystals of differing sizes then the measurement of the line half width can not be

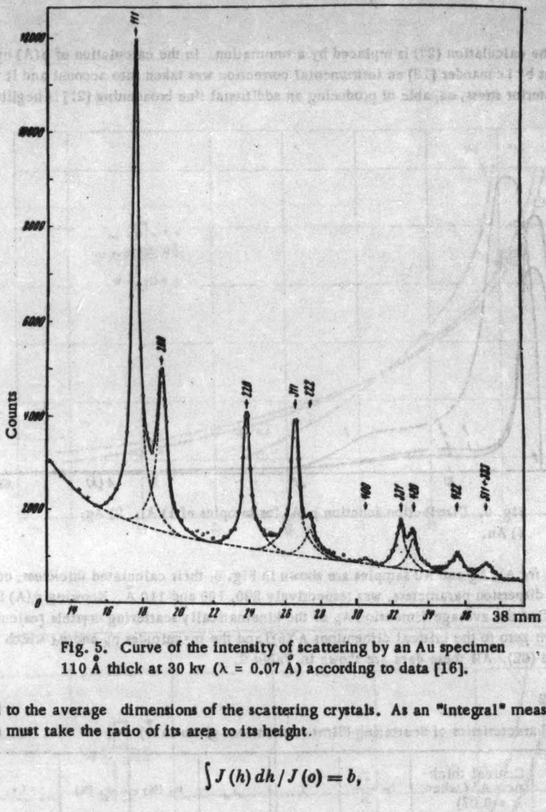

Fig. 5. Curve of the intensity of scattering by an Au specimen 110 Å thick at 30 kv ($\lambda = 0.07$ Å) according to data [16].

strictly related to the average dimensions of the scattering crystals. As an "integral" measure of the half width of the line one must take the ratio of its area to its height.

$$\int J(h)\,dh / J(o) = b, \tag{25}$$

where h is the distance* from the center of the line in $Å^{-1}$. The reciprocal magnitude b, as shown by Bertaut [19], defines the ratio of the average quadratic size of the crystals to their average size

$$l = b^{-1} = \overline{A^2} / \overline{A}, \tag{26}$$

where A is the dimension of the crystals in a direction perpendicular to the reflecting plane. It has been shown in [19] that the second derivative of the Fourier transformation J(h) makes it possible to find the distribution function p(A). To find p(A) the author [20] used the ratio

---

* This differs from § 1, 2 (where it was assumed that $h = h_3$) now $h = h_1$ (or h_2), and corresponds to the distance r in the electron diffraction pattern plane, so that $h = (L\lambda)^{-1} r$.

$$p(A) = \int_0^\infty J(h)\,h^2 \cos 2\pi\, hA\, dh. \tag{27}$$

Practically, the calculation (27) is replaced by a summation. In the calculation of p (A) by the intensity curves as carried out by Lennander [16] an instrumental correction was taken into account and it was also shown that the effect of interior stress, capable of producing an additional line broadening [21] is neglibibly small.

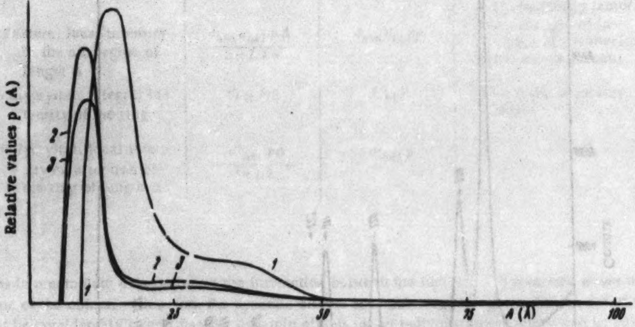

Fig. 6. Distribution function p (A) for samples of 1) Al; 2) Ag; 3) Au.

p (A) functions for Al, Ag and Au samples are shown in Fig. 6; their calculated thickness, computed in [16] from geometric dispersion parameters, was respectively 290, 100 and 110 Å. Knowing p (A) it is easy to calculate $\overline{A}$, $\overline{A^2}$, to find the average dimension A_k of the kinematically scattering crystals [calculating p (A) within the limits from zero to the critical dimensions A'(5)] and the magnitudes p_k and p_d which enter into the formulas (21) and (22). All these data are shown in Table 2.

TABLE 2

Certain Characteristics of Scattering Films (dimensions given in Å)

Element	Critical thickness A' (when λ = 0.07)	$1-\frac{\overline{A'}}{\overline{A}}$	$\overline{A}$	$\overline{A}_K$	p_K (%)	p_d (%)	• l •
Al	100	50	26	23	97,5	2,5	100
Ag	40	35	17	14	91	9	95
Au	30	39	18	13	85	15	80

First of all it must be noted that the p (A) functions (Fig. 6) show a maximum at an unexpectedly small value of A of the order of 11 Å for Au and Ag and 15 Å for Al, first falling rapidly, then decreasing slowly, but still showing certain finite values within the range up to 100 Å for Au and Ag and up to 170 Å for Al (this part of the curve is not shown in Fig. 6). This causes us to think that with the condensation of metal in a vacuum a large quantity of crystals of a certain minimal size is first formed from the vapor and further growth is carried on from there. This minimal size is greater for low melting metals.

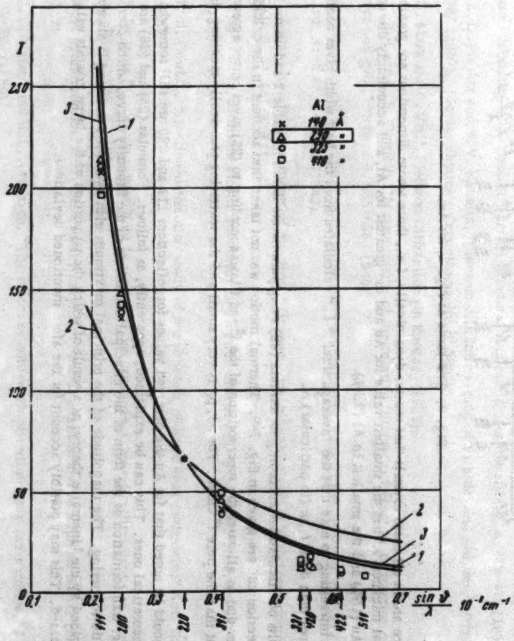

Fig. 7. Comparison of experimental data obtained in paper [16] for Al with the curves for: 1) f^2; 2) f; 3) an intermediate curve calculated by means of formulas (22).

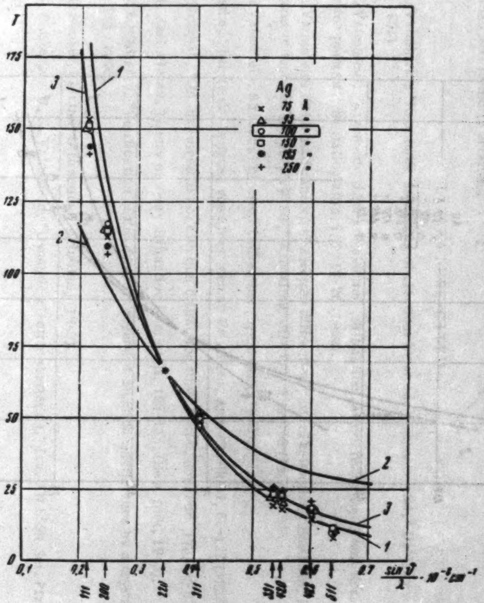

Fig. 8. The same as Fig. 7, for Ag.

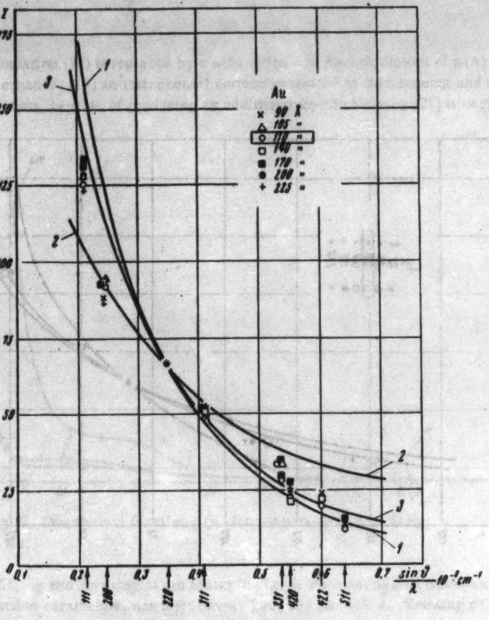

Fig. 9. The same as Fig. 7, for Au.

There are in all cases crystals that scatter dynamically, i.e., those whose dimensions are greater than A'. The critical thickness A' has the smallest value for Au and the greatest for Al, and accordingly the greatest p_d occurs in Au (15%) and the smallest in Al (2.5%).

It is interesting to note that the "average size," " l ," calculated from the half width gives considerably higher values than does l or (in particular) $\overline{A}$.

Results of calculations according to formula (22) using parameters shown in Table 2 and normalized according to reflection 220 are given in Fig. 7-9. Thermal motion was not taken into account in the calculations. It can be seen that in all cases the superposition of the f^2 and $\underline{f}$ laws according to (22) gives better agreement with experiment than the pure f^2 curve. For Al, p_d is very small and the scattering practically speaking, is purely kinematic.

It should be noted that for Au the observed values for reflections 111 and 220 are still somewhat lower than the theoretical ones. This can be explained, apparently, as follows. Formulas (25) and (26) are based on a Fourier transformation of the form of the principal maximum of the intensity curve, which corresponds to kinematic scattering. The magnitude of the principal maximum with dynamic scattering is always smaller than prescribed by the kinematic theory, as a result of which the p_d portion of the large crystals will be somewhat decreased. This may possibly account for the afore-mentioned deviations.

SUMMARY

The use of integral intensity formulas with kinematic and dynamic scattering of electrons in an ideal crystal makes it possible to deduce practical formulas for the intensity of samples consisting of a large number of crystals. The sample structure can be described by means of the distribution function of crystals according to angles and also according to size. The general formulas thus obtained are correct for boundary cases of purely kinematic or purely dynamic scattering and for the general case of intermediate scattering. Comparison of the formulas with experimental data on electron scattering in polycrystalline samples of Al, Ag and Au gives a better result than that formerly obtained.

LITERATURE CITED

[1] B. K. Vainshtein, "Kinematic scattering of electrons by an ideal monocrystal," Doklady Akad. Nauk 104, 537-539 (1955).

[2] B. K. Vainshtein, "Kinematic theory of electron diffraction pattern reflection intensities, I. Point electron diffraction patterns," Kristallografiia, I, 1, 17-26 (1956).

[3] B. K. Vainshtein, "Kinematic theory of electron diffraction pattern reflection intensities, II. Electron diffraction patterns of textures and polycrystals," Kristallografiia I, 2, 150-158 (1956).

[4] B. K. Vainshtein, Structural Electron Diffraction [in Russian] (1956).

[5] H. Bethe, Theorie der Beugung von Electronen an Kristallen, Ann. Physik 87, 55-129 (1928).

[6] M. Blackman, "On the intensities of electron diffraction rings," Proc. Roy. Soc. 173, 68-82 (1939).

[7] W. H. Zachariasen, Theory of x-ray diffraction in crystals. 123-135. (New York, 1945).

[8] C. H. McGillavry, "Verification of the dynamic theory of electron interference by a crystal lattice," Physica 7, 329-343 (1940).

[9] Z. G. Pinsker, Electron Diffraction [in Russian] (1949).

[10] Z. G. Pinsker, and B. K. Vainshtein, "Dynamic electron scattering," Izv. AN SSSR Ser. Fiz. 14, 2, 212-222 (1950).

[11] B. K. Vainshtein and A. N. Lobachev, "On the determination of the nature of electron scattering (dynamic and kinematic) in electron diffraction structural studies," Kristallografiia, I, 4, 472-473 (1956).

[12] Z. G. Pinsker and S. V. Kaverin, "Electron diffraction study of carbides and nitrides," Kristallografiia, 2, 3, 386-392 (1957). [Soviet Physics – Crystallography, p. 380.

[13] G. Mark and P. Virl', Electron Diffraction [in Russian] (1933).

[14] T. Tol and L. S. Ornstein, "Measurements of the relative intensity of electron diffraction pattern of copper, silver and gold," Physica 7, 685-696 (1940).

[15] I. I. Iamzin and Z. G. Pinsker, "Atomic electron scattering," Trudy Inst. Krist. 5, 69-112 (1949); Doklady Akad. Nauk 65, 645-648 (1949).

[16] S. Lennander, "Measurements of electron diffractions intensities by means of Geiger counters," Arkiv för Fysik 8, 54, 551-613 (1954).

[17] J. A. Hoerny, Multiple elastic scattering in electron diffraction by crystals. Phys, Rev., 102, 1534-1542 (1956).

[18] J. M. Cowley, "Electron-diffraction study of the structure of basic lead carbonate," Acta Cryst. 9, 391-396 (1955).

[19] F. Bertaut, "Etude aux rayons X de la repartion des dimensions des cristallites dans une poudre cristalline," Compt. Rend., 228, 492-494 (1949).

[20] A. I. Kitaigorodskii, x-ray Structural Analysis of Fine Crystalline and Amorphous Bodies [in Russian] 132-135 (1952).

[21] B. E. Warren and B. L. Averbach, "The effect of cold-work distortion on x-ray patterns," J. Appl. Phys. 21, 595-599 (1950).

Institute of Crystallography
Acad. Sci. USSR

Received February 26, 1957

THE THEORY OF THE RELATION BETWEEN STRUCTURE AMPLITUDES AND METHODS OF DIRECT ANALYSIS OF CRYSTAL STRUCTURES

A.I. Kitaigorodskii

The law of predominant positivity of $F_H F_K F_{H+K}$ has been elucidated, a new method of its use for direct structure analysis being proposed. It has been demonstrated that statistical theories are of secondary importance both for proving and applying this law.

§ 1. The Law of Predominant Positivity of the Structure Product

In 1952 Sayre [1] and Cochran [2] first drew attention to a very interesting fact. If we form the product $F_H F_K F_{H+K}$ of unitary structure amplitudes for any centrosymmetric crystal, then among these products (let us call them structure products – they will in future be denoted by X) there will be more positive quantities than negative. The proportion of positive X_{HK} increases as the absolute value of the structure product increases.

This observation was used with success by Zachariasen [3] in structure analysis. The signs of all the amplitudes were determined by the direct method, without any assumptions concerning the structure under consideration.

In the years which followed, the law of predominant positivity was used by many authors as a method of direct analysis. Sometimes the investigators were unsuccessful, but in other cases the structural problem was successfully solved.

The divergence of opinions as regards the possibilities of application of the law of predominant positivity is due to misconceptions of the basis of this remarkable law. Therefore, before discussing the possible ways of direct crystal structure analysis, it is necessary to explain the nature of the above law.

In the early work of the author [4], in the paper [5] and in a series of others, it was shown that the law of predominant positivity of the structure product could be deduced from the assumption of the uniform distribution of the cosines which appear in the expression for the structure amplitude.

However, the weakness of this explanation is evident as soon as we consider the full universality of this law. It is strictly obeyed even by crystals in which the atoms occupy special positions, in spite of the fact that in these cases the arguments of the trigonometric functions can only take a limited number of discrete values, and it is not possible to talk of a uniform distribution.

If the values of the amplitudes and the structure factors are continuously distributed, we may in principle construct an experimental distribution function $f(X_{HK})$. The schematic form of this function, which may be established by calculation from experimental data, is given in Fig. 1. The characteristic features of this function are as follows: near the center of the distribution it coincides with the Gaussian curve, the mean of which is displaced to the right; for negative X the curve falls more quickly and for $X = 0.125$ reaches zero, as X is always greater than -0.125. For X positive the curve drops slowly and in general P(X) is distinct from zero right up to X equal to a few tenths.

Evidently a distribution function of this type expresses the law of predominant positivity of the structure product.

What is the reason for the fact that the area under the positive part of the curve is greater and consequently the structure factor is more often positive than negative ? In the following section it will be shown that the reason for this is that the determinant relating the structure amplitudes is always positive.

Does the distribution of the arguments of the trigonometric functions play any role in this? It can be shown that this distribution does effect the form of the curve. In particular, because of the equality of the distribution of the arguments, the maximum of the curve $f(X_K)$ is displaced to the right. However, the basic result – the presence of a tail in the positive region, which ensures the preponderance of large structure factors, is the consequence of the positive nature of the determinant.

This tail remains for any distribution of the arguments, including one which is discrete. Therefore the law of predominant positivity of the structure product must be considered as a consequence only of the positive nature of the determinant.

§ 2. The Basis of the Law of Predominant Positivity of the Structure Product

We find in the work of Karle and Hauptmann [7], and also of Goedkoop [8], a generalization of the inequalities of Harker and Kasper [6].

In the paper [9] it was shown that the essence of these generalizations is the posibility of representing unitary structure amplitudes as cosines of the angles between N-dimensional vectors.

Let us consider m arbitrary points of the reciprocal lattice, including the origin. The corresponding unitary structure amplitudes are expressed as

$$F_p = \sum_{j=1}^{N} n_j \exp 2\pi i \boldsymbol{H}_p \boldsymbol{r}_j.$$

We introduce the quantities

$$G_p = \sum_{j=1}^{N} e_j n_j^{1/2} \exp 2\pi i \boldsymbol{H}_p \boldsymbol{r}_j, \tag{1}$$

which we shall consider as vectors in an N-dimensional space with orthogonal coordinate vectors e_j. Since the n_j are positive $n_j^{1/2}$ are real numbers. Therefore the vector G_p is of unit length,

$$G_p G_p^* = \sum_{j=1}^{N} n_j = 1,$$

while the scalar product

$$G_p G_q' = \sum_{j=1}^{N} n_j \exp 2\pi i (\boldsymbol{H}_p - \boldsymbol{H}_q) \boldsymbol{r}_j = F_{pq} \tag{2}$$

are equal to unitary structure amplitudes of the reciprocal lattice point $H_p - H_q$. The structure amplitudes are the cosines of the angles between the vectors G.

As we know from geometry, the determinant $\| F_{pq} \|$, known as the Gramme determinant, is greater than zero for $m < N$.

The inequality

$$\|F_{pq}\| > 0 \quad \text{for} \quad m < N \qquad (3)$$

is the fundamental equation relating structure amplitudes.

Since the diagonal elements of the determinant equal 1 we have, by well known formulas,

$$\|F_{pq}\| = 1 - \sum F_H^2 + \sum_H \sum_K F_H F_K F_{H+K} - \ldots > 0. \qquad (4)$$

The important terms of the series are those written above. In view of the fact that the sum of the series is positive, the third term, i.e., the sum of the structure products must be positive. Hence it follows that the majority of the structure products must be positive. Hence we have proved the law of predominant positivity of structure products, at least for the cases in which they have a large absolute value.

From equation (4) it also follows that for large values of $|F|$, which appear in the determinant of order m, not only the majority but all the structure products will be positive. For this to be true [10] we need the condition $|F_{pq}| > \delta$ for all $|F_{pq}|$, where δ is the root of the equation

$$1 - \frac{m(m-1)}{2}\delta^2 - \sum_{k=3}^{m}(-1)^k\left[\frac{k-1}{k!}\frac{m}{(m-k)!} - \frac{4(m-2)!}{(m-k)!\,(k-3)!}\right]\cdot|F|^k = 0. \qquad (5)$$

For $m = 3$ $\delta = 0.5$, for $m = 10$ $\delta = 0.3$, etc. To simplify the calculations in the deduction of (5) all the $|F|$ are considered identical. Our rule $X_{HK} > 0$, if $|X_{HK}| > \frac{1}{8}$ is contained in this equation.

§ 3. The Limits of the Possible Values of the Structure Amplitude [9]

Since for $m < N$ the Gramme determinant, calculated for the vectors G_p, is greater than zero, then the vectors G_p are linearly independent; this enables us to choose the unit orthogonal vector e_i of the N-dimensional space such that

$$G_p = \sum_{j=1}^{p} \alpha_{pj} e_j. \qquad (6)$$

Let m-1 of the first vectors G_p be fixed. Then the last vector G_m cannot be arbitrary, as the cosines of its angles with the other vectors $G_1, G_2, \ldots$, which equal respectively $F_{1m}, F_{2m}, \ldots$, are fixed. We further assume that we are given all the structure amplitudes besides $G_m G_{m-1} = F_{m,m-1}$, and we will calculate the possible variation of the vector G_m. It is evident that the end of the vector C_m lies on the plane satisfying the equation

$$(xG_p) = F_{mp} \quad \text{for} \quad p = 1, \ldots, m-2. \qquad (7)$$

Since the end of the vector G_m lies on the surface of an m-dimensional sphere, it describes a region cut out on the sphere by the plane (7). The components of G_m have orthogonal unit vectors which are fixed, except for e_{m-1} and e_m. The plane (7) is parallel to the plane e_{m-1}. The projection of G_m on this plane is $\alpha_{m,m-1}e_{m-1} + \alpha_{mm}e_m$. Introducing the azimuthal angle $\varphi = \arctan \alpha_{mm}/\alpha_{m,m-1}$ we may, given the other F_{pq}, express all the possible values of $F_{m,m-1}$ in terms of one parameter.

To do this we need to express α_{pq} in terms of F_{pq}, forming the scalar product between the vectors (6). Consequently we get, for p ranging up to m−2,

$$F_{p1}=\alpha_{p1};\ \alpha^2_{22}=1-\alpha^{21}_{2}$$
$$F_{p2}=\alpha_{p1}\alpha_{21}+\alpha_{p2}\alpha_{22};\ \alpha^2_{33}=1-\alpha^2_{31}-\alpha^2_{32}$$
$$F_{p3}=\alpha_{p1}\alpha_{31}+\alpha_{p2}\alpha_{32}+\alpha_{p3}\alpha_{33};\ \alpha^2_{44}=1-\alpha^2_{41}-\alpha^2_{42}-\alpha^2_{43}$$

the values of all the α_{pq} up to $\alpha_{m,m-2}$.

Taking into account the fact that

$$\alpha^2_{mm}+\alpha^2_{m,\,m-1}=1-\alpha^2_{m1}-\alpha^2_{m1}-\ldots-\alpha^2_{m,\,m-2},$$

and using the relation

$$\alpha^2_{m,\,m}+\alpha^2_{m\ m-1}=\alpha^2_{m,\,m-1}/\cos^2\varphi,$$

we may express

$$F_{m,m-1}=\sum_{p-1}^{m-1}\alpha_{pm}\alpha_{p,\,m-1}$$

in terms of the remaining F_{pq} and the azimuthal angle φ.

So that the text should not be unwieldy, we quote only the formulas for F_{32} and F_{43}.

$$F_{32}=F_{21}F_{31}+\sqrt{(1-F_{21})^2(1-F^2_{31})}\cos\varphi$$
$$F_{43}=F_{31}F_{41}+\frac{1}{1-F^2_{21}}(F_{23}-F_{21}F_{31})(F_{42}-F_{21}F_{41})+$$
$$+\sqrt{\left[1-F^2_{31}-\frac{1}{1-F^2}(F_{32}-F_{21}F_{31})^2\right]\left[1-F^2_{41}-\frac{1}{1-F^2_{21}}(F_{42}-F_{21}F_{41})^2\right]}\cdot\cos\varphi. \tag{9}$$

For any $F_{m,m-1}$ the formula will be of the form

$$F_{m,\,m-1}=A+B\cos\varphi, \tag{10}$$

where A and B are expressed in terms of F_{pq}. From (10) we may immediately determine, first, the average value of $F_{m,m=1}$ which equals A, and also the extreme values A ± B. Equation (10) contains the whole of the relation between structure amplitudes. The known inequalities which exist between amplitudes are a consequence of equation (10).

§ 4. The Probability of a Positive Structure Product

The condition for the positivity of the Gramme determinant led us to the law of predominant positivity of the structure product.

What can be said about the sign of any one structure product? In many cases the fundamental equation relating structural amplitudes enables us to state that a structure product is definitely positive. However, in other cases this is not possible, and then we may put the question of the probability that a given structure product $F_H F_K F_{H+K}$ is positive.

According to (8)

$$F_{K+H} = F_H F_K + \sqrt{(1 - F_H^2)(1 - F_K^2)} \cos \varphi,$$

where φ is a parameter, the variation of which covers all structures with given values of F_H and F_K.

Let F_{K+H} change by dF_{K+H} for a change $d\varphi$ in φ. The probabilities that the structure is characterized by the parameter φ, and that it has amplitude F_{K+H} are the same, i.e.,

$$P(F_{K+H})\, dF = P(\varphi)\, d\varphi,$$

but the probability densities are different. The proportion of structures which have a given value of the structure product is characterized by the function $P(\varphi)$, but not $P(F)$:

$$P(\varphi) = \frac{dF}{d\varphi} P(F)$$

or

$$P(\varphi) = \sqrt{1 - F_H^2 - F_K^2 - F_{K-H} + 2F_H F_K F_{K+H}}\, P(F).$$

The probability of a structure for which the structure product is positive equals:

$$W_+ = \frac{1}{1+\varepsilon},$$

where

$$\varepsilon = \sqrt{\frac{1 - F_H^2 - F_K^2 - F_{K-H}^2 - 2\,|F_H F_K F_{K+H}|}{1 - F_H^2 - F_K^2 - F_K^2 - F_{K-H}^2 + 2\,|F_H F_K F_{K+H}|}\, \frac{P(F_-)}{P(F_+)}}.$$

The calculation of $P(F)$ has been carried out by a series of workers [4, 5, 11] on the assumption of uniform distribution of the trigonometric functions which appear in the expression for the structure amplitude. In the majority of cases a sufficiently good approximation is provided by the formula first deduced by the author [4], according to which

$$\frac{P(F^-)}{F(F_+)} = \exp - 2N\,|F_H F_K F_{H-K}|,$$

where N is the effective number of atoms in the cell.

If the structure product is small in absolute magnitude the first factor in ε is near to 1 and we obtain the earlier formula which the author obtained for W

$$W = \frac{1}{1+e^{-2NX}}.$$

The main error of the papers [5, 7, 11] and of several other authors who have considered the problem is the identification of the probability P(F) with the probability of the structure which has a given F.

The formulas of these authors (which are self-consistent) naturally cannot give distribution functions for the structure product which are observed experimentally.

§ 5. Methods of Direct Analysis of a Structure

If the structure product is positive with a probability of greater than ½, then under certain conditions it is in general possible to apply the so-called statistical method for the determination of signs, and this consists basically of the use of the Zachariasen equality.

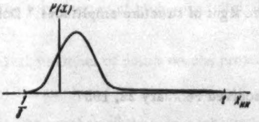

Fig. 1

Practical applications of this method have shown that it only leads to success when the signs of at least 10-20 strong amplitudes can be reliably determined.

The attempts of Karle and Hauptmann to show that the statistical method is not needed in this initial stage were unjustified. The fact is that there are very few strong structure products of the type $F_H^2 F_{2H}$, and that structure products of higher orders of type $F_H^2 F_K^2 F_{2H+2K}$) have a predominant positivity which is much less clearly expressed [10, 12].

In which cases can the first signs of the structure amplitudes be determinated by the direct method? In those cases in which we have among the structure products some which are reliably known to be positive. The direct method of analysis must begin with the selection of reliably positive structure products.

If among the amplitudes we have dozens which are large and near to 0.5 then the problem can be solved simply and quickly. If the structure is more complex and the maximum unitary structure amplitudes are of order 0.3-0.4, then the selection of the positive structure products can be made only if the strong amplitudes make up a Gramme determinant of sufficiently high order.

However, a more important consideration is that the selection of positive structure products serves not only as the first stage of direct analysis.

There is no doubt that the selection of reliably positive products can be carried far enough to make possible the construction of a series for the electron density.

The application of statistical considerations even to later stages of structure analysis is not necessary although it may be expedient.

The possibilities of the direct analysis of a structure by the method of selection of positive structure products are not yet quite clear and need study with the help of highspeed calculating machines.

The theoretical analysis [10] shows that direct methods are at any rate useful for structures with less than 100 effective atoms in the unit cell.

LITERATURE CITED

[1] D. Sayre, "The squaring method," Acta Cryst. 5, 60 (1952).

[2] W. Cochran, "A relation between the signs of structure products," Acta Cryst. 5, 65 (1952).

[3] W. H. Zachariasen, "A new analytical method for solving complex crystal structures," Acta Cryst. 5, 68 (1952).

[4] A. I. Kitaigorodskii, "The statistical method for the determination of signs," J. Exptl.-Theoret. Phys. (USSR) 24, 747 (1953); "The theory of the statistical method for the determination of signs," Doklady Akad. Nauk SSSR 94, 225 (1954).

[5] J. Karle and H. Hauptmann, "The probability distribution of the magnitude of a structure product," Acta Cryst. 6, 131 (1953).

[6] D. Harker and J. Kasper, Acta Cryst. 1, 70 (1948).

[7] J. Karle and H. Hauptmann, "The phases and magnitudes of structure products," Acta Cryst. 3, 181 (1950).

[8] J. A. Goedkoop, "Remarks on the theory of phase limiting inequalities and equalities," Acta Cryst. 3, 374 (1950).

[9] A. I. Kitaigorodskii, "The theory of the relation between structure amplitudes," Doklady Akad. Nauk SSSR 105, 482 (1955).

[10] A. I. Kitaigorodskii, The Theory of Structure Analysis, (1957).*

[11] E. F. Bertaut, "Fonctions de repartition," Acta Cryst. 8, 823 (1955).

[12] A. I. Kitaigorodskii, "The theory of the distribution of the signs of structure amplitudes," Doklady Akad. Nauk SSSR 101, 73 (1955).

Institute of Heteroorganic Compounds

Received February 22, 1957

---

* In Russian.

THE AUTOMATIC SYNTHESIS OF A TWO-DIMENSIONAL REPRESENTATION OF ATOMIC STRUCTURES

V.I. Vlasenko and G.S. Zhdanov

The problem is solved by converting the numerical tables obtained from high-speed digital computers into the electron density map. In order to fulfill this operation it is necessary to construct a two dimensional model of the electron density, then to dissect this model with a series of planes parallel to the XY-plane and to register the lines of intersection on a flat screen. All these operations are made by the electronic equipment. Thus an electron density map is obtained on the cathode-ray tube in a few seconds.

Statement of the problem. From the summation of the Fourier series the electronic calculators produce numerical tables [1, 2] which are then used in further analysis (the determination of the coordinates of the maxima, the calculation of interatomic distances, etc.). For this purpose it is desirable to carry out a quick survey of the results obtained. Numerical tables are of no use for this.

The introduction of high-speed digital computers alters on several counts the calculation of the Fourier synthesis:

a) the number of points on one projection reaches 10,000 or more;

b) the number of calculations of sections of the three-dimensional series may reach many dozens;

c) the number of digits in each number maybe greater than for the method of strips.

The machines produce a large amount of numerical material. In connection with this there arises the problem of the automatic processing of the numerical results obtained from the electronic calculating machines.

One of the first tasks in this direction is to devise an automatic method of synthesizing a representation of the electron density or of the Patterson function, which are obtained by the summation of Fourier series on an electronic calculating machine [3].

Two methods of synthesis of the representation. The important step in the synthesis is the two-dimensional interpolation from the initial data to obtain a continuous model of the function.

There are two possible methods of synthesis, which lead to:

a) a mosaic representation, or

b) a representation by contours.

In the mosaic case, use is made of the ability of the eye to see a large number of similar elements as a single unit (analogous to two-dimensional interpolation). The production of a mosaic representation is simple, but the results are rather coarse and can only serve as a preparatory analysis of the electron density function, which will latter be improved by the use of the necessary data from the numerical table.

In the second method the two-dimensional interpolation is carried out by a machine. The electron density function can be represented more accurately by the contour method.

The mosaic representation. The mosaic representation may be composed of various elements, the most convenient of which are colored squares.

To synthesize the colored mosaic one must carry out the following operations in an arrangement the block-scheme of which is shown in Fig. 1. The signal from the calculating machine 1 (usually this is the value of the function at one point, expressed in the binary system) enters the sorter 2. Depending on the size of this value there appears at one of the ten outputs to the sorter one pulse which corresponds to the automatic choice of one of the ten ranges.

This pulse enters the printer 3 which consists of ten type elements. When a pulse passes through the solenoid of a type element, the element is set in motion and makes an imprint of the corresponding color on the paper 4, which is fixed onto a drum.

The calculating machine gives in succession the results, which are then printed line by line in the form of squares of various colors, and thus the whole mosaic representation of the function is made up.

Figure 2 shows a contour representation of a function, made by hand from the numerical table in the usual way. The colored mosaic representation is only a little less clear than the contour representation.

The contour representation. The electron density function varies smoothly between maxima and minima and this reduces interpolation errors. The numerical results of the summation of the series, which are obtained as the output of the calculating machines, are passed into a special sorter, in which each number, which is expressed as a sum of impulses, is turned into one impulse with an amplitude proportional to the magnitude of the number. From a series of impulses along a line of the network of calculated values a continuous curve is formed by means of interpolation. This curve approximates to the function along a certain line.

The process of one-dimensional interpolation along the X-axis (Fig. 3) is the first stage of the reconstruction. One-dimensional interpolation parallel to the X-axis along all the lines of the table can not, however, lead to a complete reconstruction of the function. After the formation of continuous functions along all the lines parallel to the X-axis and their registration in a special accumulator, it becomes possible to carry out interpolation parallel to the Y-axis (Fig. 3).

The above transverse interpolation is based on the use of the data obtained in the first interpolation, which can be taken out of the accumulator in the desired order. Transverse interpolation can be carried out many times, since the curves in the accumulator are continuous and it is possible to obtain values of the function for any given value of X. As a result of transverse interpolation for a sufficient number of curves parallel to the Y-axis, a "continuous" two-dimensional surface is obtained – a reconstruction of the electron density function.

The final stage of the synthesis of the representation of the structure is the section of the model obtained of the two-dimensional function, consisting of the curve 4 (Fig. 3), by the planes 5 which are parallel to the XY plane, and the registration of the points of intersection 6 on a two-dimensional carrier, for which we may use either paper or the screen of a cathode-ray tube.

The section process is carried out in order, as the model of the function does not exist as a whole unit in time, and it is only because of the large number of points registered on the flat carrier that we may observe the representation of the reconstructed function as a whole unit. The points appear successively on the carrier in the order 1-2-3-4-5-6, etc., as shown in Fig. 4, i.e., along the lines. These lines cover the field of the representation, and, as a result, the points of equal level form contours.

The repetition of the reconstruction process with the next section of the model at a different level gives another set of contours which are registered together with those obtained above. (Fig. 4b).

Photoelectric reconstruction. The first stage of the reconstruction is the drawing of graphs for all the lines of the table. Each line of the table is automatically turned into a continuous smooth function 1 (Fig. 5) and is put on the drum in the form of a graph [4]. This process can be carried out in parallel with the summation of the Fourier series on the calculating machine. After all the graphs have been put on to the drum, the motor 3 is switched on and the drum begins to rotate with constant speed. Then the reading of the graphs drawn on the paper is carried out transversely (with respect to the direction of the recording). A narrow beam of light cuts the line of the graph and then its axis. When the beam cuts the black line the amount of light

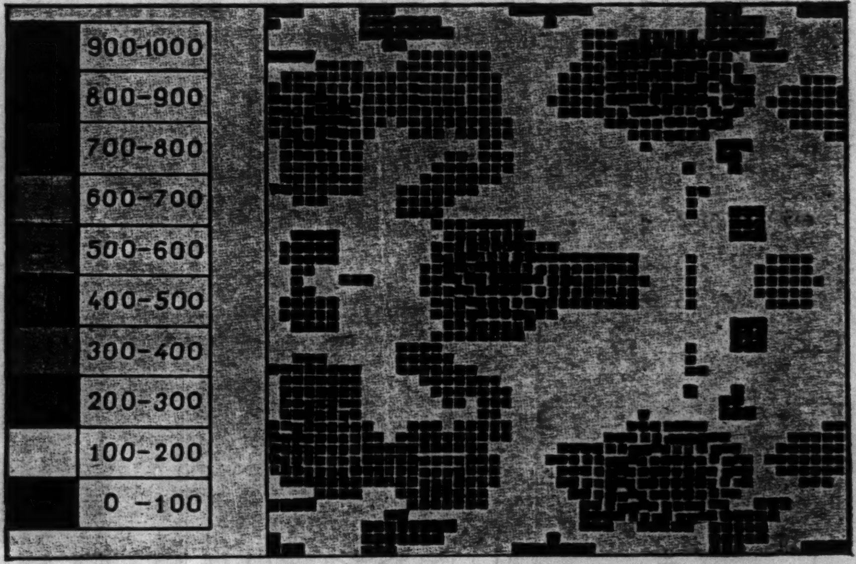
900-1000
800-900
700-800
600-700
500-600
400-500
300-400
200-300
100-200
0 -100

Color mosaic representation of the atomic structure of anosovite. a) Assumed designation of magnitude of electron density by color; b) mosaic representation of structure. (Publisher's note – This illustration appeared in color in the Russian original.)

reflected from the paper is reduced and the impulse from the photoelement is smaller. It is evident that the time between the impulses due to the intersection of the light beam with the axis and with the graph is proportional to the distance between the points of intersection, since the velocity of the paper is constant. As a result the photoelement gives an output of a series of phase-modulated impulses, which are then fed into the demodulator 6 where a curve is formed which is equivalent to curve 4 in Fig. 3. The curves are fed into the amplitude discriminator 7, where the points of equal height are sorted out. These points are marked by impulses, which appear in the output of the discriminator when the initial intensity is equal to a given level. These impulses are transferred into the registration block 8, which actuates the recording element 9 and prints points on the paper. These points, as was shown above (see Fig. 4) form a contour. The process of reconstuction of the function and the registration of its representation occupies several minutes.

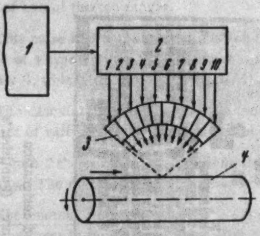

Fig. 1.

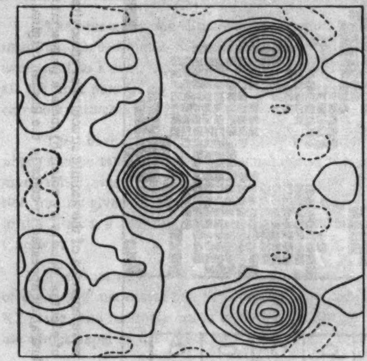

Fig. 2.

The magnetic representation. The processes described above for the synthesis of a representation of the electron density function can also be carried out using electronic apparatus which works with high speed. The accumulation of the intermediate data, which are obtained as the result of the first interpolation along the X-axis, can be carried out on a magnetic drum [2, 6]. The calculations of the necessary quantities and further work, i.e., the second interpolation, the sorting of the points of equal height and other operations are carried out in the electronic circuits of the apparatus.

On the surface of the magnetic drum it is necessary to record the curves corresponding to all the lines of the table in a corresponding number of lines parallel to the X-axis. Each curve occupies one circular path on the surface of the drum.

The first interpolation and the recording of the curves on the magnetic drum can be carried out in parallel with the solution of the problem as the results come out of the machine.

When all the results given by the calculating machine are recorded on the drum, the reconstruction apparatus, the block-scheme of which is shown in Fig. 6, begins to operate.

As the drum 1 revolves the reading of the recorded curves is carried out simultaneously by all the reading heads. In the circuit of each reading head 2 there is an amplifier 3 and a gate 4. The gate is usually shut and is only opened at the moment of arrival of a directing impulse from the commutator 5.

The magnitudes of the various quantities pass through the gate and enter the main bus bar in the form of short impulses. With the help of the commutator the gates of the reading system open successively at equal time intervals from the first channel to the last, and because of this one cycle of operation of the commutator produces a series of amplitude modulated pulses in the bus bar. This process is equivalent to the transverse reading of all the curves recorded on the drum. The direction of the transverse reading which is carried out using the gate and the commutator coincides with the direction of the axis of the drum.

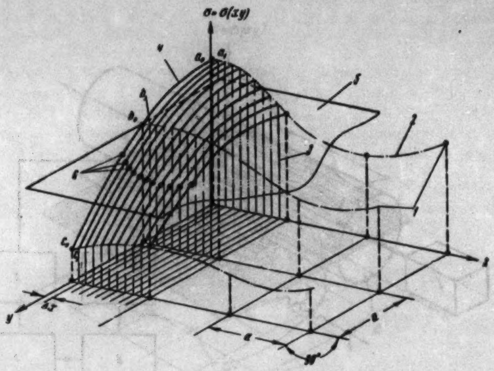

Fig. 3.

Then a curve is formed from the amplitude modulated impulses which appear in the main bus bar of the demodulator 7, i.e., the second interpolation is carried out parallel to the Y-axis (see Fig. 3).

One cycle of the work of the commutator produces one curve, which is obtained as the result of transverse reading parallel to the axis of the rotating magnetic drum. After the drum has been rotated through a certain angle the process is repeated.

By repeating the transverse reading cycle after very small angles of rotation of the drum, a large number of curves may be obtained and this determines the number of lines in the representation.

The curves are fed into the amplitude discriminator 8, the output from which is in the form of pulses which correspond to a given level of electron density. These impulses are recorded on the screen of the cathode-ray tube 9, the sequence of their appearance is shown in Fig. 4.

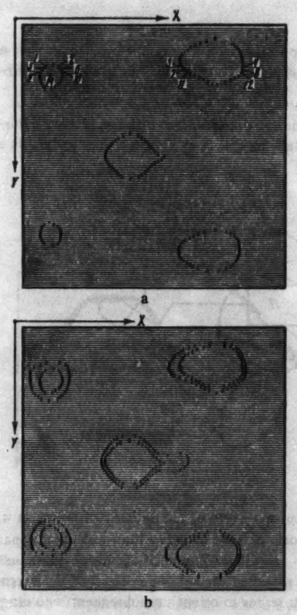

a

b

Fig. 4.

In the apparatus just described the "line and frame" synchronization of the operation of the elements of the scheme plays an important part. For the line synchronization the cycle of the opening of the gates 4 must proceed at the same time and with the same speed as the displacement of the lines in the tube 9. When the gate 1 opens, the beam of the tube 9 must be at the left hand side of the screen and when the gate n opens the beam must be on the right of the screen. This is achieved by the commutator 5 receiving a synchronizing pulse from the saw-tooth generator 12, which feeds the deflecting plates of the tube 9.

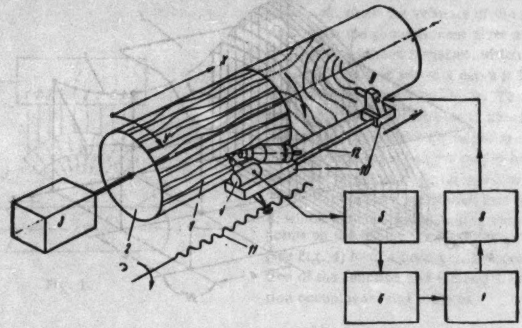

Fig. 5.

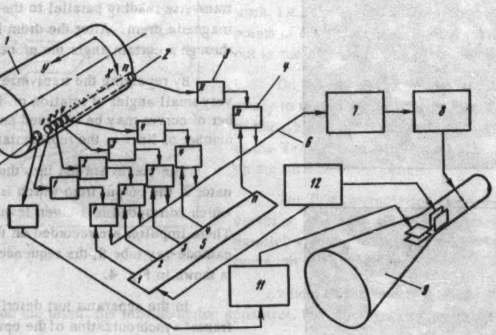

Fig. 6.

The synchronizing pulse excites the commutator and carries out the cycle of the opening of the gates 4. As a commutator we may use a moving register on ferrite ring cores or a set of delay lines and other apparatus. The frame synchronization is effected by a single pulse from the special reading head 10, which starts the saw-tooth generator 11. When the first electron density curve is recorded around the cylinder of the magnetic drum, the writing head 10 makes a record of a single pulse which serves to orient the subsequent recording of all the curves on the magnetic drum, as this pulse shows the position of the origin of all the curves written on the drum. Thus, the beginning of the magnetic model function is denoted by a pulse counted by the head 10,

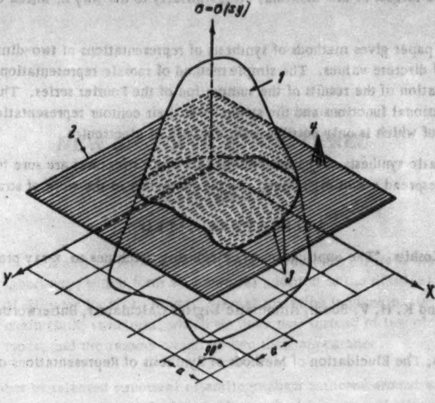

Fig. 7.

and the starting of the generator by this pulse ensures that the representation of the reconstructed function coincides with the edges of the screen of the cathode-ray tube.

As an experimental check of the suggested method of synthesis of a contour representation, a model was made which corresponded to the block scheme shown in Fig. 6, with, however, a small number of reading heads. For the check we took a simple two-dimensional function in the form of a single maximum, as shown in Fig. 7. This function was modelled in the electronic circuits of the mock-up and was cut by a plane at an arbitrary level. The result of this intersection was registered on the screen of the cathode-ray tube (Fig. 8). The small number of lines which were used in this synthesis (not more than 120), the nonlinearity of the line deployment and certain peculiarities of the amplitude discriminator lead to the coarse structure of the contour lines and to the breaking of the closed contour. An increase in the number of lines, an improvement of the linearity of the line deployment and improvements to the amplitude discriminator will doubtless remove the breaks and increase the sharpness of the contours. Figure 8 also shows the structure of a contour line, consisting of dashes made by the electron beam on the screen of the tube.

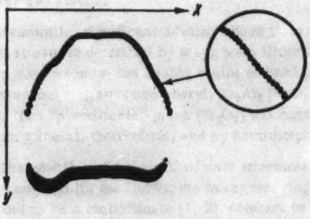

Fig. 8.

The representation of the function can be obtained within a few seconds of the completion of the summation of the Fourier series on the calculating machine.

For steady revolution of the magnetic drum the modelling of the function and the synthesis of the complete representation on the screen take place in one revolution. Since the afterglow of the screen is small the representation disappears and then the whole cycle of the synthesis is repeated. Modern types of magnetic drums enable speeds of up to 100 revolutions per second to be used, i.e., the representation of the function may appear and disappear 100 times a second. This dynamic method of modelling opens up additional possibilities for the investigation of the electron density function [3].

It is also possible to change the coordinate angle of the representation, to expand it along either the X or Y axes, to examine certain parts of the representation in a magnified form, to displace the representation on the screen in any direction, to change the contrast of the representation, i.e., to increase the difference between the smallest and largest of the maxima, etc., similarly to the way in which this is done in Pepinsky's machine XRAC [7].

Conclusion. The paper gives methods of synthesis of representations of two-dimensional functions which are described by a set of discrete values. The simple method of mosaic representation may find application in a preparatory examination of the results of the summation of the Fourier series. The method of dynamic modelling of two-dimensional functions and the synthesis of their contour representation have great possibilities, the realization of which is only possible with the help of electronics.

Methods of automatic synthesis of representations of atomic structures are sure to find application in connection with the widespread use of high-speed digital computers in the work of structure analysis.

LITERATURE CITED

[1] M. A. Porai-Koshits, "The application of calculating machines to x-ray problems," Kristallografiia (USSR) 1, 2 (1956).

[2] A. D. Booth and K. H. V. Booth, Automatic Digital Calculators, Butterworth Scientific Publications (London, 1955).

[3] V. I. Vlasenko, The Elucidation of Methods of Synthesis of Representations of Atomic Structures (Dissertation) (1956).

[4] George J. Mosons, "Analog interpolation for automatic control," J. Assoc. Comput. Machinery, 2, 2 (1956).

[5] V. V. Elmor and N. Sands, Electronics in Nuclear Physics [Russian translation] (1951).

[6] J. L. Douce and J. C. West, The Application of Analog Techniques to a Continuously Rotating Magnetic Drum, IRE Transactions of Instrumentation PGI-5, (1956) pp. 107-112.

[7] R. Pepinsky, Computing Methods and Phase Problems in x-Ray Crystal Analysis, x-Ray Crystal Analysis Lab., Pennsylvania State College (1952).

L. Ia. Karpov Institute of Physical Chemistry

Received February 22, 1957

NEW SILICATE STRUCTURES

N. V. Belov

A short review of about 10 such structures, all from the author's laboratory, which form a substantial addition to the classical system of silicates by W. L. Bragg. Special attention is given to six types of chain (lath) structures, which we have now instead of two classical types, and the reasons which govern their appearance.

In 1924-28, a number of talented structural crystallographers gathered around W. L. Bragg in Manchester (Pauling, Zachariasen, Warren, West, Naray-Svabo, Taylor) and with great enthusiasm made the first analyses of silicate structures. Their remarkable results were collected by Bragg in his "The Structure of Silicates" (1930-1931). The data and diagrams from this book and particularly those pertaining to the basic type of silicate structures entered into all courses in crystallography, geochemistry and mineralogy, and became frozen, as it were, to be repeated in the same form for 25 years. This stagnation reflected the actual state of affairs, at least in the years immediately after 1931 when Bragg's laboratory ceased to exist and its workers moved on to other subjects.

The work on silicate structures was renewed only after the second world war, when new scientists entered the field armed with more powerful methods of x-ray analysis permitting structural determinations of complex silicates of low symmetry by means of 40 or 50 parameters. Perhaps because of this complexity, the results of these studies were very slow in coming to the attention of crystallochemists and mineralogists. Moreover, much of the new work on the silicates was done in the USSR, published in Soviet journals and received little notice in the reviews abroad.

Meanwhile, significant advances have been made in recent years in the study of silicate structures. Almost all structures described by Bragg were illustrated by a single example. The chains $[SiO_3]_\infty$ were illustrated by pyroxenes only; the double chains or bands, by the amphiboles. Bragg mentioned only one metasilicate with hexagonal ring structure—beryl, $Be_3Al_2[Si_6O_{18}]$ — and one with trigonal ring structure—benitoite, $BaTi[Si_3O_9]$. The "pyrosilicate" group $[Si_2O_7]$ was considered exceptionally rare and was represented by a very rare scandium mineral, thortveitite, and by hemimorphite, whose structure is in doubt even now.

The new investigations of silicate structures have provided at least one more example for each of Bragg's types. Long ago (in the USSR), the hexagonal ring structure was found in dioptase—$Cu_6[Si_6O_{18}]\cdot H_2O$ — which turned out to be a metasilicate [1, 2], contrary to Bragg's statement (after Rammelsberg) that it is an orthosilicate with an impossible, from modern crystallochemical point of view, formula, $CuSiO_2(OH)_2$. The second example of a silicate with trigonal ring structure is the zirconium silicate catapleite, $Na_2Zr[Si_3O_9]\cdot 2H_2O$ from Khibina [3].

The metasilicate chains $[SiO_3]_\infty$, geometrically identical with pyroxene chains, have been found in a silicate [4] with the ratio O : Si of $4\frac{1}{2}$ rather than 3. This mineral is ramsayite—$Na_2Ti_2[Si_2O_9]$. A new type of cyclosilicate structure was discovered [5], the two-tier hexagonal ring $[Si_{12}O_{30}]$ in the very rare mineral milarite, $KCa_2(Si_2Be)[Si_{12}O_{30}]$. The remark that milarite is very rare has lost its significance since 1955 when it was shown [6, 7] that the rather neglected fact that cordierites of nearly identical composition may be either uniaxial or biaxial depends on structural differences; the biaxial cordierites have hexagonal rings of the beryl type $[(Si, Al)_6O_{18}]$, while in the uniaxial cordierites the rings are of the two-tier milarite type $[(Si, Al)_{12}O_{30}]$.

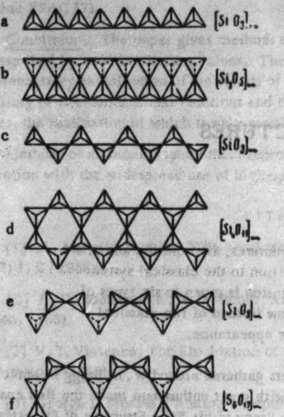

Fig. 1. Different types of infinite silica chains. a) The simple st chain — SiO_3 ∞; b) sillimanite c) pyroxene, d) amphibole; e) wollastonite; f) xonotlite.

The group $[Si_2O_7]$ has been found in many minerals and not only in those with formulas suggesting this structure, such as cuspidine, $Ca_4[Si_2O_7]F_2$ [8], or tilleyite, $Ca_5[Si_2O_7](CO_3)_2$ [9]; but, unexpectedly, in such generally known minerals as ilvaite, epidote and zoisite with the empirical orthosilicate formulas which had never been questioned by mineralogists and chemists. It is necessary here to recall the lone voice of Sobolev [10], who predicted the "pyrosilicate" nature of epidote long before any structural work had been done on it.

In ilvaite [11] all silica is concentrated in the $[S_2O_7]$ groups, since $CaFe'''Fe''_2\,Si_2O_8 \cdot OH = CaFe'''Fe''_2O\,[Si_2O_7]OH$, but in epidote [12], and zoisite [13] the structure contains both the orthosilicate and the "pyrosilicate" groups: $Ca_2Al_2Fe\,Si_3O_{12}OH = Ca_2Al_2FeO\,[SiO_4]\,[Si_2O_7]\,OH$. The eighth ion of oxygen in the formula of ilvaite and the twelfth ion of oxygen in epidote do not enter into the silicate radical. In ramsayite, $Na_2Ti_2[Si_2O_9] = Na_2Ti_2O_3\,[Si_2O_6]$ three oxygen ions out of nine are not tied in the silicpn tetrahedra.

In the pyroxenes and in ramsayite, as has been pointed out, in spite of the difference in their empirical formulas, the chains $[SiO_3]_\infty$ are geometrically identical. In the pyroxenoid wollastonite, $CaSiO_3$, the chain structure $[SiO_3]_\infty$ is present [14] but it is quite different geometrically. Linking of two pyroxene (ramsayite) chains parallel to the mirror plane results in the amphibole band with the formula $[Si_4O_{11}]_\infty$ with hexagonal links (Fig. 1, d), but the coupling of wollastonite chains gives a band $[Si_6O_{17}]_\infty$ with octagonal links (Fig. 1, f). This band was discovered in a mineral of the wollastonite group, xonotlite, $6CaSiO_3 \cdot H_2O = Ca_6[Si_6O_{17}](OH)_2$, (important because of its role in the setting of cement and its hardness).

Instead of the two types of infinite chains of silicate tetrahedra figured in all texts based on Bragg's classical "The Structure of Silicates," six types are distinguished now (Fig. 1), three types of single chains with the same formula $[SiO_3]_\infty$ but geometrically different and three types of double chains with the formulas $[Si_2O_5]_\infty$, $[Si_4O_{11}]_\infty$ and $[Si_6O_{17}]_\infty$.*

The single chains of type c with the formula $[SiO_3]_\infty$ are characteristic of pyroxenes and of ramsayite; the single chains with the same formula but geometrically different e are found in wollastonite. The double chains, d, with the formula $[Si_4O_{11}]_\infty$ are typical of amphiboles, and those of type f $[Si_6O_{17}]_\infty$ of xonotlite.

The simplest type of single chain, a, with the formula $[WO_3]_\infty$ is known at present only in the copper metagermanate $CuGeO_3$, and the corresponding double chain (type b), in sillimanite, in which Si ions alternate with Al ions, forming bands with the formula $[SiAlO_5]_\infty$.

The ideas about the role of the silicate radicals have changed also. It was believed in the past that these radicals with their characteristic geometry—rings, chains, bands, sheets, three-dimensional frameworks—determined the morphological properties of the minerals because of their special rigidity, but now [16] it has become evident that the great strength of the silicate radicals does not make them rigid; on the contrary, they have a marked capacity for adapting themselves to the morphological characters of the other components of structure.

---

* These formulas result from the following "condensations" of two simple chains: $2SiO_3 - O = [Si_2O_5]_\infty$, $4SiO_3 - O = [Si_4O_{11}]_\infty$, $6SiO_3 - O = [Si_6O_{17}]_\infty$.

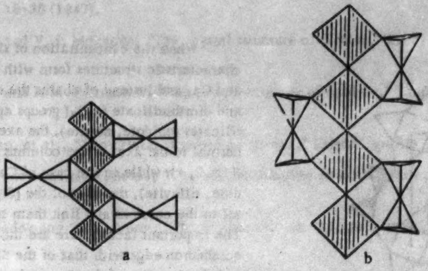

Fig. 2. Positions of the groups $[Si_2O_7]$. a) In minerals with columns of Al octahedra (epidote), b) in minerals with columns of Ca octaheda (cuspidine).

The ideas about the role of the silicate radicals have changed also. It was believed in the past that these radicals with their characteristic geometry—rings, chains, bands, sheets, three-dimensional frameworks—determined the morphological properties of the minerals because of their special rigidity, but now [16] it has become evident that the great strength of the silicate radicals does not make them rigid; on the contrary, they have a marked capacity for adapting themselves to the morphological characters of the other components of structure.

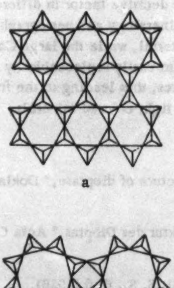

Fig. 3. Silicate sheets $[Si_2O_5]_\infty$. a) Hexagonal; b) tetragonal (undeformed).

Thus one of the few cubic tectosilicates (aluminosilicates), sodalite, owes its high symmetry to the large chlorine ions around which the aluminosilicate net forms "chinese lanterns" united into a lacy framework. The central part of the rhombohedral structure of dioptase consists of very rigid rhombohedral rings of six H_2O molecules as if carved out of ice structure and these are associated with hexagonal $[Si_6O_{18}]$ rings similar to those of beryl in composition but very different geometrically; the rings $[Si_6O_{18}]$ in beryl, in addition to the six-fold axis, have also an equatorial plane of symmetry, while in dioptase three silicon-tetrahedra point up and three down in obedience to the rhombohedral symmetry of the $(H_2O)_6$ rings of the ice structure.

The infinite (alumino) silicate sheets in platy silicates are the result of accommodation of the silicate radicals to the platy structures consisting of Mg(Fe) and Al octahedra characteristic of brucite, hydrargillite and even of corundum and occurring in talc, pyrophyllite, clays, micas and chlorites.

In the silicates characterized by elongated habit (columnar or acicular) columns of Mg(Fe), Ti or Al octahedra (pyroxenes, ramsayite, amphiboles), or of large Ca octahedra (wollastonite, xonotlite) are always found. If sufficient silica is present in the chemical formula, silicate chains and bands stretch parallel to the columns of octahedra, the type of chain depending on whether the octahedra are Mg(Fe) and Al, on the one hand, or Ca, on the other. Because of the considerable difference in the size of the octahedral edges, the Mg(Fe) and Al silicates are associated with chains of types a, b, c, and d of Fig. 1 while Ca silicates are associated with chains having larger links of types e and f.

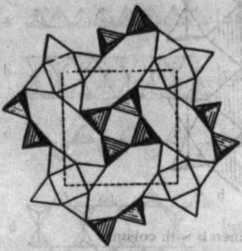

Fig. 4. Tetragonal silicate sheet in apophyllite.

When the concentration of silica is low, very characteristic structures form with columns of Mg, Al and Ca, and instead of chains the orthosilicate $[SiO_4]$ and diorthosilicate $[S_2O_7]$ groups appear. In the aluminosilicates (epidote, zoisite), the axes of the latter are normal to the axes of the columns of the Al octahedra (Fig. 2, a), while in the case of Ca octahedra (cuspidine, tilleyite), the axes of the $[Si_2O_7]$ groups are parallel to the columns and link them together (Fig. 2, b). The important factors here are the equality of an Al octahedron edge with that of the Si tetrahedron edge and the equality of the Ca octahedron edge to the height of the two joined silicon tetrahedra in the $[Si_2O_7]$ group.

With sufficient concentration of silica, the Mg(Fe) and Al cations are associated with bands with hexagonal links, while the Ca cations are associated with chains with octagonal links. With still higher concentration of silica, or with substitution of Al for a part of the Si ions in the tetrahedra, double chains unite into sheets without changing the form of their links, and as a result there are hexagonal sheets (pseudohexagonal) with six (continuously linked) rings in Mg(Fe) and Al silicates (Fig. 3, a) and tetragonal sheets with eight rings in the Ca silicates (Fig. 3, b). Geometry allows structures consisting of hexagonal rings only, but octagonal rings must necessarily alternate with square rings (Fig. 3, b). Large octagonal rings in the sheets are usually deformed with preservation of the four-fold symmetry axis as shown in Fig. 4, representing a sheet of the tetragonal mica, apophyllite. Hexagonal sheets do not usually condense into three-dimensional frameworks, and tetragonal sheets of the apophyllite type are rare since most of them condense into three-dimensional frameworks, mainly feldspars. Thus the decisive factor in differentiation of rocks into leucocratic and melanocratic components, so important in mineralogy and petrography, is the size of the cations; the smaller cations, Mg and Al, form melanocratic material, while the large Ca cations form the leucocratic material. The standard size of Mg and Al ions makes them easily replaceable by other ions, some of which are colored and especially by Fe in different oxidation states, thus leading to the formation of dark minerals. The large Ca ions are not readily replaced and tend to form light colored minerals.

LITERATURE CITED

[1] N. V. Belov, V. P. Butuzov and N. L. Golovastikov, "The crystal structure of dioptase," Doklady Akad. Nauk, SSSR, 87, 6 (1952).

[2] H. G. Heide, K. Boll-Dornberger, E. Thilo and E. M. Thilo, "Die Struktur des Dioptas," Acta Cryst., 8, 425-430 (1955).

[3] B. K. Brunowski, "Die Struktur des Katapleits" Acta Phys. Chem. U. R. S. S., 6, 6 (1936).

[4] N. V. Belov and L. M. Beliaev, "The crystal structure of ramsayite," Doklady, Akad. Nauk, SSSR, 69, 2 (1949).

[5] N. V. Belov and T. N. Tarkhova, "The crystal structure of milarite," Trudy Inst. Krist. 6, 83-140 (1951).

[6] A. Miyashiro, "Osumilite, a new silicate mineral and its crystal structure," Am. Mineral. 41, 104-116 (1956).

[7] N. V. Belov, Studies in Structural Mineralogy VII [in Russian] "Uniaxial cordierites," Collection, L'vov Geol. Soc. 10, 30-31 (1956).

[8] R. F. Smirnova, et al., "The crystal structure of cuspidine," Zap. Vsesoiuzn. Min. Ob-va 84, 21 (1955).

[9] J. V. Smits, "The crystal structure of tilleyite," Acta Cryst. 6, 9-18 (1953).

[10] V. S. Sobolev, "The significance of the coordination number of aluminum in silicates," Min. Sb. L'vovsk Geol. Ob-va 1, 16-30 (1947).

[11] N. V. Belov and V. I. Mokeeva, "The crystal structure of ilvaite," Trudy Inst. Krist. 9, 49-104 (1954).

[12] N. V. Belov and I. M. Rumanova, "The crystal structure of epidote," Trans. Inst. Krist. 9, 105-165 (1954).

[13] E. G. Fesenko, et al., "The crystal structure of zoisite," Kristallografiia 1, 2 (1956).

[14] Kh. S. Mamedov and N. V. Belov, "The crystal structure of wollastonite," Doklady Akad. Nauk SSSR, 107, 3 (1956).

[15] Kh. S. Mamedov and N. V. Belov, "The crystal structure of xonotlite," Zap. Vsesoiuzn. Min. Ob-va 85, 1 (1956).

[16] N. V. Belov, in the book: Studies in Structural Mineralogy, VI [in Russian],9 (1955), Collection, L'vov Geological Society.

Institute of Crystallography,
Academy of Science, USSR

Received March 11, 1957

THE ATOMIC CRYSTAL STRUCTURES OF COMPLEX ACID-AMINE NICKEL COMPOUNDS

M.A. Porai-Koshits, E.K. Iukhno, A.S. Antsishkina and L.M. Dikareva

An x-ray structure investigation of six complex nickel compounds has beeh carried out: $Ni(C_5H_5N)_4X_2$, where X = Br, NCS; $Ni(NH_3)_4X_2$, where $X = NO_2$, NCS; $NH_4Ni(NH_3)_3(NCS)_3$; $(NH_4)_2, Ni(NH_3)_2(NCS)_4$.

It is found that all the four thiocyanate-amine compounds are complex mononuclear compounds, all compounds of the NiA_4X_2 type characterized by a molecular octahedral complex.

Interatomic nickel-addend distances and the character of the chemical bonds in thiocyanate groups are established.

Some results of the crystallochemical investigation of complex compounds of bivalent cobalt and nickel have been published in reference [1]. An account is given here of the results of investigating six more acid-amine nickel compounds:

1) $Ni(C_5H_5N)_4Br_2$;
2) $Ni(C_5H_5N)_4(NCS)_2$;
3) $Ni(NH_3)_4(NO_2)_2$;
4) $Ni(NH_3)_4(NCS)_2$;
5) $NH_4[Ni(NH_3)_3(NCS)_3]$;
6) $(NH_4)_2[Ni(NH_3)_2(NCS)_4]\cdot H_2O$.

The first four compounds provide data for deciding on the structure of compounds of the NiA_4X_2 type, i.e., the location of the acid radicals with respect to the Ni atom. The available structural data on this question are extremely scarce; aside from the crystal structure of $NiPy_4Cl_2$ [2], there are only data concerning $Ni(CH_3COO)_2\cdot 4H_2O$ [3] and $Ni[SC(NH_2)_2]_4Cl_2$ [16]. In all three cases the acid radicals enter into the inner sphere of the complex.

The thiocyano-ammonium nickel compounds $Ni(NH_3)_4(NCS)_2$ are obtained by the addition of ammonia in an aqueous solution with Ni^{++}, NH_4^+ and NCS^- ions. Depending on the concentration and amount of NH_3, compounds of the four compositions indicated above separate out, and the question is posed whether these compounds — in the crystalline state — are binary salts or are complex.

The determination of the interatomic distances between a complex-forming atom and its addends, as always, permits a judgment about the character of the chemical reaction and the degree of stability of the complexes. It is regrettable that a precise determination of the distances was not possible in all cases.

Yet another problem in the structural investigation was the determination of the configuration, dimensions and orientation of the thiocyanate groups and the comparison of the results with the data of other investigations. Data on the crystallographic and crystallooptical character of all five compounds are given in Table 1.

TABLE 1

Crystallographic, Crystallooptical and Magnetic Characteristics of Crystals of Nitro- and Thiocyano-Ammonium Nickel Compounds

$Ni(C_5H_5N)_4Br_2$	$Ni(C_5H_5N)_4(NCS)_2$	$Ni(NH_3)_4(NO_2)_2$	$Ni(NH_3)_4(NCS)_2$	$i(NH_{3/3}(NCS)_2$	$NH_4[Ni(NH_3)_3(NCS)_3]$	$(NH_4)_2[Ni(NH_3)_2(NCS)_6]H_2O$
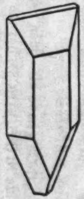	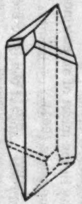	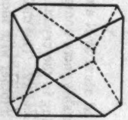	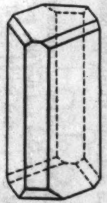	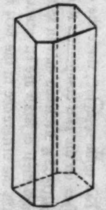	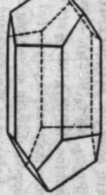	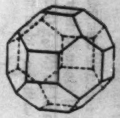
Fig. A	Fig. B	Fig. C	Fig. D	Fig. E	Fig. F	Fig. G
Green rhombic crystals	Sky-blue monoclinic crystals	Purple-red monoclinic crystals	Dark-blue monoclinic crystals	Blue-green rhombic crystals	Blue-violet trigonal crystals	Dark-blue cubic crystals
		$a:b:c=$ $=1.54:1:0.895$	$a:b:c=$ $=1.40:1:0.70$	$a:b:c=$ $=1.057:1:0.730$	$a:c=0.919$	
$a=15.8\pm0.1kX$ $b=9.3$ $c=14.2$	$a=12.3\pm0.1kX$ $b=13.2$ $c=16.2$ $\beta=120°$	$a=10.77\pm0.0.2kX$ $b=6.85$ $c=6.14$ $\beta=128°$ *	$a=11.46\pm0.02$ $b=8.18$ $c=5.68$ $\beta=105°$	$a=11.08\pm0.02$ $b=10.48$ $c=7.65$	$a=10.23$ $c=11.13$	$a=13.41$
N=4	N=4	N=2	N=2	N=4	N=3	N=6
$\sigma=1,67$ g/см³	$\sigma=1.40$ g/см³	$\sigma=1.72$ g/см³	$\sigma=1.55$ g/см³	$\sigma=1.603$ g/см³	$\sigma=1.493$ g/см³	$\sigma=1.523$ g/см³
F. gr. Pna	F. gr. $C2/c$ (or Cc)	F. gr. $C2/m$	F. gr. $C2/m$	F. gr. $Pbnm$	F. gr. $C\,3_121$	F. gr. $I\,23$
$n_g=1.700$	$n_g=1.718$	$n_g=1.660\pm0.003$	$n_g=1.674\pm0.003$	$n_g=1,748\pm0,003$		
$n_m=1.692$	$n_m=1.680$	$n_m=1.598$	$n_m=1.618$	$n_m=1.732$	$n_m=1.658$	$n=1.654$
$n_p=1.682$	$n_p=1.642$	$n_p=1.491$	$n_p=1.561$	$n_p=1.568$	$n_p=1.650$	
$\mu_{eff}=3.03$ BM	$\mu_{eff}=3.01$ BM	$\mu_{eff}=3,18$ BM	$\mu_{eff}=3.31$ BM	$\mu_{eff}=3.11$ BM	$\mu_{eff}=3.26$ BM	$\mu_{eff}=3.17$ BM
piezoeffect +	piezoeffect −	piezoeffect −	piezoeffect −	piezoeffect −	piezoeffect +	piezoeffect +

---

* Axis X of $Ni(NH_3)_4(NO_2)_2$ corresponds to direction [102] of $Ni(NH_3)_4(NCS)_2$.

All the experimental data were obtained by the method of photographing the reciprocal lattice (Mo-emission). The intensities were estimated with a calibrated density scale. Only the polarization and Lorentz factors were taken into account.

The first stages of the analysis were done with the aid of interatomic function distributions (both on the projections and, as necessary, in cross sections), and thereafter with the aid of electron density distributions, except in cases where centers of inversion were absent. In the examination of Ni $(NH_3)_3(NCS)_2$ the refinement of the atomic coordinates and the interatomic distances was accomplished with the aid of the "differential synthesis" method on the universal electronic computer BESM [4].

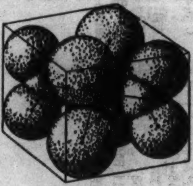

Fig. 1. Molecule of nickel-dinitrotetrammine, Ni $(NH_3)_4(NO_2)_2$.

Nickel compounds of the NiA_4X_2 type as a rule have a blue or green color [for example, Ni $(NH_3)_4(NCS)_2$, $NiPy_4Cl_2$, $NiPy_4Br_2$, $NiPy_4(NCS)_2$]. Crystals of nickel-dinitrotetrammine Ni $(NH_3)_4(NO_2)_2$ are quite anomalous in this regard – they have a purple-red color. It was natural to suppose that the anomalous color is connected with the character of the bonds and perhaps with a change in coordination of the nickel atoms. The latter supposition had to be rejected, since the crystallographic and x-ray data on the two compounds Ni $(NH_3)_4(NO_2)_2$ and Ni $(NH_3)_4(NCS)_2$ disclosed that in spite of the entirely different color their crystals are structurally isomorphic, although with the difference in the NO_2 and NCS addends there cannot be strict isomorphism.

The structural examination of nickel- dinitro- and dithiocyanotetrammine was facilitated by the fact that only two molecules fit into the base-centered unit cell of the crystal.

As a result of the examination it was clear that both substances have molecular structures in the crystalline state: the Ni atoms are surrounded by an octahedron with four NH_3 groups and two NO_2 groups (correspondingly NCS) in the trans-position, as in $NiPy_4Cl_2$ crystals. In spite of the fact that the structural investigation of the Ni $(C_5H_5N)_4Br_2$ and Ni $(C_5H_5N)_4(NCS)_2$ compounds is not quite complete, it is established that here also the acid radicals Br and NCS have direct contact with the Ni atoms. Thus all of these compounds are constructed from hexacoordination molecular compounds $[NiA_4X_2]$.

Both the nitro and thiocyano groups are connected with the central Ni atom by N atoms. Owing to the V-shaped form of the NO_2 group, the Ni $(NH_3)_4(NO_2)_2$ molecule is considerably more compact and, roughly speaking, has the rhombic prism form (Fig. 1), convenient for close packing in the crystal. The general structural patterns are given in Fig. 2 in the form of projections on planes xy and xz. The molecules are arranged in layers, parallel to the plane (102); the layers are superimposed on one another with successive displacements in just one direction according to the scheme in Fig. 3. From the packing standpoint the crystal is "four-story."*

It is clear that each successive layer of molecules can in principle be superimposed with a displacement both in the positive and in the negative direction. This explains why in the midst of an enormous number of growing crystals only isolated chance specimens were not twins along plane (001).

The molecule of nickel-dithiocyanotetrammine is considerably less compact owing to the presence of "tails," formed by linear NCS groups stretched out in the direction of the SCN – Ni – NCS bond. It therefore seems paradoxical that the molecules are packed in the crystal in the same type of structure as the Ni $(NH_3)_4(NO_2)_2$ molecules, and the difference consists only in a change in the relative dimensions of the edges a, b, c of the cell, so that the space in the second compound is not made use of as well as in the first: the packing coefficients in the first and second compounds equal respectively 0.742 and 0.721.

The crystal structures of nickel-dithiocyanotriammine Ni $(NH_3)_3(NCS)_2$ have also been mentioned in reference [1]. This compound also is molecular. The complex molecule Ni $(NH_3)_3(NCS)_2$ has the form of a tetragonal pyramid with the Ni atom at the origin (coordination number 5). The coordination of Ni adds up to 6 on

---

* Through every four stories the molecules are superimposed precisely one above another, which produces the rhombic pseudosymmetry in the projection on plane xz. An analogous structural pattern is 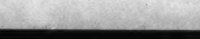 [5].

account of the S atom from the thiocyano group of the adjoining molecule (Scheme 1). This compound is the antianalog of K-tetrathiocyanocadmate, $K_2Cd(SCN)_4 \cdot 2H_2O$; in the latter, four thiocyano groups are distributed around Cd in a square and connected with it through the S atoms; the coordination of Cd adds up to six on account of the two N atoms from the thiocyano groups of the adjoining complex ions [6].

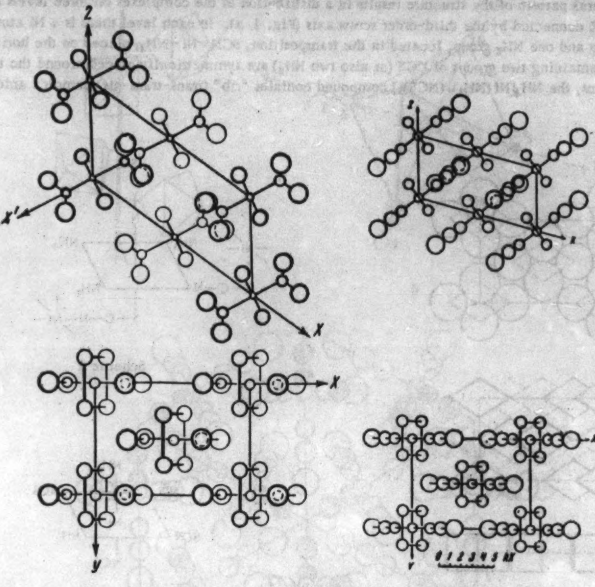

a b

Fig. 2. The structural pattern in a crystal of nickel-dinitrotetrammine $Ni(NH_3)_4(NO_2)_2$ (a) and nickel-dithiocyanotetrammine $Ni(NH_3)_4(NCS)_2$ (b). Projection on planes (010) and (001). X' – the direction of axis assumed in measuring the crystal of $Ni(NH_3)_4(NO_2)_2$, X – for arrangement assumed in measuring the crystal of $Ni(NH_3)_4(NCS)_2$.

Crystals of ammonium trithiocyanotriamminonickelate $NH_4[Ni(NH_3)_3(NCS)_3]$ are obtained in the form of coarse (a centimeter and more) monocrystals. The considerable piezoelectric effect,* approaching the value of the quartz piezoeffect, in conjunction with the capacity for growth, imparts to these crystals a practical interest.

The trigonal crystals of $NH_4[Ni(NH_3)_3(NCS)_3]$ have a much more complex structure. Their analysis was hampered by the absence of centers of inversion. There was no certainty even that this was a complex compound, for it can also have a purely ionic structure: $Ni^{++} \cdot (NH_4)^+ \cdot 3(NCS)^- \cdot 3NH_3$, similar to crystals of $Ba(SCN)_2 \cdot 2H_2O$ [7] (the isolated Ba^{++} ions, the $(SCN)^-$ ions grouped in pairs in the antiparallel position and the molecules of water). There might also be expected the binary salts $Ni(NCS)_2 \cdot NH_4NCS \cdot 3NH_3$ in analogy with $Hg(SCN)_2 \cdot NH_4NCS$, consisting in the crystalline state of molecules of $Hg(SCN)_2$ and ions of NH_4^+ and NCS^- [8].

---

* The piezoelectric effect was measured by V. A. Koptsik (the physical faculty of MGU), for which the authors express appreciation.

The structural investigation did however reveal the existence of octahedral complex ions $[Ni(NH_3)_3(NCS)_3]^-$ in the crystal.

The thiocyano groups are connected with the Ni atom through the N atoms and are placed almost precisely in line with the direction of the Ni–N bond.

The general pattern of the structure results in a distribution of the complexes on three levels along the principal axis Z connected by the third-order screw axis (Fig. 4, a). In each level there is a Ni atom, one thiocyano group and one NH_3 group, located in the transposition, SCN–Ni–NH_3, placed on the horizontal twofold axis; the remaining two groups of NCS (as also two NH_3) are symmetrically placed around the twofold axis (Fig. 4, b). Thus, the $NH_4[Ni(NH_3)_3(NCS)_3]$ compound contains "rib" (trans-trans-cis) complex anions (Scheme 2).

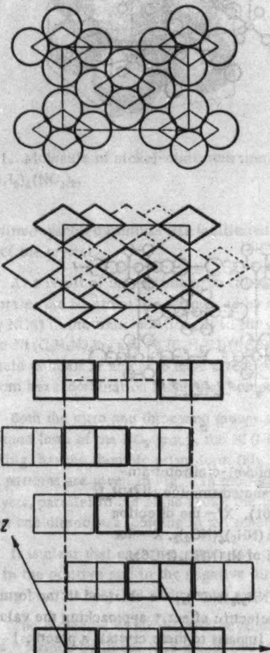

Fig. 3. Scheme of superposition of layers in the structure of nickel-dinitrotetrammine.

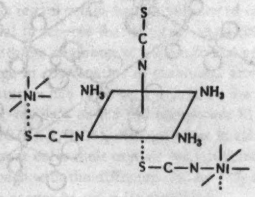

Scheme 1

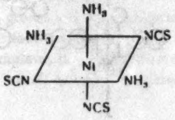

Scheme 2

The NH_4^+ ions are located between the layers of the complexes (at heights 1/6, 3/6 and 5/6). Each NH_4 is surrounded in an octahedron by six S atoms from the thiocyano groups.

If the complexes are formally considered as packed "spheres," then the structure will be analogous to NaCl: the NH_4^+ ions occupy all the octahedral voids of the three-layer (rhombohedral) packing. In another aspect the Ni and S atoms are arranged in the pattern of the face-centered cubic lattice of the perovskite type out of cubo-octahedra and octahedra, alternating along the principal axis: the cubo-octahedra out of the S atoms are occupied by the Ni atoms (and the remaining addends of the complex anion), and the octahedra by the NH_4 cations.

Somewhat different formulas may also be ascribed to the $(NH_4)_2[Ni(NH_3)_2(NCS)_4] \cdot H_2O$ compound if it be assumed that it is purely ionic or binary, made from NH_4NCS molecules and complex molecules (or ions) or, lastly, is purely complex.

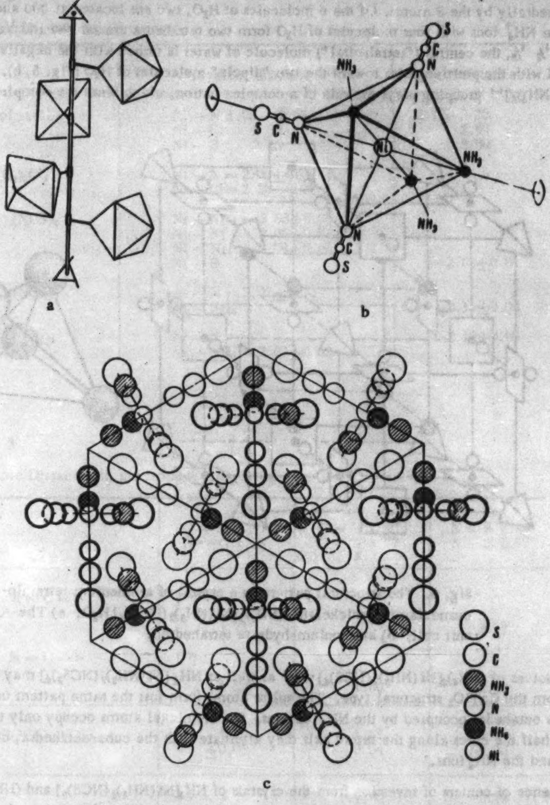

Fig. 4. The structural pattern in a crystal of ammonium trithiocyanotriamminonickelate, $NH_4[Ni(NH_3)_3(NCS)_3]$. a) symmetrical connection of complexes with one another; b) symmetry of the complex; c) projection of the structure on plane (001).

The structural analysis showed that this compound in the solid state is a complex one with the formula $(NH_4)_2^+[Ni(NH_3)_2(NCS)_4]^{--}H_2O$. The ions $[Ni(NH_3)_2(NCS)_4]^{--}$ have trans-structure. The thiocyano groups here are also connected with the Ni atoms through the N atoms.

The cubic crystals of NH_4-tetrathiocyanodiamminonickelate as well as of trithiocyanonickelate do not have centers of inversion (group I 23; N = 6). The structural pattern can be described in the following manner. The unit cell is divided into eight cubelets with edges a/2 (Fig. 5, a). The Ni atoms of the complex ions

$[Ni(NH_3)_2(NCS)_4]^{--}$ are placed in six of the eight vertices of the cubelets; points 000 and ½ ½ ½ of the cell remain free. The $NH_3-Ni-NH_3$ bonds are oriented along the edges of the cubelets, and the $SCN-Ni-NCS$ bonds along the diagonals of their base, while the S atoms prove to be approximately in the centers of the faces of the cubelets. Of the 12 NH_4^+ ions in the cell, 8 are placed in the body-centers of the cubelets and are surrounded octahedrally by the S atoms. Of the 6 molecules of H_2O, two are located at 000 and ½ ½ ½. The remaining four NH_4^+ ions with four molecules of H_2O form two tetrahedra around 000 and ½ ½ ½. Located at 000 or ½ ½ ½, the central ("tetrahedral") molecule of water is turned with the negative poles toward the two NH_4^+, and with the positive poles toward the two "dipole" molecules of H_2O (Fig. 5, b). On the whole the $[H_2O(H_2O)_2 \cdot (NH_4)_2]^{++}$ grouping plays the role of a complex cation, which binds the complex Ni anions.

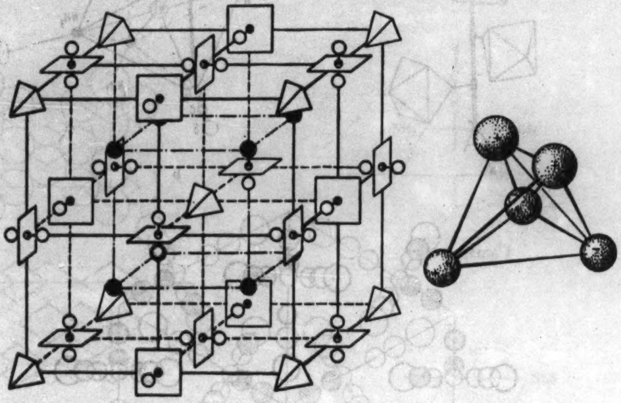

a b

Fig. 5. The structural pattern in a crystal of ammonium tetrathiocyanodiamminonickelate, $(NH_4)_2[Ni(NH_3)_2(NCS)_4]H_2O$. a) The unit cell; b) ammonium-hydrate tetrahedron.

The structure of $(NH_4)_2[Ni(NH_3)_2(NCS)_4] \cdot H_2O$ as well as $NH_4[Ni(NH_3)_3(NCS_3)_4]$ may be formally described, proceeding from the $CaTiO_3$ structural type. The sulfur atoms form just the same pattern of cubo-octahedra and octahedra, the octahedra occupied by the NH_4^+ cations. But the nickel atoms occupy only three-fourths of cubo-octahedra; in half the cores along the tetrad axis they alternate with the cubo-octahedra, occupied by the molecules of H_2O and the NH_4 ions.

The absence of centers of inversion from the crystals of $NH_4[Ni(NH_3)_3(NCS)_3]$ and $(NH_4)_2[Ni(NH_3)_2(NCS)_4] \cdot H_2O$ prevents an exact determination of the metal-addend distances and the distances in the thiocyano groups. The data on the Ni-addend distances, obtained in the structural analyses of $Ni(NH_3)_4(NO_2)_2$, $Ni(NH_3)_4(NCS)_2$ and $Ni(NH_3)_3(NCS)_2$ and also $Ni(C_5H_5N)_4Cl_2$, are assembled in Table 2. Even with the very same octahedral configuration of complexes and approximately the same magnetic moments, indicating the presence of two uncoupled electrons, the character of the bond in these compounds is somewhat different. In B $Ni(C_5H_5N)_4Cl_2$ and $Ni(NH_3)_3(NCS)_2$ all the Ni-addend distances approach the covalent (with the exception of Ni–S in the second compound – the distance from Ni to the sixth addend, S from the adjoining molecule). In $Ni(NH_3)_4(NCS)_2$ and $Ni(NH_3)_4(NO_2)_2$ some of the bonds are weakened: in the first, $Ni-NH_3$; in the second, however, the $Ni-NO_2$ bonds. It is interesting to note that two essentially different metal – NH_3 distances are also found in platinum compounds; one is of the order 2.0 A (for example, in Gerhardt salts, $Pt(NH_3)_2Cl_4$-trans [9], in Gros salts, $[Pt(NH_3)_4Cl_2]Cl_2$ [10]), the other is of the order 2.17 A (Cleve salt, $Pt(NH_3)_2Cl$-cis [11], Rieset's second base, $Pt(NH_3)_2Cl_2$-trans [12]).

In regard to the distances Me$-NO_2$ and Me$-$NCS, analogous systematic data on the element Me are as yet lacking.

TABLE 2

Interatomic Ni-addend Distances

	Covalent distance	Ionic distance
Sum of radii	Ni — N 1.95 — 2.05	2.15—2.25
	Ni — Cl 2.38	2.60
	Ni — S 2.25	2.60
$Ni(NC_5H_5)_4Cl_2$	Ni — N = 2.00±0.05	
	Ni — Cl = 2.39±0.01	
$Ni(NH_3)_2(NCS)_2$	$Ni - NH_3 = 2.08\pm0.05$	
	$Ni - N_I = 2.08\pm0.04$	
	$Ni - N_{II} = 2.04\pm0.04$	
	Ni — S	=2.62±0.01
$Ni(NH_3)_4(NCS)_2$	Ni — N = 2.07±0.03	
	$Ni - NH_3$	=2.15±0.02
$Ni(NH_3)_4(NO_2)_2$	Ni — N	=2.15±0.03
	$Ni - NH_3 = 2.07\pm0.03$	

TABLE 3

Interatomic Distances in the Isothiocyano Group

	N = C 1.26 N≡C 1.15	C = S 1.60 C — S 1.77	N ∼ S 2.86 N ∼ S 2.92
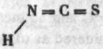	[14] 1.21	1.57	2.78
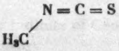	[15] 1.22	1.56	2.78
$Ni(NH_3)_4(NCS)_2$	1.20 ±0.05	1.61 ±0.04	2.81 ±0.03
$Ni(NH_3)_2(NCS)_2$	I 1.16 ±0.05 II 1.13 ±0.05	1.63 ±0.04 1.70 ±0.04	2.79 ±0.03 2.83 ±0.03

For the structure of Ni $(NH_3)_4(NO_2)_2$ it is characteristic that simultaneously with an increase in the Ni$-NO_2$ distance some decrease is observed (in comparison with the usual intermolecular) in the O$-NH_3$ distance at the contacts of adjoining molecules, which makes probable the presence of weak hydrogen bonds between the molecules. It is very likely that the anomalous coloring of the Ni $(NH_3)_4(NO_2)_2$ crystals is connected with the weakening of the Ni$-NO_2$ bonds, i.e., with the occurrence of NO_2-groups in an unusual valence state.

In Table 3 are shown the interatomic distances in the thiocyano groups. Comparison with the microwave

spectra data for isothiocyanic acid and methyl isothiocyanate shows that in $Ni(NH_3)_2(NCS)_2$ there is a considerable decrease in the N−C distance and an increase in the C−S distance. It appears that the bond between N and C here should be viewed as triple. This is in keeping with the geometry of the atomic arrangement: in agreement with the theory, the conjugate $Ni-N\equiv C$ bonds are placed in a straight line. The absence (or insignificance) of an analogous decrease of distance in $Ni(NH_3)_4(NCS)_2$ is rather strange, besides which the disposition of the Ni−N bond and the linear NCS group practically in a straight line rejects the combination of $Ni-N=C=S$ bonds, which require an angle with N ~ 100°, and the distance Ni−N equal to 2.07 A prevents treating the bond as ionic.

It should be noted that the C coordinate is not determined as exactly as the rest of the atoms, and it is possible that the distance N−C is a few hundredths A lower than that which results from analysis of the electron density. It is probably necessary to consider the Ni−N bond as intermediate between covalent and ionic, and the N−C bond as intermediate between double and triple.*

SUMMARY

1. In crystals of complex compounds of the NiA_4X_2 type that have been investigated so far, the Ni atom has octahedral coordination. The acid radicals enter into the inner sphere of the complex.

2. Compounds of $Ni(NH_3)_4X_2$ with X = NO_2 and NCS are iso-structural (if the difference in form of the NO_2- and NCS-groups is disregarded).

3. Thiocyano-ammonium Ni compounds of complex composition have in the crystalline state the structure of complex compounds. In $NH_4[Ni(NH_3)_3\cdot(NCS)_3]$ the complexes have octahedral trans-trans-cis structure; in $(NH_4)_2[Ni(NH_3)_2\cdot(NCS)_4]\cdot H_2O$ − trans-structure.

4. The compounds of Ni with thiocyano groups which were investigated are isothiocyanate complex compounds; the thiocyano groups are attached to the Ni atom by N atoms.

5. The NCS group is linear and is placed in line with the Ni−N bond.

6. In spite of the identical geometry of the complexes the character of the metal-addend bonds is different in different compounds: in $Ni(C_5H_5N)_4Cl_2$ all the bonds are covalent; in $Ni(NH_3)_4(NCS)_2$ the $Ni-NH_3$ bonds are weakened, in $Ni(NH_3)_4(NO_2)_2$ the $Ni-NO_2$ bonds are weakened. In the latter compound there probably are molecular hydrogen bonds. The anomalous red color of the crystals probably has some connection with the unusual valence state of the nitro group.

7. In the $Ni(NH_3)_3(NCS)_2$ compound there is a decrease in the distance N−C and an increase in C−S in comparison with those characteristic for $N=C=S$. The N−C bond should be considered as triple. In $Ni(NH_3)_4(NCS)_2$ this effect is less significant.

LITERATURE CITED

[1] M. A. Porai-Koshits, "X-ray examination of complex bivalent cobalt and nickel compounds," Trudy Inst. Krist. 10, 117 (1954).

[2] M. A. Porai-Koshits and A. S. Antsishkina, "The crystal structures of nickel-dichlorotetrapyridine and cobalt-dichlorotetrapyridine," Izv. Sektora Platiny 29, 19 (1955).

[3] J. N. Niekerk and F. R. L. Schoening, "The crystal structures of nickel acetate, $Ni(CH_3COO)_2\cdot 4H_2O$, and cobalt acetate, $Co(CH_3COO)_2\cdot 4H_2O$," Acta Cryst. 6, 609 (1953).

---

* It is curious to note that in the $K_2Co(NCS)_4\cdot 4H_2O$ compound, investigated by Zhdanov and Zvonkova [13], with the distance Co − N = 2.15 A (considerably greater than that observed in the nickel compounds, and signifying in the authors' opinion the predominant ionic character of the bonds) the thiocyano group is turned toward the bond at a 100° angle, i.e., as if the combination of single and double covalent bonds $Co^{\;N=C=S}$ had been accomplished.

[4] M. A. Porai-Koshits, "Refinement of the crystal structure parameters of nickel-triaminodithiocyanate (II) and cesium tetrachlorocobaltate by Fourier differential synthesis on the electronic computer," Izv. AN SSSR Ser. Fiz. 20, 740 (1956).

[5] R. Hulme, "The structure of p-di-isocyanobenzene," Acta Cryst. 5, 144 (1952).

[6] Z. V. Zvonkova, "The crystal structure of thiocyanates. VI. The crystal structures of complex zinc, cadmium and mercury tetrathiocyanates," Zhur. Fiz. Khim. 26, 1798 (1952); VII. "The crystal structure of complex platinum tetrathiocyanate," Zhur. Fiz. Khim. 26, 1804 (1952); VIII. "The crystal structure of complex rhodium hexathiocyanate," Zhur. Fiz. Khim. 27, 100 (1953).

[7] Z. V. Zvonkova and G. S. Zhdanov, "X-ray examination of $Ba(SCN)_2 \cdot 2H_2O$ crystals," Zhur. Fiz. Khim. 24, 1345 (1950).

[8] G. S. Zhdanov and V. V. Sanadze, "The crystal structure of thiocyanate. IV. X-ray examination of the crystal structure of $Hg(SCN)_2 \cdot ASCN$; A—K, NH_4," Zhur. Fiz. Khim. 26, 469 (1952).

[9] G. B. Bokii, M. A. Porai-Koshits and G. N. Tishchenko, "Refinement of atomic coordinates in the structure of Gerhardt salts, trans-$Pt(NH_3)_2Cl_4$," Izv. AN SSSR, OKhN 5, 481 (1951).

[10] M. A. Porai-Koshits and E. M. Romanova, "Refinement of interatomic distances in the crystal structure of trans-dichlorotetrammine chloride of platinum of valence 4," Izv. Sektora Platiny 28, 282 (1954).

[11] G. B. Bokii, G. A. Kukina and M. A. Porai-Koshits, "X-ray examination of platinum cis-tetrachlorodiammine crystals," Izv. Sektora Platiny 29, 5 (1955).

[12] M. A. Porai-Koshits, "The crystal structures of trans-dichlorodiammine platinum salts," Trudy Inst. Krist. 9, 229 (1954).

[13] G. S. Zhdanov and Z. V. Zvonkova, "The crystal structure of thiocyanates. II. The crystal structure of potassium tetrathiocyanocobaltate," Zhur. Fiz. Khim. 24, 1339 (1950).

[14] C. J. Beard and B. P. Dailey, "Microwave spectrum and structure of isothiocyanic acid," J. Chem. Phys. 15, 762 (1947).

[15] C. J. Beard and B. P. Dailey, "The structure and dipole moment of isothiocyanic acid," J. Chem. Phys. 18, 1437 (1950); Erratum, J. Chem. Phys. 19, 975 (1951).

[16] L. Cavalca, M. Nardelli and A. Braibanti, "La struttura cristallina del cloruro di tetratiourea-nichello (II)," Gazz. Chim. Ital. 86, 942 (1956).

N. S. Kurnakov Institute of General and
Inorganic Chemistry
M. V. Lomonosov Moscow State University

Received February 22, 1957

X-RAY INVESTIGATION OF CRYSTALS OF SOME FERROCENE DERIVATIVES

Iu. T. Struchkov and T.L. Khotsianova

The investigation of substituted ferrocene derivatives was undertaken in order to determine the configuration of their molecules in the crystal, since several configurations corresponding to different optical isomers are theoretically possible. It is also necessary to ascertain which are the determining factors in the choice of the configuration realized in the crystal; the specific interaction of the substituents or the tendency toward a minimum of steric hindrance in the molecule and toward a maximum packing density.

The crystals of diketoferrocenes are characterized by the following data:

	$Fe(C_5H_4COC_6H_5)_2$	$Fe(C_5H_4COCH_3)_2$	$Fe(C_5H_4COC_2H_5)_2$	$Fe(C_5H_4COC_3H_7)_2$
a (A)	11.69±0.02	14.89±0.07	13.40±0.04	11.84±0.11
b (A)	25.36±0.05	13.03±0.06	5.8±0.04	14.02±0.12
c (A)	6.27±0.01	5.90±0.03	37.92±0.12	9.74±0.05
β	90°±1°	90°±1°	—	—
n	4	4	8	4
Space group	$P2_1/n$	$P2_1/a$	*Pbca*	*Aba*

The most detailed structure examination is that of dibenzoylferrocene. The preliminary data on the structure amplitude signs were obtained by minimization of the three-dimensional Patterson function and by the statistical method. The atomic coordinates are established from the three-dimensional electron density map. The bond lengths have the following values: Fe−C = 2.05 ± 0.02 A; C−C = 1.41 ± 0.03 A (in the ferrocene ring); 1.39 ± 0.03 A (in the benzene rings) and 1.52 ± 0.02 A (between the atoms of the rings and the atoms of the keto groups); C = O = 1.21 ± 0.01 A. The benzene groups are not in the planes of the five-membered rings, but are brought out from them by rotation around the single C−C bonds. This leads to reduction of the steric hindrance in the molecule. In the crystal the molecule has an asymmetric configuration, which corresponds to the optical 1,2'-isomer, assuming the following numeration of atoms of the ferrocene ring:

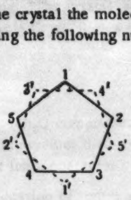

The determination of structure amplitude signs for diacetyl-, dipropionyl- and dibutyrylferrocenes was difficult because, owing to the special values of the coordinates, the iron atom does not take part in all of the reflections. Nevertheless a comparison of the unit cells of dibenzoyl-, diacetyl- and dipropionylferrocenes indicates their similarity and allowed an approximate orientation of the molecules in the cells of two adjoining compounds to be proposed. This approximate orientation was made more precise by the two-dimensional map, which also indicates a 1,2'-configuration. The molecule of dibutyrylferrocene occupies a peculiar position in the crystal, with symmetry 2; its position in the cell is also determined by the two-dimensional map.

Some other di-substituted compounds are at present being investigated: bis(p-bromophenyl)ferrocene, dimethyl ester of ferrocenedicarboxylic acid and dialkylferrocenes.

Institute of Heteroorganic Compounds

Received February 22, 1957

THE CRYSTAL STRUCTURES OF DIPHENYL HALOGEN COMPOUNDS

T.L. Khotsianova and Iu.T. Struchkov

The present work is part of an investigation by the authors of halogen compounds, i.e., compounds containing a halogen atom. X = Cl, Br, I in the valence state $>X^+ \leftrightarrow >X^-$. The best known representatives of this class of compounds have the formula 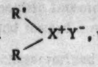 $\overset{R'}{\underset{R}{>}}X^+Y^-$, where R and R' are organic radicals, and Y^- is the anion of Cl^-, Br^-, I^-, BF_4^-, etc. The cases are well-known when the "anion" and the "cation" of the halogen compound are parts of one molecule, for example in phenyliodoniumdimedone 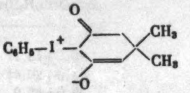

From the chemical standpoint, the investigation of similar compounds is of interest for determining the nature of the X–Y bond, which in a number of cases is not purely ionic and has an intermediate character, and for determining the valence configuration of the central atom of halogen X.

The crystals of diphenyliodonium chloride and iodide are isomorphous.

	$(C_2H_5)_2$ ICl	$(C_6H_5)_2$I
a. A	20.81±0.06	22.08±0.10
b. A	5.82±0.02	6.27±0.03
c. A	20.26±0.06	20.42±0.08
β	102°34′±30′	101°±1°
n	8	8
Space group	*C*2 / *c*	*C*2 / *c*

After the determination of the coordinates of the heavy atoms from the two-dimensional Patterson map P (x 0 z) and the Harker cross section, the structures of these compounds were refined by the calculation of the three-dimensional electron density map.

The lengths of the bonds have the following values: C–I = 2.08 A, I–Cl = 3.08A, I–I = 3.29 A. The I–Cl and I–I bonds are noticeably longer than the covalent and close to the ionic. The molecules of both compounds have a T-shaped configuration: C–I–C = 98°, C–I–Cl = 87° and 174°. The benzene rings are rotated around the I–C bonds relative to the plane C–I–C. In the crystal the molecules are united in "dimeric" pairs at the centers of symmetry ¼ ¼ 0, being bound by their own polar portions; the distances between them (I...Cl = 3.20 A, I.....I = 3.34 A) prove to be noticeably less than the sums of the Van der Waals radii. In the iodide crystals the intra- and intermolecular distance I...I is practically the same, so that this structure can be considered ionic. The packing of the nonpolar portions of the molecules (benzene rings) is accomplished with the usual density (Van der Waals radii I–2.1 A, C–1.8 A, H–1.1 A).

The crystals of the fluoroborates of diphenyliodonium, diphenylbromonium and diphenylchloronium proved to be nonisomorphous:

	$[(C_6H_5)_2I][BF_4]$	$[(C_6H_5)_2Br][BF_4]$	$[(C_6H_5)_2Cl][BF_4]$
a. A	6.05 ± 0.03	8.16 ± 0.03	18.85 ± 0.05
b. A	12.80 ± 0.04	14.80 ± 0.03	8.51 ± 0.02
c. A	17.26 ± 0.05	10.17 ± 0.10	21.60 ± 0.08
β	97°15′ ± 20′	96°30′ ± 30	125°20′ ± 30′
n	4	4	8
Space group.	$P2_1/c$	$P2_1/c$	$P2_1/c$

For determining the structure of diphenyliodonium fluoroborate, the two-dimensional Patterson functions, calculated from the 0k*l*, 1k*l*, and 3k*l* reflections, and the three-dimensional electron density map were used. The structural investigations of the fluoroborates of diphenylbromonium and diphenylchloronium were carried out in less detail; a further refinement is proposed, carried out by the calculation of the three-dimensional electron density map. In these purely ionic structures the cations have an angular configuration in which the angle C−X−C is more than 90°, and the benzene rings are brought out from the plane C−X−C for elimination of the steric hindrance. The packing of these large-scale cations and tetrahedral anions $[BF_4]^-$ is interesting.

The noncentrosymmetric structure of the binary compound $(C_6H_5)_2ICl \cdot HgCl_2$ is determined by three Patterson projections and by electron density. The crystals belong to the space group $P\,2_1\,2_1\,2_1$ with four molecules in the cell (a = 13.5 ± 0.05 A, b = 5.82 ± 0.03 A, c = 18.60 ± 0.10 A). The molecules of $HgCl_2(C_6H_5)_2ICl$ lose their individuality: the structure is ionic and is formed by infinite ionic segments $[HgCl_3]^-_{\infty}$, being extended lengthwise from 2_1 [010]. The coordination polyhedrons of the Hg atoms are distorted trigonal bipyramids with common faces. The cations $(C_6H_5)_2I^+$ have an angular configuration.

Institute of Heteroorganic Compounds

Received February 22, 1957

ELECTRON DIFFRACTION STUDY OF NITRIDES AND CARBIDES OF TRANSITION METALS

Z.G. Pinsker and S.V. Kaverin

Electron diffraction studies of Fe, Cr, Mo, W and some carbides of Fe have been in progress. Structural data concerning the phases Fe_4N, Fe_2N, Fe_3N, CrN, MoN, Mo_2N, WN, W_2N, Fe_3C, Fe_4C and others have been obtained. In the course of studying nitridation processes, the phenomenon of nondiffusional rearrangement for Fe-, Cr- and Mo-nitrides has been discovered and investigated.

Carbides and nitrides of transition metals form an interesting group of crystallographic phases from the standpoint of many current problems in crystallochemistry. Meanwhile our knowledge of these phases and their crystallographic structure is far from being complete. The difficulty in forming the isolated nitrides or carbides, the insufficient sensitivity of the x-ray method for determining the positions of the nitrogen and carbon atoms, as well as other factors, limit the possibilities for x-ray analysis in this field.

In recent years a number of electron diffraction studies devoted to the formation processes of nitrides and carbides and to the structure of these phases have been published [1-10]. These researches were carried out either on films obtained by processing metallic layers in the appropriate gaseous medium, with vacuum condensation, or on carbide powders. Although the first method (processed films obtained in vacuum) does not exactly fulfill certain important technical objectives, it has a number of material advantages and interesting features, which are summarized in the following.

1. Purity of original metallic layers.

2. Ease in obtaining as desired both monocrystalline and polycrystalline samples of the phases being studied. The first are convenient for purposes of (qualitative) phase analysis and determination of the mutual orientation in various phase transitions; the second, for quantitative measurements of intensities necessary for a detailed structural investigation.

3. The possibility of the formation of separate phases.

4. The high diffusion rate of nitrogen and carbon into thin films.

5. The feasibility of using electron diffraction for localizing the light atoms in the lattice.

The chief difficulties of the method in question are: the absence of direct data on the chemical composition of the separate phases, which is, however, often the case with x-ray analysis, and the presence of dynamic diffusion of small crystals with linear dimension $> 3–5 \cdot 10^{-6}$ cm.

In the present report are cited some results of investigations of nitridation processes and gaseous cementation of Fe, Cr, Mo and W films and the corresponding phase structures.

EXPERIMENTAL METHODS

For obtaining the original films, Fe, Mo and W were vaporized from 0.3-0.5 mm diameter wires which had been heated up by the passage of a current. The vaporization of chromium was effected from molybdenum wire, electrolytically chrome-plated. After sublimation, salt crystals coated with films of the metal were subjected to annealing with a view to further recrystallization and achievement of equilibrium. Figs. 1 and 2 represent typical electron diffraction patterns from the original metallic films.

Proceeding to the nitridation of the films, it will be noted first of all that the system used here is wholly analogous to the process of commercial nitridation in a stream of ammonia. A greater temperature range is covered (on the low side). The diagram of the apparatus for nitridation is given in Fig. 3.

In the nitridation process the ammonia decomposes on the surface of the metal into nitrogen and hydrogen; this reversible reaction does not take place with appreciable speed until 275°C is reached, when the rate quickly increases with the temperature. In the equilibrium state in a closed space at 627°C, the dissociation reaches 99.8%, i.e., goes practically to completion. In the NH_3 stream the degree of dissociation drops considerably. The formation of nitrides by the action of ammonia on iron (or another metal) proceeds according to the formula:

$$2x\mathrm{Fe} + 2\mathrm{NH}_3 \rightleftharpoons 2\mathrm{Fe}_x\mathrm{N} + 3\mathrm{H}_2.$$

The reaction will proceed to the right provided that the escaping nitrogen is trapped by the metal and is removed from the gaseous phase. In the reverse direction, the reaction of nitride dissociation is determined by the desorption rate of the nitrogen and does not depend on the nitrogen content in the sample.

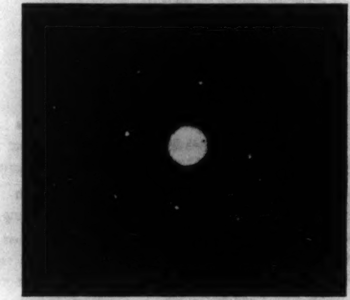

Fig. 1. Electron diffraction pattern from monocrystalline film of iron.

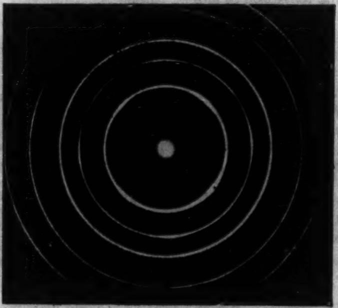

Fig. 2. Electron diffraction pattern from polycrystalline film of chromium.

The diffusion of nitrogen inside the granule (crystal particle) is the limiting factor in the formation of nitrides. In the course of the reaction the rate of formation of new nitrides will fall and at a definite stage it equals the rate of the reverse processes [11]. In order to shift the reaction toward the formation of a nitride with low nitrogen content, it is necessary to change the ratio of active nitrogen and ammonia, to introduce, for example, a preliminary dissociation. As the curves presented in [11] show, the smaller the concentration of NH_3 in the gaseous phase at a given temperature, the lower is the nitrogen content in the nitride so formed. By using the appropriate equilibrium conditions, it was possible to dissociate the Fe, Cr, Mo and W nitrides and to isolate in pure form the lower nitrides Fe_4N, Mo_2N and the higher Fe_3N, Fe_2N, CrN, MoN etc.

The conditions for the formation of these nitrides will be given below.

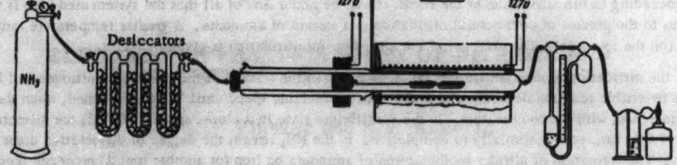

Fig. 3. Diagram of apparatus for nitridation of metallic films.

The process of gaseous cementation is in many respects like the process of nitridation but it also has peculiarities of its own.

1. Nitrides of the elements under study, beginning with iron, are relatively more resistant to oxidation than are carbides.

2. Nitridation is carried out in an atmosphere completely free of oxygen, and gaseous cementation is carried out in the majority of cases in a stream of CO. At temperatures of 400° and higher, CO is oxidized with the formation of atomic carbon

$$2CO \rightarrow CO_2 + \overset{\uparrow}{C};$$

but CO_2 is an oxidizing agent, and with a certain CO_2 and CO ratio this composition becomes useless for processing films. In the present experiments for cementation in a stream of CO, two systems were used.

1. A system with a stream of gas passing through it (see Fig. 4). In this the gas goes through a careful scrubbing and then enters the oven. The iron carbides Fe_3C and Fe_4C described in [5] were thus obtained.

2. A system with gas circulation. For better purification of the gas, the apparatus was first flushed with either CO or H_2 from 3 to 5 times. After this, part of the system was disconnected, and with the help of a pump, the gas was driven through the oven and the purifying system, comprising copper filings for oxygen absorption, desiccator (silica gel) and a Dewar flask for freezing out the CO_2. The second system functions much more stably, but it does not allow the ratio of active gas to be regulated, as is done in nitridation.

A system similar to nitridation can be used in this case if hydrocarbons serve as the active gas.

For the first experiments acetylene is most practicable. However, at normal pressure and a temperature higher than 300°C it very quickly decomposes with the formation of a large amount of carbon, which is deposited on the sample in the form of carbon black and makes a film useless for further electron diffraction study. In order to reduce the amount of precipitating carbon, the cementation had to be carried out in a vacuum of 10^{-2} mm Hg. In this atmosphere the same carbides were successfully obtained as in the stream of CO.

The FeN system. Fundamental results obtained by using the simplest method of nitridation have been presented in [4]. Diffraction from the γ-phase was observed only in common with diffraction from the hexagonal phase and it was usually represented by a few reflections. In these studies there was discovered the interesting phenomenon of a kinetic increase in the domain of existence of the γ-phase, which was made manifest by a considerable range of values for the period of the lattice: from a = 3.79, corresponding to x-ray data, to a = 3.91-3.92 A. This phenomenon can be understood if it be assumed that during nitridation the formation of nitride phases high in nitrogen occurs by way of superposition of two processes: diffusion with saturation by nitrogen of a poorer phase and the reorganization of the iron atoms in a new structure capable of absorbing a relatively large amount of nitrogen. In that case, with a high diffusion rate of nitrogen in the γ -phase, supersaturation can be reached in view of the delay in the reorganization γ ' → ε . What is the structural picture of this supersaturation ? An attempt can be made to decide this question by a careful study of the changes in intensity of the electron diffraction pattern reflections, which should be observed with so considerable an increase in the period of the lattice.

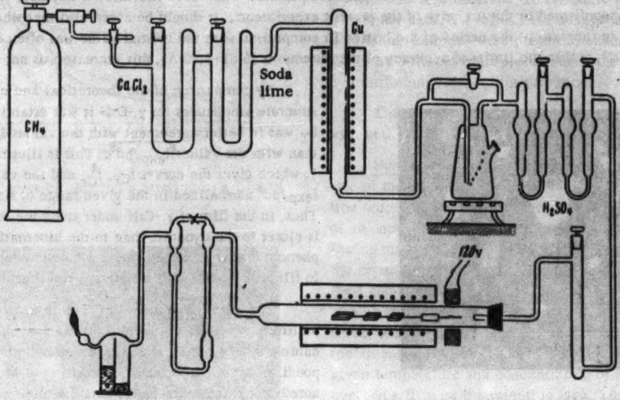

Fig. 4. Diagram of apparatus for cementation of films in a stream of gas passing through.

In the work referred to, a preliminary study was made of the hexagonal iron nitrides using a trial method and a geometric analysis of structures based on a quantitative determination of the intensities. A characteristic picture was established of the gradual enrichment by nitrogen of the hexagonal lattice of iron atoms with the formation of four ε -phases.

Further experiments have been conducted on the nitridation of iron films using a preliminary dissociation of ammonia.* These studies have demonstrated the accuracy of the above-described systems for control of reactions between ammonia and metal. For the first time, so far as is known, the γ -phase was obtained in pure form, from which different electron diffraction patterns were obtained (Figs. 5 and 6). The characteristic property of these electron diffraction patterns is the adequate intensity of the reflections 100, 110, 210 etc., owing to scattering from the primitive lattice formed by the nitrogen atoms. This circumstance is a graphic illustration of the high sensitivity of the electron diffraction method for the detection of light atoms. F^2 and F-series were calculated from the electron diffraction patterns of polycrystalline films of Fe_4N, on the basis of a qualitative determination of the intensities. In addition, by an F-series cross section in the direction of the space diagonal [111], a maximum in the center of the cell corresponding to the nitrogen atom was discovered, together with a maximum at the origin of the coordinates (Fe atom).

The Cr–N system. The notes given here will be brief, since a more detailed study is being completed with the assistance of L. N. Abrosimova.

In the Cr–N system the following are known from x-rays data: the hexagonal β -phase (Cr_2N) with periods a = 2.747 – 2.77 and c/a = 1.616 – 1.63; ε -phase (CrN; a = 2.75 A and c = 4.415 A); and the cubic γ -phase (CrN; a = 4.14 A). Note should be taken here of the poor reliability of data on the composition and periods of the lattices of hexagonal phases, and the interesting nature of the cubic phase CrN.

---

* Graduate students Velina and Nozik of the Gorkii University have taken part in this experimental series.

This phase has a structure of the NaCl type, in which the nitrogen atom has the "radius" of 2.07 − 1.27 = 0.80 A, which exceeds considerably the known value for R_N = 0.71 A; in the Fe_4N lattice the nitrogen, also located in the octahedral hollow, has a radius equal to 1.90 − 1.26 = 0.64 A.

In the initial experiments in chromium nitridation,* a cubic phase was obtained with period a = 4.14 A, in accordance with x-ray data. Electron diffraction patterns from this phase correspond to the normal structure of the NaCl type. Using iron filings as catalyst, a further series of experiments** gave a good idea of the formation conditions of this phase. In the absence of filings, a complex polyphase system is formed containing a number of hexagonal nitrides with as yet unestablished periods. The above indicated x-ray data for hexagonal nitrides are unconfirmed in the majority of the present experiments. It should be noted also that whereas in the case of Fe_3N an increase in the period of the lattice in comparison with the normal value was often observed, in the case of CrN, within the limits of accuracy of measurements (0.01-0.02 A), this increase was not observed.

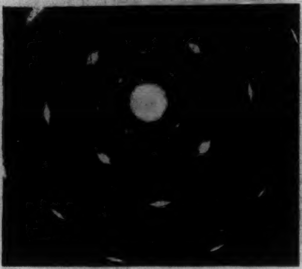

Fig. 5. Electron diffraction pattern from monocrystalline film of Fe_4N with "normal" period a = 3.79 A.

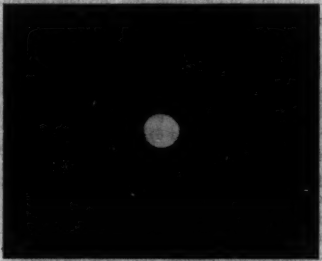

Fig. 6. Electron diffraction pattern from monocrystalline film of Fe_4N with increased period.

By comparison of the theoretical and experimental structure amplitudes for γ-CrN it was established that F_T was in better agreement with the values I_{exp}/pd^2 than with the values $\sqrt{I_{exp}/pd^2}$. This is illustrated in Fig. 7, which gives the curves f_{Cr}, f_{Cr}^2 and the values of I_{exp}/pd^2 normalized in the given range of $\sin\vartheta/\lambda$. Thus, in the film of γ-CrN under study the scattering is closer to the dynamic than to the kinematic. This phenomenon is at present being studied systematically in films of γ-CrN with a different small crystal size.

The Mo−N system. In [7] are presented some preliminary results of electron diffraction studies of the cubic phase of Mo_2N, and also hexagonal phases corresponding to the theoretical composition of MoN. It is noted that existing structural data for these phases undoubtedly require further study.

Thus, in the case of γ-Mo_2N, the structure of which has in its base a cubic face-centered lattice of Mo atoms, the nitrogen is represented by two atoms in the unit cell. The invariable presence on the electron diffraction patterns of reflections 100, 110 etc., is evidence of order in the arrangement of the nitrogen atoms in this structure. With two atoms in the cell, the only possible solution is a model in which one atom fits into the center of the cell ($\frac{1}{2}$ $\frac{1}{2}$ $\frac{1}{2}$), and the other is placed statistically in position in the middle of one of the edges ($\frac{1}{2}$ 0 0, 0 $\frac{1}{2}$ 0, 0 0 $\frac{1}{2}$). This rather artificial model has not as yet been confirmed in the present experiments. Potential maxima in the centers of the octahedra in one-dimensional sections along directions [111] and [100] of the γ-Mo_2N lattice have a ratio of heights equal to ~ 0.95 instead of 3.

In this connection it should be noted that here, as in the case of CrN, the scattering in some specimens lies between the dynamic and the kinematic, which must be taken into account in the determination of the structure amplitudes.

There is much confusion about the structures of the hexagonal phases of the composition ~ MoN. Our data only partially agree with the final results of Schönberg [12], because we have discovered the presence of two hexagonal lattices.

---

* With the assistance of graduate student M. Vasilevskaia.

** With the help of technical assistant L. Abrosimova.

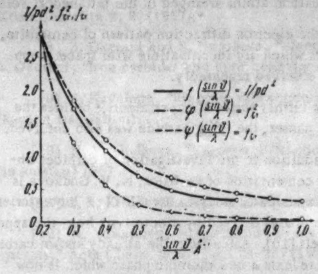

Fig. 7. Curves of electron scattering in a film of CrN.

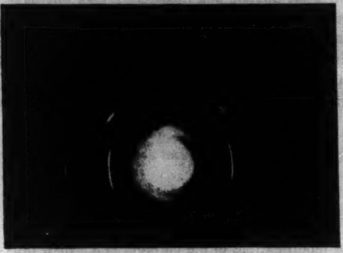

Fig. 8. Electron diffraction pattern from hexagonal W nitride.

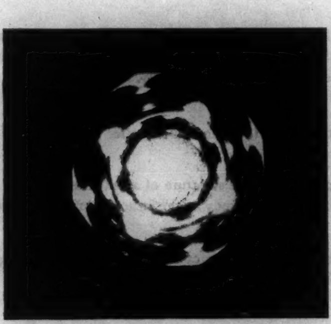

Fig. 9. Electron diffraction pattern from film of Cr nitrides, confirming nondiffusional conversion, cubic → hexagonal.

The W–N system.* Data on this system are extremely limited. In the literature there are indications of the existence of a cubic nitride γ-W_2N, analogous to γ-Mo_2N, and a hexagonal nitride WN. Nitridation of films of metallic W has been carried out by the present authors at temperatures of 700-600°C in a two-hour period. Lines of a cubic nitride with a period a = 4.118 A were observed, in complete agreement with x-ray data. As regards the hexagonal nitride, laminated structures were observed, characterized either by different multiple values of the period c or by insufficient order in this direction.

The period a of the hexagonal cell, in accordance with new x-ray data, equals 2.89 A (Fig. 8).

Nondiffusional Conversion in phase transitions. One of the material results of our study of the nitridation process in Fe films on rock salt is the observance of an unusual mechanism of the phase transition $\gamma' \rightarrow \epsilon$. During nitridation, when the saturation by nitrogen of the crystal particles of the γ'-phase comes to an end, their conversion to the ϵ-phase takes place by means of a nondiffusional reorganization of the iron lattice. Under ordinary conditions, for example in a massive specimen, no further processes would take place at the given temperature and concentration of nitrogen. However, in a film on the orienting face (100) of the rock salt, the crystals of the ϵ-phase, which have been termed regenerated, prove to be unstable. Their faces were found to be oriented parallel to the indicated face of NaCl, which in the new hexagonal axes is irrational. Therefore, with a somewhat longer time in the oven, recrystallization occurs with the formation of recrystallized small crystals of the ϵ-phase with plane $(11\bar{2}0)$ oriented parallel to the face of the cube of salt. The processes described, as shown in detail in [6], are very well established by the characteristic picture of the distribution of nodes on the rings of the hexagonal nitride, in particular by the presence of four pairs of nodes on the ring $(10\bar{1}1)$.

Further, in the study of the nitridation processes of Cr, Mo and W, completely analogous electron diffraction patterns were obtained (Fig. 9), from which it can be concluded that the phenomena described are general for processes on orienting surfaces.

The cementation of films and the structure of carbides. The results of our studies of the cementation of Fe films have been presented in [5]. In similar films the following carbide phases were observed: cementite, a hexagonal carbide and a hitherto unknown cubic phase with period a = 3.875 A. For cementite and the hexagonal carbide, periods in good agreement with the x-ray data were found. By analysis of the electron diffraction pattern of the cubic carbide (Fig. 10) it was established

---

* These preliminary results were obtained with the assistance of graduate student K. Tiul'nikova. A systematic investigation of the given system is being carried out by V. I. Khitrova.

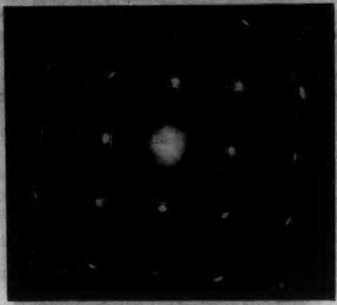

Fig. 10. Electron diffraction pattern from monocrystal α-Fe and polycrystal Fe_4C.

that its probable composition corresponds to the formula FeC_4, and the structure is characterized by a small distortion of the face-centered lattice of the iron atoms with the carbon atoms arranged in the tetrahedral voids.

In the electron diffraction pattern of cementite, reflections which are incompatible with space group D_{2h}^{16} were observed repeatedly.

In a further series of experiments,* besides the indicated phases, the Hägg carbide was also observed.

In addition to the investigation of carbides obtained by cementation of Fe films, N. V. Gudkova is making a systematic study in our GIFTI** laboratories of carbide phases derived by electrolysis from the appropriate steels [10]. Aside from the already known carbides, this study reveals a new rhombic phase which is now being investigated.

Finally, there is the recent work of the Japanese investigators Oketani and Nagakura [8, 9], who have studied carbides obtained by the action of a $CO + H_2$ mixture on Fe films coated with a fine powder of reduced iron. They have observed the hexagonal carbide (ϵ), the Hagg carbide χ and cementite θ. In studying the phase transitions $\epsilon \rightarrow \chi \rightarrow \theta$ and the further decomposition of Fe and C in the carbides during heating, they come to the conclusion that these transitions are of an allotropic nature and that the indicated carbide phases either have the same composition or are phases of variable composition in a wide range of carbon concentrations.

All of the foregoing characterizes the difficulty and complexity of the problems associated with the investigation of carbide phases in the Fe – C system.

LITERATURE CITED

[1] L. J. E. Hofer, E. M. Cohn and W. C. Peebles, "The modifications of the carbide, Fe_2C, their properties and identification," J. Am. Chem. Soc. 71, 189 (1949); E. M. Cohn and L. J. E. Hofer, "Some thermal reactions of the higher iron carbides," J. Chem. Phys. 21, 354 (1953); J. T. McCartney, L. J. E. Hofer, B. Seligman, J. A. Lecky, W. C. Peebles and R. B. Anderson, "Electron and x-ray diffraction studies of iron Fischer-Tropsch catalysts," J. Phys. Chem. 57, 730-736 (1953).

[2] J. J. Trillat and S. Oketani, "Etude par diffraction electronique de la cementation du fer par l'oxyde de carbone," Metalux & Corrosion 25, 302 (1950); "Etude par diffraction electronique de la cementation du fer," C. R. Acad. Science 230, 2203 (1950); "Cementation de cristaux uniques de fer," C. R. Acad. Science 233, 51 (1951).

[3] J. J. Trillat, S. Oketani, "Sur les relations d'orientation entre la cementite et le fer – α," Acta Cryst. 5, 469-471 (1952).

[4] Z. G. Pinsker and S. V. Kaverin, "Electron diffraction study of the structure of a cubic nitride of iron," Doklady Akad. Nauk SSSR 95, 797-799 (1954); "Electron diffraction study of the structure of hexagonal nitrides of iron," Doklady Akad. Nauk SSSR 96, 519-522 (1954).

[5] Z. G. Pinsker and S. V. Kaverin, "Electron diffraction study of the structure of the iron carbide Fe_4C," Kristallografiia 1, 1, 66-72 (1956).

---

*Calculated with the assistance of graduate student A. Smolinaia.

** Gor'kii Research Institute of Physics and Technology.

[6] Z. G. Pinsker and S. V. Kaverin, "The mechanism of phase transitions and nondiffusional transitions and nondiffusional transitions in the nitridation of iron," Trudy Inst. Krist. Akad. Nauk 12, 3-17 (1956).

[7] Z. G. Pinsker, S. V. Kaverin and N. V. Troitskaia, "Electron diffraction study of molybdenum nitrides," Kristallografiia 2, 2, (1957).*

[8] S. Oketani and S. Nagakura, "Electron diffraction study of iron carbides," (1956) (Russian translation); S. Oketani, "Iron carbides and their behavior in steel tempering," (1956) (Russian translation).

[9] S. Nagakura, "Electron diffraction study of iron carbides. Phase transitions of carbides," (1956) (Russian translation).

[10] N. V. Gudkova, "Electron diffraction study of iron carbides," Metal Physics and Metallography [in Russian] 1957.

[11] I. R. Krichevskii and N. E. Khazanova, J. Tech. Phys. (USSR) 21, 719 (1947).

[12] N. Schönberg, "Contribution to the knowledge of the molybdenum-nitrogen and the tungsten-nitrogen systems," Acta Chem. Scand. 8, 204-207 (1954).

Institute of Crystallography
Academy of Sciences USSR

Received March 7, 1957

---

* [See Soviet Physics — Crystallography].

DETERMINATION OF THE STRUCTURE OF CELADONITE BY ELECTRON DIFFRACTION

B.B. Zviagin

The possibilities of electron diffraction are realized for the complete determination of the structure of celadonite $K_{0.8}(M_{0.7}Fe_{1.4})[Al_{0.4}Si_{3.6}O_{10}](OH)_2$. The unit cell is a = 5.20; b = 9.00; c = 10.25 kX; $\beta = 100.1°$. Using Fourier syntheses the atomic coordinates and interatomic distances were found. The mean ratio of linear dimensions of octahedrons and tetrahedrons $k \simeq 1.11$. A number of distortions of ideal arrangements and regular forms of the polyhedrons and of the central locations in them of the cations were revealed.

Structural analysis of layered silicates is based on the concepts of their structure generalized from experimental data mainly in the works of Pauling [1], Bragg [2] and Belov [3]. These concepts deal with different types of layers conceived as definite combinations of two-dimensional tetrahedral and octahedral sheets, with the degree to which these polyhedra are populated by cations and with the character of the interlayer fill. They permit determination of the following structural details: 1) the manner of linkage (one of three) of two adjacent sheets; 2) their mutual orientation; 3) the form of the tetrahedral sheets which depends on the relative linear dimensions of the tetrahedra and octahedra; 4) distortion of the regular form of the polyhedra and displacement of cations from their central positions; 5) the exact interlayer structure; and 6) the arrangement of the layers in the structure. These characteristics have been established for only a few minerals and incompletely for most of these. Certain details have been obtained for some kaolinites and micas by the trial and error method from powder photographs.

Complete structural determinations have been made only for the coarsely crystalline varieties of these minerals, vermiculite and dickite, by the use of single crystals and application of harmonic analysis.

The electron diffraction method allows considerable advance in the study of the finely dispersed varieties of layered silicates and of clay minerals in particular. In the electron diffraction photographs the oblique structure of these minerals gives reflections distributed in two-dimensions and systematically grouped along ellipses according to their indices [4-7] thus permitting more accurate determination of reflection intensities.

The present investigation was based on electron diffraction photographs of samples of celadonite taken by E. K. Lazarenko [8], K. M. Malkova [9] and V. P. Shashkina. The best photographs were those of K. M. Malkina's sample 43-B. She also provided the structural-chemical formulas of celadonite.

The computation of theoretical structure amplitudes was based on the approximate formula $K_{0.8}(Mg_{0.7}Fe_{1.4})[Al_{0.4}Si_{3.6}O_{10}](OH)_2$ in which small amounts of other elements are neglected and potassium ions are substituted for $(H_3O)^{+1}$.

The investigations were carried out mainly on the electronograph EM-4 with focal length of 350 mm and a 4.5 by 6 cm^2 screen. Both transmission (from very thin films on a celluloid base) (Fig. 1) and reflection [7] (from precipitates on polished stainless steel) photographs were made. The latter, although they differed because of the ribbon-like form of celadonite from the photographs described in article [10], nevertheless contained reflections from 001. According to [7] the elongation corresponds to axis a, while the direction across the ribbon coincides with axis b. The determination of intensities was made on photographs with short exposures which showed a number of very weak reflections. The electron-diffraction apparatus at the Institute of Crystallography gave photographs 13 × 18cm² with a large diffraction field. Altogether it was possible to register 400 reflections.

The transformation of intensities I to the squares of structure amplitudes F^2 was made by the relation [4].

$$|F\ (hkl)|^2 \approx \frac{I_{hkl}}{pd_{hk0}} \qquad \text{(p – multiplicity factor)}$$

Even before construction of the syntheses, during the geometric analysis of the photographs, it was possible to arrive at a number of conclusions concerning the structure of layered silicates on the basis of the data concerning their unit cells, space groups and true and minimum values of c. Celadonite gives photographs of high quality with sharp reflections independent of the index k which indicates that it possesses a perfect structure.

The dimensions of the unit cell are [5]: a = 5.20 kX, b = 9.00 kX, c = 10.25 kX., β = 100.1°.

According to the value of the period c, which is small and sharp, celadonite consists of orderly stacking of three-layer silicate units with one-layer period.

Since the octahedra of the silicate layers share their edges, the structure they form is rigid, and the linear dimensions l of the octahedra determine the dimensions a and b of the unit cell. If it is assumed that the octahedra are regular, then

$$a = l\sqrt{3}, \quad b = 3l.$$

On the other hand, since the tetrahedra are linked by their vertices, the pattern of the net they form, as noted by Belov [11], may correspond to different values of a and b without any change in the linear dimensions l' of the tetrahedra, the variation in form being produced by the rotation of the tetrahedra about normals from the vertices to the linked bases. If the pattern of the net corresponding to the closest packing of anions, for which $l = l'$ is taken as the initial one, then any random pattern of regular tetrahedra can be obtained from it by the displacement t of the linked vertices along the three bisectrices of the initial pattern (which make 120° angles with each other) to the positions of the linked vertices in the new pattern. It is convenient to use the tetrahedral edges on these bisectrices $s = \frac{3t}{2}$ (Fig. 2).

If $l = kl'$, then between s (expressed as a fraction of the period a) and k, there exists the following relation:

$$s = \left(1 \pm \frac{\sqrt{4-3k^2}}{k}\right)/4.$$

According to this formula $k \geq 2/\sqrt{3}$. If $k \geq 2/\sqrt{3}$, two values of s correspond to each value of k.

If k = 1, $s_1 = 0$, which corresponds to the cubic closest packing, $s_2 = {}^1/_2$ corresponds to hexagonal packing. In both cases the openings in the tetrahedral net are triangles with sides $2l$ but with reversed orientation. For $k = 2/\sqrt{3}$, $s = {}^1/_4$ and the openings are regular hexagons with sides $l' = \frac{l\sqrt{3}}{2}$.

For intermediate values of k, $0 < s_1 < {}^1/_4$, and ${}^1/_4 < s_2 < {}^1/_2$, the openings are ditrigonal in both cases, but with reversed position of the angles $\gtrless 120°$.

The altitude of an octahedron can be expressed in terms of a since

$$h = \frac{l\sqrt{6}}{3} = \frac{a\sqrt{2}}{3}.$$

Comparing 4h and $\underline{c}\sin\beta$ for the triple-layer structures, the value of $\underline{k}$ may be estimated. A more exact determination of $\underline{k}$ can be obtained from projections of the syntheses of F^2 series on x0z and 0yz planes. Moreover, these projections show orientation of the sheets with respect to each other and their linkage in the layer.

In case of celadonite these projections (Fig. 3) clarified the main features of its structure which were taken as the basis for a model for computing structure amplitudes whose signs were then used in the construction of the F-series syntheses. The structure amplitudes were computed by the formulas given above, using atomic factors from Vainshtein's tables [4] for the model with $C_2^3h = C_m^3$ symmetry, with $k = 1.11$, $s = 0.135$.

Two projections of the syntheses of the F-series should suffice to determine the structure of celadonite completely. And, indeed, they showed clearly all the atoms in the structure.

However, the peaks for Si atoms are superimposed in the x0z projection (Fig. 4) on those for $O_{tetr.2}$ and in the 0yz projection on the peaks for $O_{tetr.1.3}$. Therefore, these projections give all coordinates except the $\underline{x}$ coordinates for $O_{tetr.2}$ and the coordinates $\underline{y}$ for $O_{tetr.1.3}$ (see also Fig. 2). In order to determine the masked peaks and their coordinates, syntheses were made omitting the Si atoms, but while the 0yz projection gave clear peaks for $O_{tetr.1.3}$, the x0z projection showed only weak peaks for $O_{tetr.2}$. A section of the F-series was then made along the x0z plane. This section (Fig. 5) showed very clearly the atoms of $O_{oct.}$, K and Mg, and, what is more important, the atoms of $O_{tetr.2}$, which lie on the $\underline{c}$ axis.

Thus Fourier syntheses completely determine the structure of celadonite.

It should be noted that the chemical composition of celadonite, even when given by a simplified formula, cannot be represented by the atoms of a single unit cell. Therefore, the determined dimensions of the unit cell are average. Different unit cells in the structure differ somewhat from each other in the position of various atoms within them and in the number of Mg atoms which occupy approximately 0.1 of the "vacant" octahedra of the dioctahedral pattern.

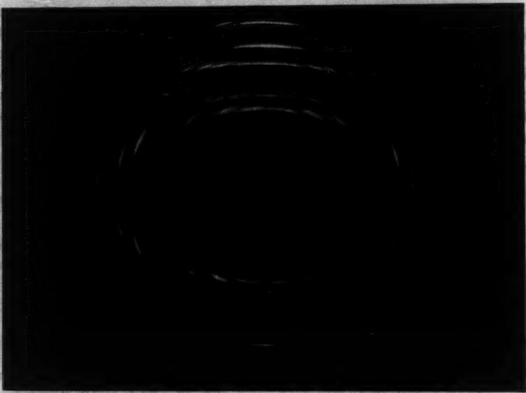

Fig. 1. Electron diffraction pattern of celadonite ($\varphi = 54°$).

Accordingly, in the syntheses given above some of the peaks are due to different atoms, for example to Si or Al, Fe or Mg.

Taking this into account, the structure of celadonite is represented by two diagrams: the normal projection on the xy0 plane (Fig. 6) which gives the coordinates of all atoms and by the three-dimensional diagram of a layer (Fig. 7) which shows all interatomic distances. For easier comparison, some of the $O_{oct.}$ and $O_{tetr.}$ atoms are numbered alike on the two diagrams.

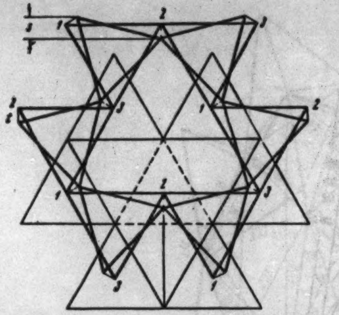

Fig. 2. Transformations of the pattern of tetrahedra (fine lines — edges of octahedra, heavy lines — edges of tetrahedra).

Taking this into account, the structure of celadonite is represented by two diagrams: the normal projection on the xy0 plane (Fig. 6) which gives the coordinates of all atoms and by the three-dimensional diagram of a layer (Fig. 7) which shows all interatomic distances. For easier comparison, some of the $O_{oct.}$ and $O_{tetr.}$ atoms are numbered alike on the two diagrams.

These diagrams show that celadonite structure deviates from the ideal structure with the closest cubic packing and is characterized by ditrigonal configuration of the tetrahedral net.

Besides this, as can be seen from Figs. 6 and 7, the celadonite structure shows a number of distortions of the ideal pattern and of the form of polyhedra as well as displacement of atoms from central positions within the polyhedra, although the average relation of the linear dimensions of the octahedra and tetrahedra is approximately the same as that taken as the basis for computing structure amplitudes. The $O_{tetr.1-3}$ atoms are shifted along the bisectrix by distance t' = 0.088a = 0.46 kX, the atoms of $O_{tetr.2}$, by t' = 0.116a = 0.6 kX; the atoms of Fe and Mg are displaced from the centers of octahedra along axis b toward the empty octahedra of the dioctahedral pattern by about 0.05 kX; the Si atoms are displaced from the centers of the tetrahedra toward their bases by about 0.1 kX; the atoms of O_{oct} deviate somewhat from their position above the Si atoms. As a result, the xy0 projection of the structure does not have a three-fold symmetry axis and of the three symmetry planes only one remains, that parallel to the monoclinic obliquity. These distortions, as shown by Fig. 7, are accompanied by certain differences in interatomic distances for like but differently positioned atoms and, as mentioned in [12], by shortening of the shared octahedral edges in relation to others.

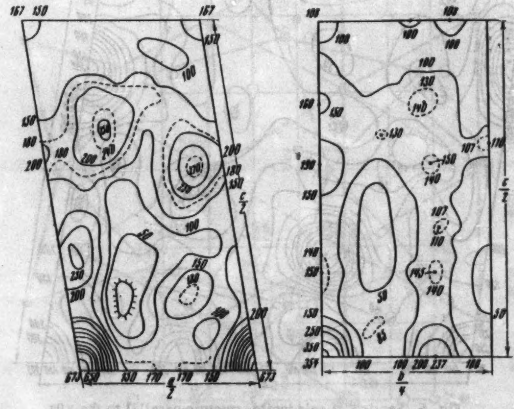

a

b

Fig. 3. Projection of the F^2-series of celadonite. a) On the x0z plane, b) on the 0yz plane.

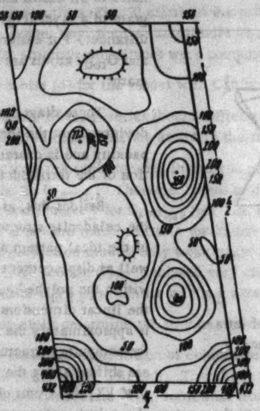

Fig. 4. Projection of the structure of celadonite on the x0z plane.

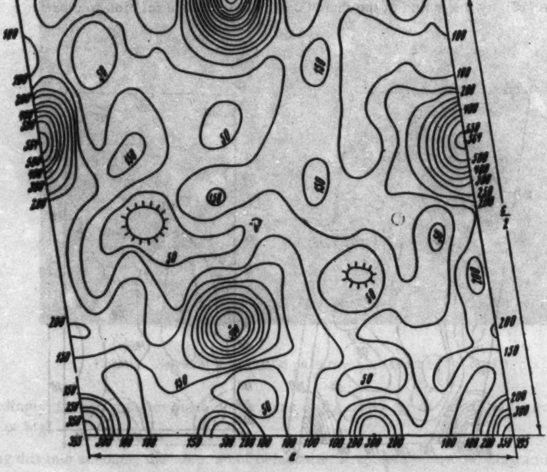

Fig. 5. Section of celadonite structure parallel to the x0z plane.

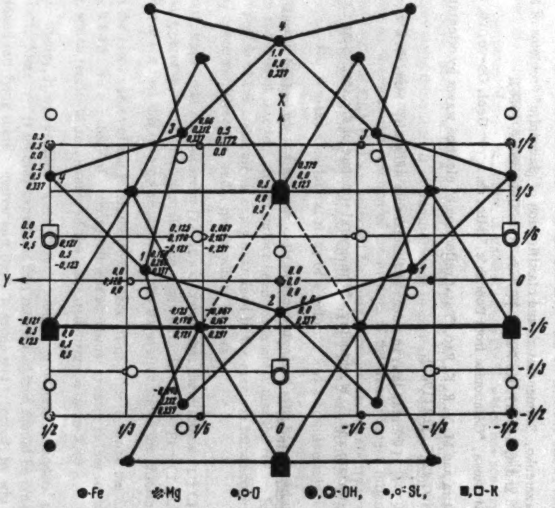
X
Y
1/2
1/3
1/6
0
-1/6
-1/3
-1/2
●-Fe
✲-Mg
●,○-O
●,○-OH,
•,∘-Si,
■,□-K

Fig. 6. Normal projection of celadonite structure on the x0y plane. Black symbols are atoms above the plane xy0, others are atoms under this plane. The numbers 0.433, 0.333, 0.291, 0.375, 0.330 and 0.121 at the center of the left tetrahedron are omitted.

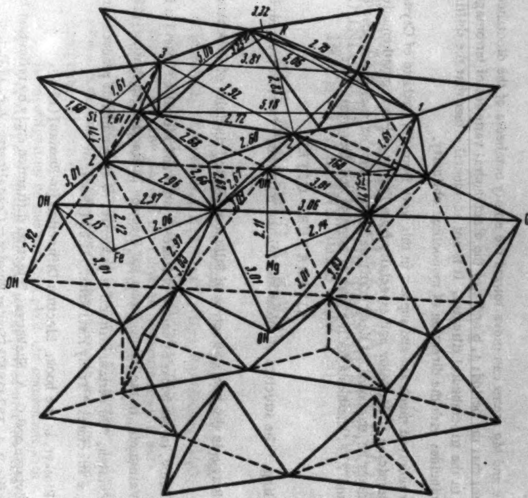
K
Si
Fe
Mg
OH
3.32
3.01
2.72
5.18
2.88
2.60
2.12
2.15
2.06
2.97
3.06
2.14
1.61

Fig. 7. A three-dimensional diagram of celadonite structure.

Evidently these distortions are due to variation in populations of the octahedra and to the interaction between the layers.

That the Fe and Mg atoms can move toward the empty octahedra of the dioctahedral pattern can be explained by the fact that the periods $\underline{a}$, $\underline{b}$ and $\underline{c}$ of the dioctahedral varieties of ferromagnesian layered silicates are smaller than in the trioctahedral silicates. It is not accidental either that the shifting of the $O_{\text{tetr.s}}$ along the bisectrices coincides with the direction of monoclinic obliquity.

The author received much aid and support in this work from the Institute of Crystallography, Acad. Sci. USSR, from Academician N. V. Belov and especially from Doctor of Physicomathematical Sciences B. K. Vainshtein. To them he expresses his deep gratitude. The author extends thanks also to E. K. Lazarenko, K. M. Malkova and V. P. Shashkina for the loan of samples and chemical data.

LITERATURE CITED

[1] L. Pauling, "The structure of micas and related minerals," Proc. Nat. Acad. Sci., U. S. 16, 123 (1930).

[2] W. L. Bragg, in the book: Structure of Silicates. Basic Principles of Geochemistry, III. [Russian translation] (1937).

[3] N. V. Belov, in the book: Structure of Ionic Crystals and Metallic Phases [in Russian] (1947).

[4] B. K. Vainshtein, in the book: Structural Electron Diffraction [in Russian] (1956).

[5] B. B. Zviagin, "On certain diffraction properties of clay minerals produced in electron diffraction patterns by oblique structures," Trudy Inst. Krist. 11, 86 (1955).

[6] Z. G. Pinsker, in the book: Electron Diffraction [in Russian] (1949).

[7] B. B. Zviagin, and G. A. Shakhova, "Electron diffraction study by reflection from powdered celadonite" Kristallografiia 2, 1, 182 (1957) [Soviet Physics — Crystallography, p. 173].

[8] K. E. Lazarenko, "Nomenclature and classification of glauconite" Problems of Mineralogy of Sedimentary Rocks, books 3 and 4, 345-379 [in Russian] (L'vov State Univ. Press, 1956).

[9] K. M. Malkova, "Celadonite from Pobuzh'e," Min. sb. L'vov Geol. Ob-vo, 10, 305 (1956).

[10] B. P. Mitra and M. V. R. K. Rao, "Basal reflection of electron waves by orientated aggregates of clay minerals. Naturwiss. 42, 5, 119 (1955).

[11] N. V. Belov, "Twinning laws in micas and micaceous minerals," Min. sb. L'vov geol. ob-va 3, 29 (1949).

[12] R. F. Newnham and G. W. Brindley, "The crystal structure of dickite," Acta Cryst. 9, 759 (1956).

All-Union Geological Institute

Received February 22, 1957

CRYSTALLOCHEMISTRY OF COMPLEX DIVALENT PLATINUM COMPOUNDS (THE EFFECT OF TRANSINFLUENCE IN CRYSTALLINE SUBSTANCES)

G.B. Bokii and G.A. Kukina

An x-ray structure investigation of the compounds K_2PtBr_4, $K[PtNH_3Cl_3]$, $K[PtNH_3Br_3]$, $K[PtNH_3Cl_3] \cdot H_2O$, $K[PtNH_3Br_3] \cdot H_2O$, $K[PtC_2H_4Cl_3] \cdot H_2O$ and $K[PtC_2H_4Br_3] \cdot H_2O$ was carried out (Tables 1-4). The plane of the ethylene molecule itself is perpendicular to that of the $[PtBr_3]$ group. In the investigated compounds "transdirecting" influence is discovered, the metal — addend distances depending on the nature of the addend in the trans-position (Table 5).

In investigations on quadrivalent platinum compounds with the help of x-ray and optical methods it was proved that the nitro group possesses a weaker transinfluence than do chlorine and bromine.

1. In the chemistry of complex compounds the most extensive generalization made in the last 30 years is the discovery by I. I. Cherniaev of the mechanism of transinfluence [1-2], which has been systematically studied.

In this Institute work has been done for a number of years on the crystallochemistry of complex compounds [3-11]. One of the studies along these lines is of transinfluence in crystals of complex compounds. In 1950 the first attempt was made to determine the interatomic distances in such complexes, where the discovery of a difference in the interatomic distances as a function of the strength of the transinfluence might be expected. The structure of Cossa salt, $K[PtNH_3Cl_3] \cdot H_2O$, was selected for study. For greater reliability it was decided to carry out these investigations simultaneously by electron diffraction and x-ray diffraction. Moreover, for increased precision it was decided to make a collateral study of a chlorine and a bromine salt.

The determination of the dimensions of the unit cells of the designated salts has already shown that x-ray data differ from those of electron diffraction. It has further been made clear that the reason for this difference is the dehydration in a vacuum of the preparations being examined in the electron microscope. Thus an anhydrous salt was studied by electron diffraction, and a monohydrate by x-ray.

In the work of Bokii, Vainshtein and Babareko [12] it was shown that the distance Pt — Cl along direction Cl — Pt — Cl is somewhat greater than the analogous distance along direction NH_3 — Pt — Cl (2.35 and 2.32 A respectively). They pointed out that this is in consequence of the transinfluence of the chlorine atom.

The difference in the cited values of the interatomic distances is negligible, since the dimension of the cell along axis b equals 8.84 A. In the study of other specimens somewhat greater values for period b were obtained (up to 9.07 A), which results in an increase of the indicated distance up to 2.40 A.

In continuing these studies, it was decided to select such compounds as have an addend possessing a stronger transinfluence than does Cl. Moreover it seemed expedient that such an addend should be constructed from light atoms. As a suitable addend satisfying these requirements the NO_2 group was selected, for which a strong transinfluence has been recognized by all chemists.

In 1952-1953 the authors determined the structure of the granular isomer $K_2[Pt(NO_2)_3Cl_3]$. However, an effect analogous to the one described above was not discovered.

During this period a refractometric method was developed for determining the structure of complex compounds [10], with the help of which it was established that the nitro group in quadrivalent platinum compounds does not possess a strong transinfluence [13]. The importance of this conclusion for the chemistry of complex compounds is that it indicates an absence of a definite gradation in the strength of transinfluence.

After examination of this peculiarity it was decided to return once more to the determination of the structure of complex divalent platinum compounds, and to take ethylene as a strongly transinfluencing addend. Zeise's salts $K[PtC_2H_4Cl_3]\cdot H_2O$ and $K[PtC_2H_4Br_3]\cdot H_2O$ were selected for study and the work on the determination of the structure of Cossa salt was renewed.

TABLE 1

	K_2PtCl_4[17,18]	$K[PtC_2H_4Cl_3]\cdot H_2O$	$K[PtNH_3Cl_3]$	$K[PtNH_3Cl_3]\cdot H_2O$
a	9.88	10.85 ± 0,02	17.6 : 2=8.8	20.88 : 2=10.44±0.05
b	(9.88)	8.53 ± 0.02	8.34(9.07) ±0.04	8.10±0.02
c	4.13	4.81 ± 0.01	4.19 ± 0.02	13.55 : 3=4.52±0.02
β	—	97°	—	—
n	2	2	4	12
Fedorov gr.	C^4/mmm	$P2_1$	*Bbmm*	*Pbna*
	K_2PtBr_4	$K[PtC_2H_4Br_3]\cdot H_2O$	$K[PtNH_3Br_3]$	$K[PtNH_3Br_3]\cdot H_2O$
a	10.14	11.38 ± 0.02	18.54 : 2 = 9.27	21.75 : 2=10.87±0.05
b	(10.14)	8.62 ± 0.02	9.2 ± 0.04	8.37 ± 0.02
c	4.22	5.01 ± 0.01	4.36 ± 0.02	14.42 : 3=4.81±0.02
β	—	97°		
n	2	2		
Fedorov gr.	C^4/mmm	$P2_1$	*Bbmm*	*Pbna*

At the end of 1954 Wunderlich and Mellor [15] published their work on the determination of Zeise's salt $K[PtC_2H_4Cl_3]\cdot H_2O$, in which it was indicated that the difference in interatomic distances is the consequence of transinfluence. After comparing the results of these authors with our own, we were fully convinced that they were in conflict. Since our study of the bromine salt had not been completed by then, we decided not to publish our own data for the time being. In 1955, a new note by the authors referred to appeared [16], with corrected coordinates. The position of the heavy atoms according to both our data and theirs is now in agreement, but the coordinates of the oxygen atoms (in the molecule of water) differ widely (see below).

In the references [15] and [16] it is indicated that the difference in the Pt – Cl distances in different directions depends on the strength of the transinfluence, but it is regrettable that the authors of these studies do not refer to the work published by us in 1951, which contains the same conclusions.

2. In the present report the following 7 structures will be examined: K_2PtBr_4, $K[PtNH_3Cl_3]$, $K[PtNH_3Br_3]$, $K[PtC_2H_4Cl_3]\cdot H_2O$, $K[PtC_2H_4Br_3]\cdot H_2O$, $K[PtNH_3Cl_3]\cdot H_2O$ and $K[PtNH_3Br_3]\cdot H_2O$. These substances belong to 4 structural types, since all the chlorine and bromine salts are correspondingly isostructural [14].

The structures of the salts listed are consistent with the structure of K_2PtCl_4. In Table 1 the cell dimensions of all these structures are given, the cell dimensions of potassium chloroplatinite being given in the base-centered aspect. From the table the similarity of the cells of all the structures is evident if the presence of pseudoperiods is taken into consideration. In Fig. 1 are given projections of the structures of K_2PtCl_4 and $K[PtC_2H_4Cl_3]\cdot H_2O$ on plane XY and XZ.

3. The dimensions of the unit cells of all the structures are determined by x-ray oscillation photographs taken with CuK_α-emission, and x-ray rotation photographs obtained with MoK_α-emission.

All the x-ray structural examinations were carried out with rotation photographs of the zero layer lines obtained with a camera for photographing the reciprocal lattice by MoK_α-emission, with rotation of the crystals along the basic crystallographic directions (axes X, Y and Z). All the compounds were analyzed with the help of projections of interatomic functions constructed on the appropriate planes. The presence in all the structures of the heavy platinum atom, and in the bromine compounds of the comparatively heavy bromine atom, allowed the coordinates of these atoms to be determined. In all cases respecting the coordinates of the heavy Pt and Br atoms the structure amplitude signs were calculated and the projections of electron density on appropriate planes were constructed. The coordinates were made more precise by means of series approximations. The intensities were estimated visually with a density scale. In the estimation of the intensities the kinematic and polarization factors were taken into account.

The central complex in the structure of Zeise's salt, located at height $\frac{1}{2}$ c, is represented in Fig. 1 b by a dotted line. The plane of the complex is located such that the direction Cl – Pt – Cl is parallel to axis Y, and the perpendicular direction is inclined slightly toward plane (001).

In Fig. 2 are given the projections of the structure of $K[PtNH_3Cl_3]$ and $K[PtNH_3Br_3] \cdot H_2O$ on plane XY and XZ. The three midpoints of the complex, located at $\frac{1}{3}$ c, are represented in Fig. 2 by a dotted line. In the first structure, as in the structure of K_2PtCl_4, the planes of all complexes are located parallel to plane XY.

In Fig. 2 b are given projections of the structure of $K[PtNH_3Br_3] \cdot H_2O$. In this structure the cell is three times as great along axis c in comparison with the preceding one. In each level the complexes are identically placed, analogous to the structure of $K[PtNH_3Cl_3]$. The direction NH_3 – Pt – Cl is parallel to axis X. The perpendicular direction Cl – Pt – Cl is inclined at an angle of ~ 26° toward the plane XY. This evidently explains the reduction of axis b of the cell in comparison with all the preceding structures.

The examination of the structures of $K[PtC_2H_4Cl_3] \cdot H_2O$ and $K[PtC_2H_4Br_3] \cdot H_2O$, apart from the answer to the basic problem – the discovery of the effect of trans-influence in modifying the interatomic distances – was even more interesting for elucidation of the location of the carbon and hydrogen atoms with respect to the group $[PtCl_3]$ and $[PtBr_3]$.

TABLE 2

Atoms		y	z
Pt	0.213	0	0.328
Cl_2	0.213	0.265	0.328
Cl_1	0.428	0	0.528
K	0.434	0.301	0.925
C_1	–0.01	0	0.30
C_2	0.04	0	0.02
H_2O	0.34	0.57	0.81

TABLE 3

Atoms	x	y	z
Pt	0.211	0	0.328
Br_2	0.211	0.281	0.328
Br_1	0.424	0	0.519
K	0.448	0.281	0.938

Extinctions lead to the space group $C_2^2 = P2_1$, i.e., the structures do not possess an inversion center. Analysis of the projections of the interatomic vector functions made it possible to determine the coordinates x and y of the Pt, Cl, Br, K and O atoms. It is regrettable that these projections are noncentrosymmetrical and analogous projections of electron density could not be constructed. The coordinates x and z of the Pt, Cl and K atoms are determined by the projection of the interatomic vector functions on plane XZ. This projection is centrosymmetrical and therefore, after calculation of the structure amplitude signs, a projection of the electron density was constructed on the indicated plane. The coordinates of the carbon and oxygen atoms were obtained, in spite of their small resolvability. In Table 2 are given the coordinates of all atoms in the structure of $K[PtC_2H_4Cl_3] \cdot H_2O$.

The presence of the heavy Pt and Br atoms in the structure of $K[PtC_2H_4Br_3] \cdot H_2O$ made it difficult to determine the coordinates of the light atoms – carbon and oxygen – although in the appropriate places insignificant indistinct maxima are observed. In Table 3 are given the coordinates of atoms in the structure of $K[PtC_2H_4Br_3] \cdot H_2O$.

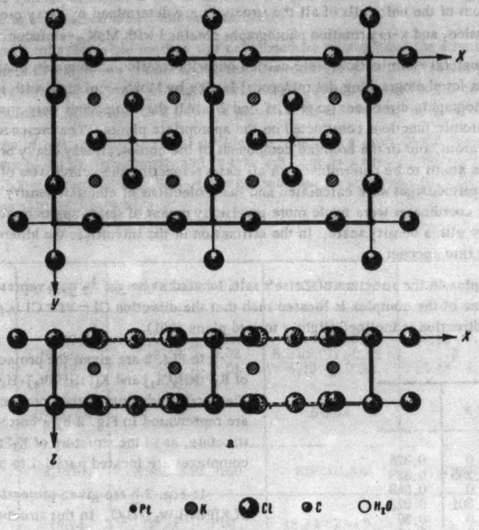
X
y
X
z
a
● Pt
● K
● Cl
● C
○ H_2O

Fig. 1a. Projection of two K_2PtCl_4 cells on plane XY in base-centered aspect.

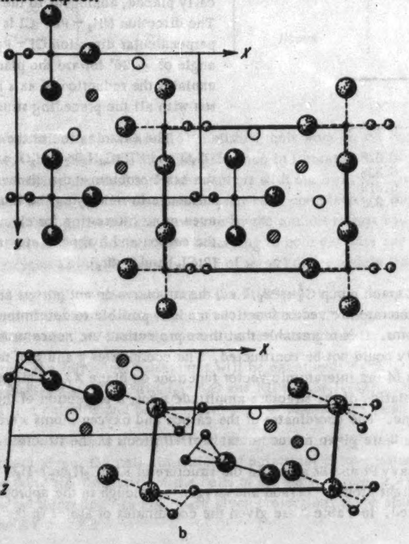

Fig. 1b. Projection of $K[PtC_2H_4Cl_3]\cdot H_2O$ on plane XY.

The interatomic distances were calculated from the coordinates of the atoms. Two of the bond lengths, Pt $-$ Cl$_{II}$ and Pt $-$ Br$_{II}$, are normal and equal 2.26 and 2.42 A respectively; the third bond length however, Pt $-$ Cl$_{I}$ and Pt $-$ Br$_{I}$, found in the transposition to the ethylene molecule, has an anomalous value equal to 2.40 and 2.50 A respectively. The strong transinfluence of the ethylene molecule is well-known, and therefore the increase in the length of bond in the direction C_2H_4 $-$ Pt $-$ Cl$_1$ and C_2H_4 $-$ Pt $-$ Br$_1$ seems perfectly natural.

As was mentioned above, analysis of the projection of electron density on plane XZ made it possible to determine the coordinates of the carbon atoms and to establish that the plane of the ethylene molecule itself is located perpendicular to the plane of the [PtCl$_3$] and [PtBr$_3$] group, and that the carbon atoms are located almost symmetrically with respect to the Pt atom, with the distance C $-$ C ~ 1.5 A.

Proceeding from the crystallochemical data, the position of the hydrogen atoms can also be determined. There are two variants of the location of the plane group C_2H_4 in the [PtC$_2$H$_4$Cl$_3$] complex. In the first variant this plane in extension passes through the line Br$_I$ $-$ Pt, in the second, it is perpendicular to this line. The calculation of the interatomic distances obtained for these two variants argues in favor of the second.

TABLE 4

Atoms	x	y	z
Pt	0.153	0.25	0
Br I	0.038	0.25	0
Br II	0.153	0.539	(0.088)
NH$_3$	0.225	0.25	0
K$_{(8)}$	0.466	0.039	0.333
K$_{(4)}$	0.462	0.25	0
H$_2$O$_{(4)}$	(0.44)	(0.25)	(0.5)
H$_2$O$_{(8)}$	(0.41)	(0.73	(0.42)

Coordinates determined only approximately are given in parentheses.

In the investigation of the structure of K[PtNH$_3$Cl$_3$]· ·H$_2$O and K[PtNH$_3$Br$_3$]·H$_2$O the space group D_{2h}^{14} = Pbna is established. The construction of a projection of the interatomic vector functions on plane XY made it possible to establish at once the location of the complex (owing to the presence of the heavy Pt atom). However, because of the low scattering power, the location of the ammonia groups and the molecules of water could not be established.

Analysis of a minimized projection showed that the complexes are oriented in the same way in all layers. The location of the potassium atoms was also established, the structure amplitude signs calculated and a projection of the electron density constructed on plane XY, the coordinates for which were taken from the projection of interatomic vectors.

A further investigation was carried out on the compound K[PtNH$_3$Br$_3$]·H$_2$O. In this it was established that the [PtNH$_3$Br$_3$] complexes are inclined with respect to axis Z approximately by a 26° angle in comparison with the anhydrous salt K[PtNH$_3$Cl$_3$]. From the projection of the electron density on plane XZ, coordinates of all the atoms were obtained, which are given in Table 4.

TABLE 5

	K$_2$PtCl$_4$	K[PtNH$_3$Cl$_3$]	K[PtC$_2$H$_4$Cl$_3$]·H$_2$O	K[PtNH$_3$Cl$_3$]·H$_2$O
Pt—Cl (a—Pt—Cl]	—	2.32	2.40 (2.38)*	2.26
Pt—Cl (Cl—Pt—Cl)	2.32	>2.35	2.26 (2.33)*	—
	K$_2$PtBr$_4$	K[PtNH$_3$Br$_3$]	K[PtC$_2$H$_4$Br$_3$]·H$_2$O	K[PtNH$_3$Br$_3$]·H$_2$O
Pt—Br (a—Pt—Br)	—	—	2.50	2.42
Pt—Br (Br—Pt—Br)	2 2	—	2.42	2.7**

---

*Calculated with the Wunderlich and Mellor data.

** Values much increased because of adverse experimental conditions (see text),

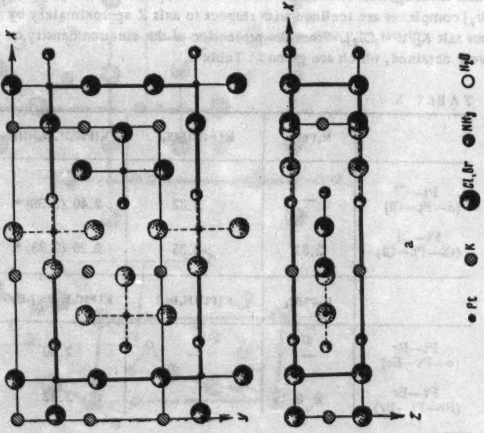
Y
y
Y
Z
a
Pt
K
Cl, Br
NH3
H2O

Fig. 2a. Projection of structure of $K[PtNH_3Cl_3]$ on plane XY.

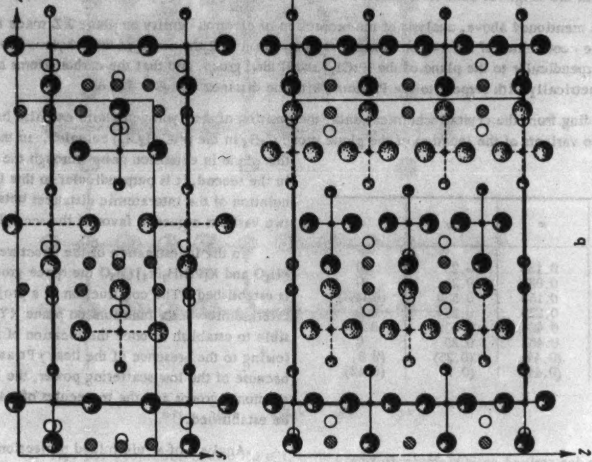

Fig. 2b. Projection of structure of $K[PtNH_3Br_3] \cdot H_2O$ on plane XY.

According to the coordinates cited, the distance $Pt - Br_I = 2.42$ A, and the distance $Pt - Br_{II} = 2.7$ A, i.e., considerably greater. This induced a more cautious approach to the handling of this value. Although the strong transinfluence of the bromine atom in divalent platinum compounds is well-known, nevertheless so considerable an increase seemed too great. For verification, a different projection was constructed and it was established that there is superimposed on the Br maximum a maximum of the series termination wave from the platinum atom. This reduces the accuracy of coordinate $\underline{z}$ of the bromine atom and apparently increases the $Pt - Br_{II}$ distance. The refinement of the angle of inclination of the complex and the coordinates of the atoms will be carried out in the future.

4. In conclusion, we discuss what effect transinfluence has on the interatomic distance.

In Table 5 are given the distances of Pt − h (in A) along the axis of the complex $\underline{a} - Pt - h$, where a = NH_3 or C_2H_4, and h = Cl or Br, and in the perpendicular direction, i.e., along the axis of the complex h − Pt − h.

From an analysis of Table 5 the conclusion may be drawn that transinfluence has a noticeable effect on the interatomic distances in the complexes: with an increase of trans-effect there is an increase also in the interatomic distances between the central atom and the labilized addend.

As a result of the increase in distance Pt − h in the direction of the maximum transinfluence, there apparently occurs a shortening of the distances to the adjoining addends − a secondary effect. It is called the cis-strengthening effect.

At the same time it is clear that the outer sphere, in particular the potassium ions or the molecules of water, can also have a strong influence on the interatomic distances in the complexes [19], as a result of which the measured values reflect an overall effect, depending on both origins − the transinfluence and the influence of the outer sphere.

LITERATURE CITED

[1] I. I. Cherniaev, "Mononitrites of divalent platinum," Izvest. Inst. Platiny 1, 4, 213 (1926).

[2] I. I. Cherniaev, "Reports of the conference on the mechanism of transinfluence, 1952," Izvest. Sektora Platiny 28 (1954).

[3] G. B. Bokii, M. A. Porai-Koshits and G. N. Tishchenko, "Refinement of coordinates of atoms in the structure of Gerhardt salts," Izvest. AN SSSR, Chemical Sciences Section 5, 2 (1951).

[4] N. V. Belov, G. B. Bokii and G. L. Trusevich, "x-Ray investigation of the structure of Gerhardt salts," Izvest. Sektora Platiny Inst. Obshchei i Neorg. Khim. AN SSSR 20, 125 (1946).

[5] N. V. Belov, G. B. Bokii and L. A. Popova, "Investigation of the structure of Gerhardt salts $[Pt(NH_3)_2Cl_4]$-trans by the harmonic analysis method," Izvest. AN SSSR Chemical Sciences Section 3, 249 (1947).

[6] G. B. Bokii and M. A. Porai-Koshits, "x-Ray investigation of Gros salts $[Pt(NH_3)_4Cl_2]Cl_2$," Izvest. Sektora Platiny Inst. Obshchei i Neorg. Khim. AN SSSR 24, 52 (1949).

[7] G. B. Bokii and L. A. Popova, "x-Ray investigation of Chugaev salt," Izvest. Sektora Platiny Inst. Obshchei i Neorg. Khim. AN SSSR 25, 156 (1950).

[8] G. B. Bokii, G. A. Kukina and M. A. Porai-Koshits, "x-Ray investigation of crystals of platinic cis-tetrachlorodiammine," Izvest. Sektora Platiny AN SSSR 29, 5 (1955).

[9] G. B. Bokii, "Crystallochemistry of the transitional series of quadrivalent platinum ammines," Izvest. AN SSSR, ser. fiz. 15, 2 (1951).

[10] G. B. Bokii, "x-Ray and crystallooptical investigations of complex platinum and cobalt compounds," Trudy Inst. Krist Akad. Nauk 10, 199 (1954).

[11] M. A. Porai-Koshits and E. M. Romanova, "Refinement of the interatomic distances in the crystal structure of trans-dichlorotetramminochloride of quadrivalent platinum," Izvest. Sektora Platiny Inst. Obshchei i Neorg. Khim. 28, 282-286 (1954).

[12] G. B. Bokii, B. K. Vainshtein and A. A. Babareko, "Electron diffraction examination and crystallo-

chemistry of K[PtNH$_3$Cl$_3$] and K[PtNH$_3$Br$_3$]," Izvest. AN SSSR, Chemical Sciences Section 6, 667-674 (1951).

[13] G. B. Bokii and S. S. Batsanov, "On the question of the quantitative character of transinfluence," Doklady Akad. Nauk SSSR 95, 6, 1205 (1954).

[14] M. N. Liashenko, "Crystals of complex compounds of the platinum group metals," Trudy Inst. Krist. 9, 335-348 (1954).

[15] J. A. Wunderlich and D. P. Mellor, "A note on the crystal structure of Zeise's salt," Acta Cryst. 7, 130 (1954).

[16] J. A. Wunderlich and D. P. Mellor, "A correction and a supplement to a note on the crystal structure of Zeise's salts," Acta Cryst. 8, 57 (1955).

[17] R. G. Dickinson, "The crystal structures of potassium chloroplatinite and of potassium and ammonium chloropallodites," J. Am. Chem. Soc. 44, 2404 (1922).

[18] N. V. Belov and V. I. Mokeeva, "The use of the method of harmonic analysis for determining the parameters of crystalline structures on standard powder x-ray photographs," Trudy Inst. Krist. 5 (1949).

[19] G. B. Bokii, "A discussion of the mechanism of transinfluence," Izvest. Sektora Platiny AN SSSR 28, 74 (1954).

The N. S. Kurnakov Institute of General and
Inorganic Chemistry

Received March 6, 1957

A CRYSTALLOCHEMICAL INVESTIGATION OF THE STRUCTURE OF SOME COMPLEX COMPOUNDS

Z.V. Zvonkova

The crystallochemical analyses of the intermolecular distances C – H...F and N – H...S = C< show some significant features of the nature of the hydrogen bond. Determination of the interatomic distances and valence angles in the structures of $F_3B - NC_5H_5$, p-$BrC_6H_4B(OH)_2$ and $S_3B_3Br_3$ made it possible to reveal the nature of the chemical bond.

The development of contemporary crystallochemistry is also of interest for the allied sciences. On the basis of crystallochemical data, individual points of a theory of the chemical bond are at present being developed. A very important development is that of the theory of the structure of complex compounds with special physicochemical properties. The present report examines some points of the crystallochemical theory of the structure of complex compounds based on work carried out in the x-ray laboratory of this Institute.

1. Intermolecular Interaction in Complex Compounds

In this field the investigations of the nature of the hydrogen bond are of the greatest theoretical and practical interest. In the paper by Zhdanov and Zvonkova at the Third International Congress of Crystallographers [1] it was reported that in the structure of $[ClTlC_6H_5]^+Cl^-$ the value $r_H = 0.74$ A was established for the molecular radius of the hydrogen atom in place of the radius $r_H = 1.17 - 1.20$ A assumed in the literature. Hence it was concluded that the strength of the hydrogen bond X – H...Y depends on the size of the angle X – H...Y and that the most stable hydrogen bonds are formed along the line of the covalent bond X – H...Y. As a result of this investigation a scheme for the phenyl ring with limiting intermolecular radii was given. These data on the phenyl ring excluded the model of the structure of triphenylene proposed by Klug, which was afterwards also experimentally confirmed in the work of Pinnock, Taylor and Lipson [2].

The question of the nature of the hydrogen bond was further developed in our subsequent studies. In the structure of $F_3B - NC_5H_5$ the value $r_H = 0.80$ was obtained (agreeing with the previous value of the intermolecular radius of the hydrogen atom [3]). The constancy of the radius of the hydrogen atom shows that the thermal vibration of this atom in the bond C – H has little effect on the magnitude of the radius. In the structure of $F_3B - NC_5H_5$ hydrogen atoms were located by electron diffraction in the C – H bonds at a distance of 1.0 A. Hence the distance F...H was obtained, equal to 1.93 A (the length of bond C – H from spectroscopic data equals 1.08 A). The distance 1.93 A, in comparison with the distance F...H equal to 2.52 A assumed earlier in the literature, is already reduced by 0.59 A even in the bond C – H...F. The change in the distance F...H from 1.93 (bond C – H...F) to 1.54 (bond N – H...F in the structure of $N_2H_6F_2$) is caused by the further increase in polarity of the bond N – H in comparison with the bond C – H and by the electrostatic interaction $N^{-\delta 2} - H^{+\delta 2} ... F^{-\delta 3}$.

According to crystallochemical considerations, the basic cause of the decrease in interatomic distances in the formation of hydrogen bonds is the decrease in the intermolecular radius of the hydrogen atom along the line of the covalent bond, which occurs on account of the drawing in of the electron cloud into the space between the nucleii and because of the increase in polarity of the bond. This explains the magnitude of the energy of the hydrogen bond. Bernal also has noticed the low electron density around the hydrogen atom of the carboxyl group in salicylic acid in comparison with the hydrogen atom of the benzene ring.

These data also indicate [4] an increase in polarity of the hydrogen bond.

Since the strength of the hydrogen bond depends on the mutual orientation of the atoms, then the change in the size of the angle $X-H\ldots Y$ with anisotropic thermal vibration of the atoms should cause a change in the strength of the hydrogen bond, whereupon this effect should be manifest in a widening of spectral lines. According to the data of G. S. Landsberg, in crystals of hydroxides the band of the OH group in the spectra narrows down sharply with a drop in temperature and is converted into one or more narrow bands.

A shift of the vibration frequency of the $X-H$ bond to the long-wave range occurs because of the lengthening of the $X-H$ bond under the influence of the directed electrostatic interaction of the polar groups. It is known that the field of a crystal increases the interatomic distances in molecules a little because of the increase in the ionic character of the bonds [5, 6].

The approximate quantum mechanical calculation of the energy of the hydrogen bond in a molecule of water, carried out recently by Coulson and Danielsson [7], after the model $\overset{\diagdown\,\diagup}{O}-H\ldots O<, -O^{-}H^{+}\ldots O< -O^{-}H-$ $-O^{+}<$, is not confirmed by the crystallochemical data.

The indicated effect of the drawing in of the electron cloud into the space between the nucleii leads to a virtual increase in the effective charge of the nucleus of the hydrogen atom and consequently to a decrease in the value of the charge of the trivalent positively charged oxygen ion.

According to our data, the asymmetry and directionality of the bonds diminish in the series of N, O, F atoms [3]. The strength of the hydrogen bond depends on the electronegativity of the atoms, and therefore it increases in the indicated series. Consequently, the presence of asymmetry of the free pair of electrons is not the principal condition for the formation of the hydrogen bond, as assumed in the quantum mechanical calculations of Fyfe [8]. In our opinion, new calculations for the hydrogen bond should be undertaken, based on the crystallochemical data.

Special opportunities for the formation of hydrogen bonds have been revealed in our investigation of the structure of Captax (2-mercaptobenzothiazole) $C_7S_2NH_5$. The original model of the structure of Captax proposed by Jeffrey is not confirmed in our work [9]. Instead of dimers of Captax molecules connected by inversion centers, we found chains of molecules directed along the second-order screw axes and connected by hydrogen bonds. In spite of the fact that the difference in the electronegativities of the atoms H ($x = 2.1$) and S ($x = 2.0$) is negligible, in the structure of Captax there is formed a strong hydrogen bond $N-H\ldots S$ (distance $N\ldots S$ equals 2.48 A), the presence of which is confirmed by spectroscopic examinations of Captax carried out by E. N. Gur'ianova and D. N. Shigorin. The crystallochemical analysis of the structure of Captax showed that the $N-H\ldots S$ atoms are not colinear, and the hydrogen bond occurs owing to the interaction of the p_{π}-electron cloud of the sulfur atom in the double bond $S=C<$ and the hydrogen atom, which has a positive charge because of the polarity of the covalent bond $N^{-\delta_2}-H^{+\delta_1}$. Consequently, strong hydrogen bonds can form in two cases: 1) along the polar covalent σ-bond and 2) in the case of groups containing π-bonds.

2. The Structure of Complex Compounds of Elements in Group III of the Periodic System

The theory of directed valency is of great importance for clearing up questions of the structure of complex compounds.

The structures of the isomorphous compounds $TlCl_3 \cdot 4H_2O$ and $TlBr_3 \cdot 4H_2O$ are worked out by the author with three projections of interatomic vector functions and of electron density [10]. The molecules of TlX_3 have a plane configuration with sp^2 directed bonds. The distances $Tl-Cl$ and $Tl-Br$ equal 2.33 and 2.46 A respectively. In Fig. 1, plotted from data in the literature, is shown the dependence of the interatomic distances of metal – chlorine $Me-Cl$ in molecules on the possible $s-p$ valence states: sp, sp^2, sp^3, p^3 and p^2. From the diagram it is apparent that the interatomic distances increase and the strength of the bond is diminished in proportion to the decrease in the degree of the s- state in the transition from the sp-hybridization of orbitals to sp^3-hybridization. The curves have a sharp inflection in the transition from $s-p$ -hybrid bonds to p- bonds. This indicates that the interatomic distances depend greatly on the degree of participation of the s- and p- states in the formation of chemical bonds. The experimental refinement of the distances in molecules of tin and lead chlorides is of interest. The magnitude of the distances $Ga-Cl$ (2.22 A) and $In-Cl$ (2.46 A) is evidence that these molecules are dimers.

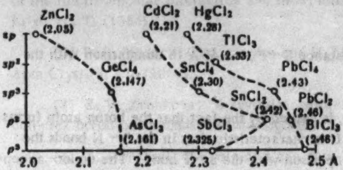

Fig. 1. Curves of the dependence of interatomic distances Me − Cl on the degree of s-, p- valence states.

TABLE 1

Ion	Radii according to Belov and Bokii (A)	Radii according to Pauling (A)	Radii according to Templeton and Carter (A)
Al^{3+}	0.57	0.50	0.51
Ga^{3+}	0.92	0.81	0.90
In^{3+}	0.97	0.93	0.72
Tl^{3+}	1.05	0.95	0.77

In the work of Templeton and Carter [11] isomorphism is indicated in the compounds $AlCl_3$, $InCl_3$, $TlCl_3$ and in a number of chlorides of rare earth elements. At the same time, the ionic radii of metals established by them differ from those proposed by other authors [12, 13] (see Table 1).

The authors [11] point out that the variations of the ionic radii affirm the difficulty in assuming single radii for thallium and indium. The distances for Tl−Cl obtained by them equal 2.55 A in $TlCl_3$ and 2.33 A in the crystal hydrate $TlCl_3 \cdot 4H_2O$. For thallium atoms a change of valence states is possible. For example, in the linear complex ion $[ClTlC_6H_5]^+Cl^-$ the distance Tl − Cl, equal to 2.27 A, corresponds to the sp-hybridization of orbitals of the thallium atom; in the compound TlI_3 the presence of Tl^+ and I_3^- ions was established [10]. The retention of the s^2-free pair of electrons by the Tl^+ ions is not an exception. According to the given directionality of the valence and the values of the interatomic distances in the structure of $Pb[(C_2H_5)_2NCS_2]_2$ the Pb − S bond is formed with an insufficient number of electrons and also the free pair of s^2-electrons are not used in the bonds [14]. In this complex compound there was obtained for the first time a pyramidal configuration of the bonds of the lead atom, established earlier by Pauling and Moore in the structure of PbO. Thus, in the chemical bonds formed by the thallium atom with halogens, the sp^2- and sp-hybridization of orbitals is used or the s^2-free pair of electrons is retained. It is therefore impossible to assume the radius of the Tl^{3+} ion to be equal to 0.77 A, as Templeton and Carter propose. It is possible that in the structure of $TlCl_3$ they obtained this value in error because of an imprecise interpretation of the structure of the monoclinic crystal system by means of a powder x-ray pattern or else this ought to be interpreted as an increase of the radius of thallium in a structure of the $AlCl_3$ type, in the formation of directed polar covalent bonds with an insufficient number of electrons. A similar variation in the length of the Hg − S bonds was established in the structures of ClHgSCN and $K_2Hg(SCN)_4$ (respectively 2.32 and 2.54 A [6]).

In crystallochemical studies great attention is paid to questions of the structure of boron compounds. A series of structures of boron trifluoride with amines (NH_3, $N(CH_3)_3$ and NH_2CH_3) have been interpreted by Hoard and his co-workers [15]. In these structures B − N distances were obtained, equal to 1.60, 1.585 and 1.57 A. However, data on the energies of formation of the compounds studied, the equilibrium constant, the rate constants of the chemical reaction, and on the basicity of the amines, show that the maximum strength of the donor-acceptor bond B − N in a series of amines and, consequently, the minimum distance B − N, must be characteristic of the compound of boron trifluoride with dimethylamine. This structure is not worked out, evidently because of the absence of an inversion center. In the structure of $F_3B-NC_5H_5$, worked out by a straightforward method, there were found more stable B − N bonds than in the amines studied earlier [3]. The distance B − N obtained in reference [7], equal to 1.53 A, corresponds to the sum of the covalent radii of the nitrogen and boron atoms without correction for electronegativity.

Of great value is the analysis of the nature of the donor-acceptor bond in complex boron compounds. In the structure of $F_3B-NC_5H_5$ the distance B − F, equal to 1.41 A, excludes the valence state $\geq B^- - N^+ \leq$, since the sum of the covalent radii of the fluorine and boron atoms equals 1.52 A. The reduction of the indicated distance by 0.11 A shows that in the structure examined there are the polar covalent bonds $B^{+\delta_1} - F^{-\delta_2}$. The value of the distance B − N, equal to 1.53 A, excludes the valence states $B^{+\delta_1} - N^{+\delta_2}$ and $B^{-\delta_1} - N^{-\delta_2}$, since the distribution of similar charges would cause an increase in the covalent interatomic distance B − N. This is apparent, for example, in the structure of B_2Cl_4 [16], where the distance $>B^{+\delta_1} - B^{+\delta_1}<$, equal to 1.80 A, is increased in comparison with the sum of the covalent radii, equal to 1.60 A. Consequently, according to the crystallochemical data, one possible valence state remains, namely:

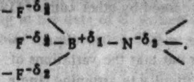

$$\begin{matrix} -F^{-\delta_2} & & & & \\ & \diagdown & & & \diagup \\ F^{-\delta_2} & - & B^{+\delta_1} - N^{-\delta_3} & & - \\ & \diagup & & & \diagdown \\ -F^{-\delta_2} & & & & \end{matrix}$$

The increase in the interatomic distance B − F to 1.41 A in comparison with the original BF_3 molecule, where the distance B − F equals 1.30 A, is caused by the fact that the boron atom forms four bonds with an insufficient number of electrons per bond. It is characteristic that in the B − N bonds the extent of the p- distance of the boron atom is increased in comparison with the B − F bond. The donor-acceptor bond $\geq B^{+\delta_1} - N^{-\delta_3} \leq$ is a polar bond with an insufficient number of electrons for the boron atom and with sp^3-hybrid orbitals of the boron atom. This conclusion is very pertinent to an explanation of the physicochemical properties of complex compounds based on their structure.

In the structure of para-bromophenylboronic acid p-$BrC_6H_5B(OH)_2$ the following distances and angles are obtained:

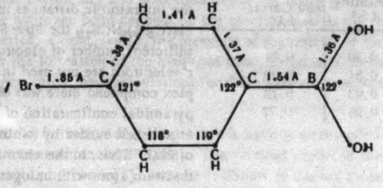

The crystallochemical rules determined earlier in the structure of molecular and complex compounds of mercury, thallium and lead show that the extent of use of the p- state of an atom of a complex-former in the chemical bond is increased in the series of addends Cl, Br, I [6]. This is a new and important factor which must be taken into account in an explanation of the properties of complex compounds.

The physicochemical properties of the derivatives of phenylboronic acid show that the dissociation constant is increased in the series F, Cl, Br, i.e., the bromine atoms in comparison, for example, with the chlorine atoms show a great mutual influence even on the remote hydrogen atoms of the OH group. Consequently, the increase in the degree of the p- state of the carbon atom in the bond $Br - C\lessgtr$ in comparison with the bond $Cl - C\lessgtr$ leads to an increase in the dissociation constant. The possibility of a change in degree of the s- or p- state of the atom in the bonds depending on the nature of the connected atoms is not usually taken into account in quantum mechanical calculations of the structure of molecules carried out by the molecular orbital method.

For confirmation of this thesis that the degree of use of the s- or p- state in the bonds of an atom of a complex-former depends on the nature of the connected addends, the author has investigated the structure of a meta-thioboric acid bromide trimer, $S_3B_3Br_3$. In this coplanar molecule the six-membered ring consists of B and S atoms. It is known that the theoretical value of the valence angles for sp^2-hybrid orbitals equals 120° and for the p^2-orbitals, 90°. It would therefore be expected that the valence angle of the boron atom SBS in the structure of $S_3B_3Br_3$ would be deformed and that its value would exceed 120°. However, the crystallochemical rules established in the analyses of the structure of complex compounds showed that atoms of elements with unfilled sp- orbitals use a greater degree of the p- state in the bonds with sulfur atoms than they do in bonds with bromine atoms [6]. Therefore the valence angle SBS must be less than the valence angle BrBS, and consequently the angle SBS must be less than 120° and the valence angle BSB more than 120°. Experimental x-ray examination confirmed the latter hypothesis.

The questions of the redistribution of the electron density between the atoms in structures of complex compounds [18] and the crystallochemical range of electronegativities of the atoms will be discussed in a special report.

LITERATURE CITED

[1] G. S. Zhdanov and Z. V. Zvonkova, "The development of crystallochemical concepts of the nature of the intermolecular interaction and intermolecular radii based on x-ray structural analysis," Trudy Inst. Krist. 10, 71 (1954).

[2] P. R. Pinnock, C. A. Taylor and H. Lipson, "A redetermination of the structure of triphenylene," Acta Cryst. 9, 173 (1956).

[3] Z. V. Zvonkova, "A crystallochemical investigation of the nature of the donor-acceptor bond in complex boron compounds," Kristallografiia 1, 73 (1956).

[4] G. D. Bernal, "Le role de l'eau dans les substances cristallisees," J. chim. phys. et phys-chim. biol. 50, 1-12 (1953). "The role of water in crystallographic substances," Uspekhi Khim. 25, 643 (1956).

[5] Z. V. Zvonkova, V. V. Samodurova and G. L. Borontsova, "New results in the crystallochemistry of complex halogen compounds of mercury," Doklady Akad. Nauk SSSR 102, 1115 (1955).

[6] Z. V. Zvonkova, "Crystallochemical investigations of the nature of the donor-acceptor bond in complex compounds," Zhur. Neorg. Khim. (in the press) (1957).

[7] C. A. Coulson and U. Danielsson, "Ionic and covalent contributions to the hydrogen bond," Arkiv Fysik 8, 239 (1954).

[8] W. S. Fyfe, "Conditions for the formation of hydrogen bonds" J. Chem. Phys. 21, 2 (1953).

[9] Iu. Tashpulatov, Z. V. Zvonkova and G. S. Zhdanov, "X-ray examination of Captax (2-mercaptobenzothiazole)," Kristallografiia 2, 38 (1957). *

[10] Z. V. Zvonkova, "The crystal structure of molecular complex thallium compounds," Zhur. Fiz. Khim. 30, 340 (1956).

[11] D. H. Templeton and G. F. Carter, "The crystal structure of yttrium trichloride and similar compounds," J. Phys. Chem. 58, 940 (1954).

[12] N. V. Belov and G. B. Bokii, "The present state of crystallochemistry and its related problems. The first conference on crystallochemistry," Izd. AN SSSR (1954).

[13] L. Pauling, The Nature of Chemical Bond [in Russian] (1947).

[14] G. S. Zhdanov, Z. V. Zvonkova and N. V. Rannev, "A structural investigation of lead diethyldithiocarbamate," Kristallografiia 1, 514 (1956).

[15] G. L. Hoard, S. Geller and T. B. Owen, "Structures of molecular addition compounds," Acta Cryst. 4, 405 (1951).

[16] M. Atoji, W. M. Lipscomb and P. J. Wheatley, "Molecular structure of diborane tetrachloride B_2Cl_4," J. Chem. Phys. 22, 1176 (1955).

[17] K. P. Coffin and S. H. Bauer, "The structures of phenylboron dichloride , B-trichloroborazole and N- trimethyl borazole as determined by electron diffraction," J. Phys. Chem. 59, 193 (1955).

[18] Z. V. Zvonkova, "On the nature of the chemical bond in complex metal thiocyanates," Zhur. Fiz. Khim. (in the press) (1957).

The L. Ia. Karpov Physical Chemistry Institute

Received February 20, 1957

---

* [Soviet Physics – Crystallography, p. 33].

DISTORTIONS OF THE CRYSTAL LATTICE IN SOLID SOLUTIONS

V.I. Iveronova, A.P. Zviagina and A.A. Katsnel'son

It is shown that mean quadratic static displacements of atoms, calculated for the elastic model of a solid solution, nearly coincide with experimental values. The dependence on the concentration evaluated by theory is also fulfilled, but there is no parallelism with difference of the atomic radii. The characteristic temperature decreases with the formation of the superstructure.

It is known that in the formation of a solid solution the mechanical properties of an alloy change, the hardness increases, the plasticity decreases, the elastic moduli change etc. Simultaneously there arise distortions of the structure which lead to a change in the intensity of the x-ray scattering (see [1-10]). This change can be calculated by introducing the factors $e^{-2\frac{\alpha \sin^2 \vartheta}{\lambda^2}}$ into the expression for the intensity. In this expression $\alpha = \alpha_{st} + \Delta B$, where α_{st} reflects the presence in the structure of static displacements connected with the different atomic volumes of the components, and ΔB characterizes the change in the value of the interatomic bonds in a solid solution, leading to a change in the characteristic temperature of the alloy and consequently also in the amplitude of the thermal vibrations of the lattice. Evidently ΔB can be both positive and negative, whereas α_{st} is positive.

An increase in the strength of a manufactured article is usually achieved by a combination of changes in the chemical composition and the processing. Plastic deformation and heat treatment, with which a special substructure is created, usually lead to a considerably greater increase in the mechanical properties than does the introduction into a solid solution of any admixture, yet with a rise in temperatures the strengthening, caused by similar effects, is removed on account of the relaxation of stresses and recrystallization. The presence in a solid solution, of components which increase the strength of the interatomic bonds, should lead to a delay in the relaxation of the stresses.

The static displacements in a solid solution would seem to depend little on the temperature. That is why a study of the character of the distortions caused by the introduction into the lattice of extraneous atoms is quite essential.

It was shown earlier [9, 10] that the intensity of the selective Bragg maxima should increase on account of the emergence of static displacements, according to the law $e^{-2\alpha \sin^2 \vartheta/\lambda^2}$,

where
$$\alpha = \frac{8\pi^2}{3}\, \overline{u_{st}^2}\,.$$

On the basis of the elastic model of a solid solution it was possible to calculate the magnitude of the mean square displacements of atoms from the equilibrium state as a function of the concentration and difference of the atomic radii of the components. For the face-centered lattice, there was obtained the expression

$$\sqrt{\overline{u_{st}^2}} = 2.8\sqrt{C}\,\Delta R, \tag{1}$$

and for the body-centered lattice the coefficient 2.8 should be replaced by 2.7.

A comparison of the experimental data for a series of solid solutions with data calculated theoretically according to formula (1) is given in Table 1. In the last column of the table are figures denoting the references from which the pertinent data were taken.

TABLE 1

No.	Alloy	Concentration of 2nd component in atomic %	Δ R in A	u_{st} theoretical	u_{st} experimental	Literature
1	Ni—Cr	22	0.04	0.052	0.07	[6]
2	Ni—Al	7.4	0.19	0.14	0.053	[6]
3	Ni—Ti	4.7	0.21	0.13	0.058	[6]
4	Ni—Fe	32	0.03	0.048	0.027	Present work
5	Cu—Au	15	0.16	0.17	0.11	[7]
6	Fe—Co	1.8	0.02	0.007	0.053	[17]
7	Fe—W	1.9	0.12	0.046	0.02	Present work
8	Fe—V	2.3	0.07	0.029	0.040	[17]
9	Fe—Nb	0.8	0.19	0.045	0.121	[17]
10	Fe—Mn	1.5	0.02	0.0067	0.084	[17]
11	Fe—Mo	1.8	0.12	0.044	0.090	[17]

The table shows that the theoretically calculated mean square displacements coincide with the experimental with respect to the order of magnitude, though correlation between the difference of the atomic radii and $\sqrt{u_{st}^2}$ is not observed.

There may be three causes for this: 1) the weakness of the elastic model of the solid solution, 2) the presence of short-range order and 3) unaccounted systematic errors in the determination of the magnitude of the static displacements.

The first cause certainly does occur. However, if it were the only one, then a comparison of the experimental and calculated magnitudes would make it possible to determine the degree of deformation of the atoms in the solid solution.

The effect of the second cause can be determined by a comparison of the degree of the short-range order in the alloy, measured by the change in the background of the x-ray pattern [8], with the magnitude of the static displacements in the same alloy. As yet there are no systematic experiments which permit such a comparison to be made. However some indirect data, as for example the effect of heat treatment on the characteristic temperature of the alloy, the effect of the degree of long-range order on the magnitude of the static displacements and on the characteristic temperature of the alloy, seem to indicate the possibility of its material effect on the experimentally observed values.

Finally, it should be borne in mind that in the determination of the static displacements substantial errors can be introduced by the effect of extinction. A method for taking into account the secondary extinction has been proposed by the authors [11]. However in the case of experiments with uniform samples, as will be shown below, the effect of a primary extinction is also possible. This is also indicated by the results in reference [12] where it is shown that the magnitude of the mean square static displacements is found to be different when determined from x-ray patterns taken with various emissions.

The dependence of the magnitude of the mean square displacements on the concentration of a solid solution in a wide range of concentrations has been detected by the authors in the alloys CuZn [3], Fe-Co [17, 18], CuSn and Ni-Fe (the present work).

The curves $u_{st} = f(c)$ for Fe-Co alloys are given in Fig. 1. In Fig. 2 are given the data converted by the authors for the alloys Ni-Cr and Ni-Ti, taken from reference [6], and in Fig. 3 for the Fe-C alloy according to [13].

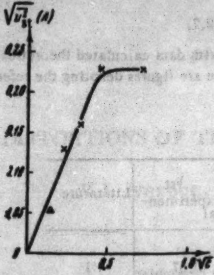

Fig. 1. The dependence of $\sqrt{\overline{u_{st}^2}}$ on the concentration in the Fe-Co alloy.
(× – according to [18], ▲ – according to [17]).

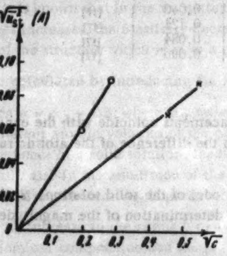

Fig. 2. The dependence of $\sqrt{\overline{u_{st}^2}}$ on the concentration in alloys Ni-Cr (×) and Ni-Ti (O).

Apparent in all curves is the linear dependence of α on the concentration at not too high concentrations, which corresponds to formula (1). The onset of saturation at high concentrations is naturally to be expected, since the use of calculations based on the elastic model of a dilute solution is inadmissible for solid solutions of high concentration. However in the case of Ni-Fe alloys the dependence of the static displacements on the concentration is represented by a curve of quite another type (Fig. 4).

It should be noted that when, in our previous work, the determination of the static displacements was carried out on powder samples, the Ni-Fe samples were monolithic. By construction of the straight line

$$\ln \frac{f_{\exp}}{f_0} = \varphi \left(\frac{\sin^2 \vartheta}{\lambda^2} \right)$$

it is possible to eliminate the effect of the secondary extinction which causes the deflection of the first points (with small hkl) from the straight line [11]. However the primary extinction should change the general slope of the f-curve and consequently its presence should lead to a diminshed value of α_{st}. Taking into account reference [12], in which as has been mentioned there is established the effect of the wavelength of the emission on the values of α_{st} obtained from experimental data, we determined the dependence of α_{st} on concentration for the Cu-Sn and Ni-Fe alloys by means of x-ray patterns taken with two types of emission. Those and other values for Cu-Sn alloys agree well. For the NiFe (32 % Fe) alloy however the value measured by the use of x-ray patterns taken with cobalt emission differs materially from that obtained by exposure with molybdenum emission (Table 3). (This latter sample was monolithic and known to be coarse-grained.) A comparison of the values of α_{st} obtained by exposure with different emissions may make it possible to judge the degree of mosaic structure of the samples.

The change of the interatomic bonds in a solid solution is determined by the magnitude of ΔB, i.e., by the change of the coefficient B in the temperature factor. We followed the change in the characteristic temperature in Ni-Fe alloys as a function of the composition, and also in Cu_3Au and Ni_3Fe as a function of the degree of long-range order. The characteristic temperature was determined by the x-ray method, with exposure at different temperatures. The x-ray patterns of the Ni-Fe alloys were taken with molybdenum emission at three temperatures (-175, 20, 215°C). The results obtained for each pair of temperatures agree approximately among themselves. The characteristic temperatures of the ordered Cu_3Au alloy are obtained by measuring the intensity of the x-ray interferences with the help of counters at two temperatures (-180 and 20°C) (see Tables 2 and 3) with copper emission.

For the ordered alloys an unexpected result was obtained indicating that with the emergence of long-range order the characteristic temperature drops.

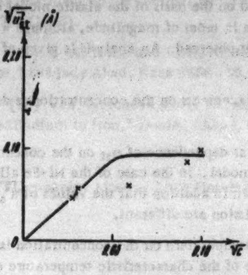

Fig. 3. The dependence of $\sqrt{\overline{u^2_{st}}}$ on the concentration in the Fe-C alloy. Along the abscissa are plotted the concentrations c/4.5 in atomic %.

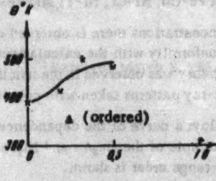

Fig. 4. The dependence of θ° on the concentration in the Ni-Fe alloy.

TABLE 2

No.	Alloy	θ, °K	No.	Alloy	θ, °K
1	$Cu_3Au_{ordered}$	240±10°	4	$Ni_3Fe_{ordered}$	480±30°
2	$Cu_3Au_{disordered}$	268*	5	$Ni_3Fe_{disordered}$	550±30°
3	Cu	320	6	Ni	400

---

* The value for the disordered alloy Cu_3Au is taken from reference [8].

TABLE 3

No.	Alloy	Characteristic temperatures				$\sqrt{\overline{u^2_{st}}}$
		calculated from 215°C and −175°C	calculated from 215°C and 20°C	calculated from 20°C and −175°C	Mean value θ	MoK_α
1	Ni	395	420	375	400	0
2	Ni—Fe(19% Fe)	420	385	455	420	0
3	Ni—Fe(32% Fe)	485	475	495	485	0.027
4	Ni—Fe(50% Fe)	475	465	480	470	0.058

The values obtained for the ordered alloy Cu_3Au approximate the results obtained in [14] and substantially disagree with the results in [15], in which the characteristic temperature is calculated from the elastic constants.

As shown in the example of the Ni_3Fe alloy, the value of the characteristic temperature of ordered alloys depends substantially on the heat treatment, which was also noted in reference [16]. Therefore a comparison of the results obtained for a disordered solid solution requires analysis of the production conditions of the alloy, i.e., analysis of the degree of short-range order.

SUMMARY

The mean square static displacements of the atoms are calculated on the basis of the elastic model of the solid solution. The experimental and calculated values of u_{st} agree in order of magnitude, although a correlation with the difference of the atomic radii required by theory is not observed. An analysis is given of the possible causes of such divergence.

The dependence of the magnitude of the mean square static displacements on the concentration is detected in the alloys of Fe-Co, Ni-Cr, Ni-Ti and Fe-C.

With low concentrations there is observed on all the curves a linear dependence of α_{st} on the concentration, which is in conformity with the calculations based on the elastic model. In the case of the Ni-Fe alloy a deviation from theory was observed in the function $\alpha = f(c)$. It is shown in addition that the values of $\overline{u^2_{st}}$ determined from x-ray patterns taken with cobalt and molybdenum emission are different.

For Ni-Fe alloys a curve of the dependence of the characteristic temperature on the concentration is constructed. In the example of the Cu_3Au and Ni_3Fe alloys the dependence of the characteristic temperature on the degree of long-range order is shown.

LITERATURE CITED

[1] V. I. Iveronova, "Distortions of the crystal lattice in solid solutions," Trudy Inst. Krist. Akad. Nauk 10, 149-157 (1954).

[2] G. M. Rovinskii, J. Exptl.-Theoret. Phys. (USSR) 7, 956 (1937).

[3] A. V. Beznosikova and V. I. Iveronova, "Atomic scattering of x-rays in copper and zinc alloys," J. Exptl.-Theoret. Phys. (USSR) 20, 6, 666-669 (1950).

[4] V. I. Iveronova, Z. I. Kuz'mina, S. S. Futergendler and E. I. Detlaf, "Atomic scattering of x-rays in solid solutions," Izv. AN SSSR Ser. Fiz. 15, 44 (1951).

[5] V. A. Il'ina, V. K. Kritskaia and G. V. Kurdiumov, "On the question of distortions of the lattice in deformed metals and solid solutions," Coll.: Problems of Metallography and the Physics of Metals [in Russian] (Metallurgy Press, 1951) pp. 222-231.

[6] G. V. Kurdiumov and N. T. Travina, "X-ray investigation of interatomic interactions in solid solutions based on nickel," Doklady Akad. Nauk SSSR 99, 77 (1954).

[7] R. A. Coyle and B. Gale, "Integrated x-ray intensity measurements from a solid solution of copper-gold," Acta Cryst. 8, 105 (1955).

[8] F. M. Herbstein, B. S. Borie and B. L. Averbach, "Local atomic displacements in solid solutions," Acta Cryst. 9, 466 (1956).

[9] K. Huang, "X-ray reflections from dilute solid solutions," Proc. Roy. Soc. 190, 102-117 (1947).

[10] V. I. Iveronova and A. P. Zviagina, "On the question of the intensity of x-ray scattering in solid solutions," Izv. AN SSSR Ser. Fiz. 20, 729 (1956).

[11] V. I. Iveronova and A. A. Katsnel'son, "On the question of the mosaic structure of crystals in polycrystalline metals," J. Tech. Phys. (USSR) 25, 4, 696-699 (1955).

[12] V. A. Il'ina and V. K. Kritskaia, "The determination of static distortions of the crystal lattice using x-rays of different wavelength," Doklady Akad. Nauk SSSR 110, 5, 765-769 (1956).*

[13] V. K. Kritskaia, G. V. Kurdiumov and N. M. Nodia, "On the bond strengths and the distortions in crystals of martensite," J. Tech. Phys. (USSR) 25, 2, 177-181 (1955).

[14] D. B. Bowen, "Debye temperature of Cu_3Au as the function of long-range order," Acta Met. 2, 4, 373 (1954).

[15] S. L. Quimby, "Variation of the mean Debye temperature of Cu_3Au between 20°C and 450°C," Phys. Rev. 95, 4, 916 (1954).

---

* [Soviet Physics — Doklady, p. 587].

[16] V. A. Il'ina, V. K. Kritskaia, G. V. Kurdiumov and T. N. Stelletskaia, "The effect of heat and mechanical treatment on the thermal factor in x-ray scattering by solid solutions," Izv. AN SSSR Ser. Fiz. 20, 7, 723-728 (1956).

[17] V. A. Il'ina and V. K. Kritskaia, "The bond strengths and static distortions in crystals of alloyed ferrite," Doklady Akad. Nauk SSSR 100, 1, 69-72 (1955).

[18] V. I. Iveronova and A. A. Katsnel'son, "Distortions of the crystal lattice in solid solutions of cobalt and palladium in iron," Doklady Akad. Nauk SSSR 99, 391-394 (1954).

M. V. Lomonosov Moscow State University

Received March 8, 1957

THE MECHANISM OF STRUCTURE TRANSFORMATIONS IN AGEHARDENING ALLOYS BASED ON NICKEL

Iu.A. Bagariatskii and Iu.D. Tiapkin

Single crystals of binary, ternary and quaternary nickel base alloys with aluminum, titanium and chromium were studied by use of the x-ray oscillating and diffuse scattering methods. The sequence of changes in atomic structure that takes place in formerly homogeneous solid solutions after quenching and annealing at 700-850°C was found.

Solid solutions of nickel with aluminum, titanium and chromium belong to the category of agehardening alloys by virtue of the noticeable decrease in solubility of the indicated elements in nickel with a drop in temperature from 1200-1300 to 700-800°C. The authors have carried out an x-ray investigation of binary, ternary and quaternary alloys, the compositions and constitutions of which are shown in Table 1. All these alloys can be divided into two groups: in the first, alloys in which the separation phase is a phase isomorphous to nickel, but with an ordered structure (the so-called γ'- or α'-phase based on the Ni_3Al compound) and in the second, alloys with the separation phase η-Ni_3Ti, which has a hexagonal close packed four-layer structure [1-5]. In the present case only the T and XT alloys belonged to the second group.

The object of the investigation was to determine what kind of atomic displacements are the means of the ultimate transformation of the single-phase (before quenching) solid solution into a two-phase system. Oscillating-crystal x-ray patterns obtained by "transmission" and by "reflection" were used, as well as pictures of diffuse scattering in those cases where it was necessary to show the presence of short-range order in the arrangement of atoms in a nickel solid solution. The process of aging was followed by measurements of the hardness of the alloys.

However the first x-ray patterns showed that in all the alloys examined after heating up to 1150-1250° and sudden cooling (quenching) the supersaturated solid solutions cannot yet be considered homogeneous: on the oscillating-crystal x-ray patterns from such alloys there are reflections characteristic of the ordered γ'-phase even in those cases where the equilibrium phase of separation is not γ', but the η-phase. The dimensions of domains with a superlattice were estimated (see Table 2) for the majority of the alloys from the spread of the superlattice reflections (Fig. 1). In some cases (alloys XT, XTA-1) the presence of a superlattice can be noted only by oscillating-crystal x-ray patterns obtained by "transmission" (thickness of crystal less than 0.1 mm), i.e., at small angles of reflection (Fig. 2). In these cases it was considered that the dimension of the domains with a superlattice is less than 50 kX.

Obtaining, by the superlattice reflections, periods of the lattices close to those for Ni_3Al (in alloys A and XA) clearly indicates that order cannot come about in the whole volume of the crystal, but occurs only in those domains where the content of aluminum or titanium approaches the stoichiometric.* This is again confirmed by the fact that the definition of the superlattice reflections depends both on the quantity of titanium and aluminum [6] and on the quenching temperature used. The enlargement of the domains having a superlattice with a drop in the quenching temperature (Fig. 1, a, b) indicates that even at a temperature of annealing below quenching the solid solution is not homogeneous and in it there already exists a submicroheterogeneity in the distribution of titanium and aluminum — in the same way that for the silver atoms in Al-Ag alloys there occurs a higher temperature of solution of the second phase [7]. However long-range order in the arrangement of the titanium and aluminum atoms in the nickel lattice probably appears in the concentrated domains only in the presence of cooling.

---

* This is even more graphically apparent in the later stages of the dissociation of the supersaturated solutions.

In alloys with small quantities of titanium and aluminum (XTA-1) the superlattice reflections, which indicate the presence of long-range order in the arrangement of atoms in a solid solution, can be observed only after quenching at 1080°, yet the pictures of the diffuse scattering of x-rays (Fig. 3) indicate a tendency toward short-range order also after quenching at a higher temperature (1250°). This tendency is found also in the stable solid solutions A-0 and T-0.

TABLE 1

Constitutions of the Principal Alloys Investigated

Designation	Composition			
	Atomic % according to chemical analyses			
	Al	Ti	Cr	Ni
I – Agehardening alloys				
A-1	14	—	—	Base
A-2	17	—	—	»
T-1	—	12	—	»
T-2	—	14	—	»
T-3	—	15	—	»
TA-1	4	7	—	»
TA-2	6	6	—	»
XA	8	—	15	»
XT	—	8.5	16.5	»
XTA-1*	2	3.5	22	»
XTA-2	5	5	15	»
II – Solid solutions				
A-0	7	—	—	Base
T-0	—	9,5	—	»

---

* Close in composition to the heat-resistant alloy of the "nimonik-80" type [16].

TABLE 2

Approximate Dimensions of Domains with Superlattice of the Ni_3Al Type in Quenched Alloys

Alloy	Quenching temperature (°C)	Dimensions (kX)	Alloy	Quenching temperature (°C)	Dimensions (kX)
A-1	1300	40—80	*XA*	1250	50—100
A-1	1250	60—120	*XT*	1250	<50
A-2	1250	100—200*	*XTA*-1	1250	—
T-1	1250	50—100	*XTA*-1	1080	<50
T-2	1250	200—400	*XTA*-2	1250	40—80
TA-2	1250	40—80			

In reference [6] 200-400 kX is denoted by mistake.

In the case of alloys A-1, A-2, T-1, T-2, TA, XT, XTA after annealing of short duration (0.5 – 2hours) at 600-700°, and sometimes also immediately after quenching, satellite-reflections are noted on the oscillating-crystal x-ray patterns, especially well marked in the case of the Ni-Al alloys (Fig. 4). These data are in complete agreement with the results of Manenc [8-10], the same interpretation of this phenomenon having been given by us [6] as by Manenc, based on the similarity of the phenomenon to that which is observed in the case of alloys of the Cu-Ni-Fe type [11, 12].

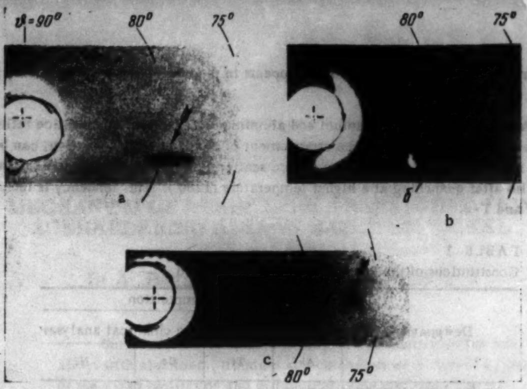

Fig. 1. Superlattice reflections 023 Fe on oscillating-crystal x-ray patterns (exposure by "reflection"; plane film, D = 40 mm) of monocrystals of Ni-Al and Ni-Ti alloys after quenching. a) alloy A-1, quenching at 1250°; b) the same, quenching at 1300°; c) alloy T-2, quenching at 1250°. K_αFe-emission.

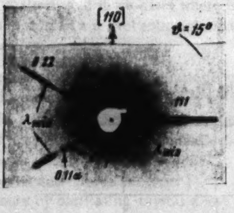

Fig. 2. Superlattice reflections 011 on oscillating crystal x-ray patterns taken by "transmission" from the quenched Ni-Cr-Ti alloy. (Composite Mo-emission, plane film, D = 40 mm). The boundary wavelength of the white spectrum is marked by streaks blackened by the primary reflections 022.

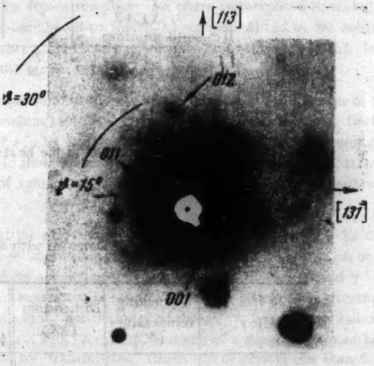

Fig. 3. X-ray pattern of the diffuse scattering (monochromatic K_αMo-emission, plane film, D = 40 mm) from a monocrystal of the Ni-Cr-Ti-Al alloy (XTA-1) after quenching at 1250°. The poorly defined superlattice spots 001, 011 and 012 are visible.

In the case of alloys A-1, A-2, T-1, T-2, TA, XT, XTA after annealing of short duration (0.5-2 hours) at 600-700°, and sometimes also immediately after quenching, satellite-reflections are noted on the oscillating-crystal x-ray patterns, especially well marked in the case of the Ni-Al alloys (Fig. 4). These data are in complete agreement with the results of Manenc [8-10], the same interpretation of this phenomenon having been given by us [6] as by Manenc, based on the similarity of the phenomenon to that which is observed in the case of alloys of the Cu-Ni-Fe type [11, 12].

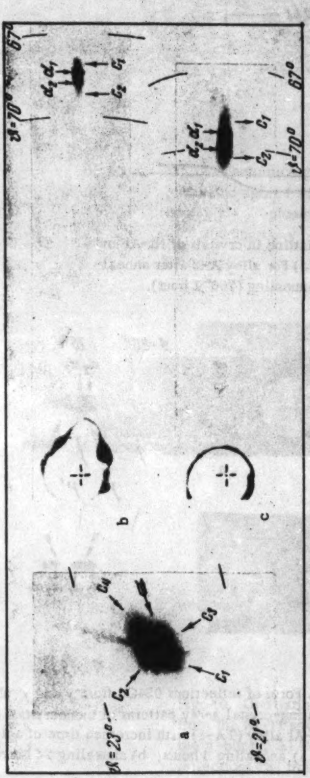

Fig. 4. Satellite reflections on oscillating-crystal x-ray patterns of monocrystals of the Ni-Al and Ni-Cr-Ti alloys at early stage of aging. a) alloy A-2, annealing 700° 1 hour, reflection 111 Cu; x 5; b) the same, annealing 2 hours, reflection 004 Ni; x 2; c) alloy XT, quenched at 1250°C, reflection 133 Cu; x2.

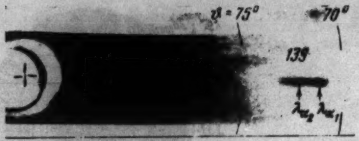

Fig. 5. Oscillating-crystal x-ray pattern of monocrystal of Ni-Al alloy (A-2) by Mo-emission after 2-hour annealing at 700°. The relatively clear reflections 139 K_{α_1} and K_{α_2} correspond to an increased period of the lattice, close to K_{aNi_3Al}, the diffuse ones at the side of the larger angle ϑ correspond to a decreased period. The intermediate period and the satellite do not come through. (Compare with Fig. 4, b).

Taking into account the necessary appearance of large elastic strains in the crystal lattice during the formation of domains with an increased lattice period and in view of the well-known work of Nabarro [13] on the advantage in this case of laminar formations, it is easy to realize also the advantage of the formation of modulated structures which cause the appearance of satellites on the x-ray patterns. It is characteristic that the period of alternation of the layers with an increased and a decreased period of the lattice (period of modulation) along axes of the type [001] depends little on the constitution of the alloy, the temperature and the time of aging. In all of the cases examined it is close to 300-400 kX.

The modulated structures were examined by means of oscillating-crystal x-ray patterns by "reflection" with hard (K_αMo) emission. As in the case of the Ni-Al alloys [6], in all of the other cases it was not possible to observe satellites of the reflections of high orders. The observed pictures (Fig. 5) could have been interpreted as an independent scattering by the domains with a superlattice (and increased period of the lattice) and by the domains poorer in titanium and aluminum. Such an interpretation is in agreement with the work in reference [14], if the period of modulation is allowed to vary.

On the basis of the results obtained graphs were constructed of the probable change in the period of the lattice $a = 2d_{(001)}$ along axes [001] of crystals of the agehardening solid solutions examined at this early stage of aging (Fig. 6).

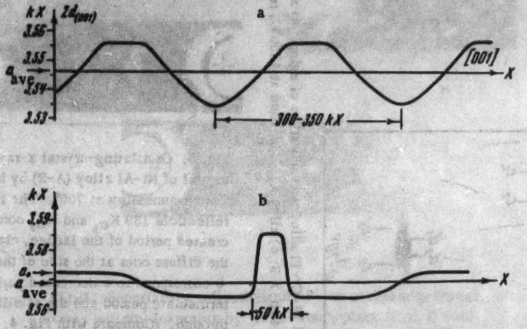

Fig. 6. Graph of change in period of the lattice in crystals of Ni-Al and Ni-Cr-Ti alloys at early stages of aging. a) For alloy A-2 after annealing (700° 2 hours); b) for alloy XT after annealing (700° 1 hour).

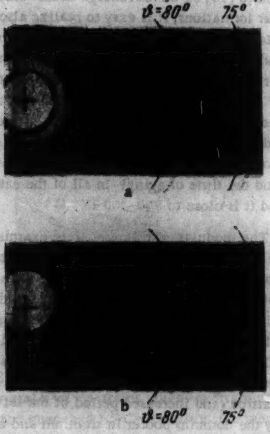

Fig. 7. Change in form of basic reflection 024 Cu and of superlattice reflection 023 Fe on oscillating-crystal x-ray patterns of monocrystals of the Ni-Al alloy (A-2) with increased time of aging at 700°. a) annealing 2 hours; b) annealing 8 hours.

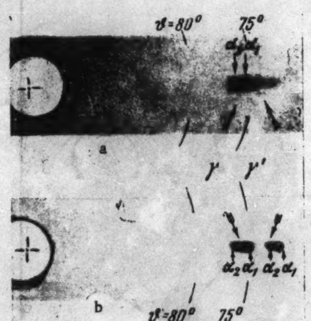

Fig. 8. Form of reflections 024Cu from γ and γ' phases on oscillating-crystal x-ray patterns of monocrystals of the Ni-Ti-Al alloy (TA-1) with increased time of aging at 800°. a) annealing 4 hours; b) annealing 24 hours.

With an increase in the aging period at 700° the basic reflections, located within the large angles ϑ (on exposure with soft radiation), quickly become diffuse and the super lattice reflections become clearer (Fig. 7); the character however of the high-order reflections (on exposure with hard radiation), changes little; only in the case of the alloy XT (and XTA) do the components corresponding to layers with an intermediate (original) period of the lattice gradually disappear. All this argues that here

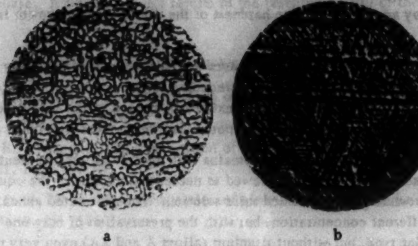

Fig. 9. Photomicrograph of the Ni-Al and Ni-Cr-Ni alloys after protracted aging (×1000). a) alloy A-2 (annealing 800° 1000 hours); $\gamma + \gamma'$-phases; b) alloy XT (annealing 900° 300 hours + 700° 300 hours); $\gamma + \eta$-phases.

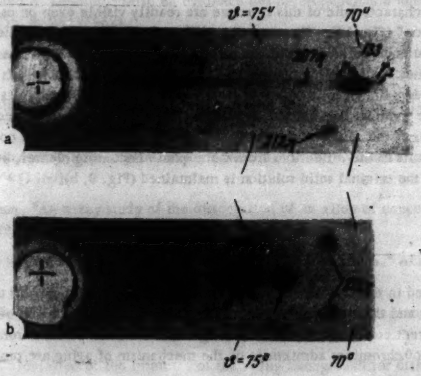

Fig. 10. Oscillating-crystal x-ray patterns (by Cu-emission) from the Ni-Ti and Ni-Cr-Ti alloys with reflections from the η-phase. a) alloy XT after annealing (850° 2 hours); two reflections 133 from the solid solution are visible; b) alloy T-3 after annealing (800° 1000 hours); condition of η-phase close to equilibrium (orientation of the crystal is different from that in photograph a).

the progressive separation of a supersaturated solid solution ends up in two phases — one with a reduced concentration of aluminum and titanium (close to equilibrium) and one with an increased concentration, close to 25 atomic % of Ti + Al; whereupon the development of the process goes, in principle, not on account of an increase in difference of concentrations, but on account of the enlargement of the submicrovolumes enriched by titanium and aluminum. In the XTA alloys this tendency is less clearly expressed; according to the x-ray patterns taken with Mo-emission there is a marked change in the concentration of an impoverished solid solution with an increase in the period of aging.

In all of the agehardening alloys examined, the growth of the nucleating γ'-phase up to dimensions of 200-400 A is accompanied by an increase in the hardness of the alloys; further growth is accompanied by a decrease in hardness.

The process of enlargement of the submicrovolumes with a superlattice evidently takes place by means of the fusion of smaller volumes characteristic of the preceding stage, as a result of which the periodicity of the alternation of the layers of equal thickness, which existed in a stage of the modulated structure, is disrupted. In the alloys XA and T-3 a modulated structure is not noted, but the process goes on in an analogous manner.

In alloys with the equilibrium phase γ', the domains with an ordered arrangement of atoms and a high concentration of aluminum and titanium can be viewed as nucleation centers of the equilibrium phase of separation, connected with the surrounding impoverished solid solution. The protracted annealing of such alloys leads to a single volume with a different concentration, but with the preservation of only one orientation of the lattices (Fig. 8). In alloys of a similar type, but without titanium (alloys A and XA) even very protracted annealing at a high temperature (1000 hours at 800°) does not lead to such a complete separation of reflections from both phases, although microstructurally the separations of the γ'-phase are clearly visible (Fig. 9, a).

The process goes on in a different fashion in those alloys in which the equilibrium phase of separation is the hexagonal η-phase. Here also there exists a stage (in particular, after a 2-hour annealing at 800-850°) when there can be noted (even in x-ray patterns obtained with soft radiation) the presence of two solid solutions, in which the titanium-rich solid solution possesses an ordered structure of the Ni_3Al type. For example, at the same time, submicrovolumes with the structure of the η-phase appear in these alloys, as shown by the x-ray pattern. Reflections characteristic of this structure are readily visible even on oscillating-crystal x-ray patterns obtained by "reflection" (Fig. 10). The somewhat diffuse form of the spots of the η-phase and the difference between the measured and equilibrium values of the periods a and c indicate the adaptation of the hexagonal lattice in these volumes to the lattice of the surrounding solid solution. Analysis of the volumes which correspond to one atom in domains of solid solutions impoverished and enriched by titanium and in domains where a lattice of the η-phase had formed, argues that the latter occurred on account of the reorganization of the lattice in domains of the solid solution enriched by titanium almost to the composition of Ni_3Ti. Very protracted annealing results in the reflections from the η-phase becoming clearer, but its regular orientation relative to the crystal of the original solid solution is maintained (Fig. 9, b):

$$(00\cdot1)\,\eta \parallel (111)\,\gamma$$
$$(11\cdot0)\,\eta \parallel (110)\,\gamma.$$

The method used in the investigation, while making it possible to specify the character of the transposition of the aluminum and titanium atoms in the lattice during the dissociation of a solid solution, does not make it possible to draw direct conclusions as to the change in distribution of the chromium atoms. Therefore considerations as to the effect of chromium admixtures on the mechanism of aging are omitted here; they are written up in reference [15].

SUMMARY

1. The dissociation (stratification) of agehardening nickel solid solutions has already begun in the process of annealing alloys at temperatures below quenching. The dimensions of the heterogeneities observed in quenched alloys depend on the content of titanium and aluminum and on the annealing temperature; they vary in the alloys investigated from 50 (and less) to 200-400 kX. In these domains there is noted a definite degree of long- or short-range order in the distribution of atoms of the Ni_3Al structural type.

2. In some alloys at an early stage of aging a modulated structure is formed, similar to that in Cu-Ni-Fe alloys, but with a period of modulation of the order of 300-400 kX.

3. In alloys with the equilibrium phase of separation γ', isomorphous (as to the type of lattice) with the original solid solution, the process of formation of particles of the phase of separation consists of the subsequent growth and separation of submicrovolumes formed during quenching, with a composition close to $(Ni, Cr)_3(Ti, Al)$ and with an ordered arrangement of atoms.

4. In alloys with the equilibrium phase of separation η, the first stage of aging is similar to that in alloys with the γ'-phase; but upon the attainment of definite dimensions by domains enriched by titanium (with superlattice of the Ni_3Al type) there takes place in them a reorganization of the cubic lattice into the hexagonal, characteristic of the η-phase. A further process results in the oriented growth of these particles — of the nucleating η-phase.

LITERATURE CITED

[1] A. Taylor and R. W. Floyd, "The constitution of nickel-rich alloys of the nickel-chromium-titanium system," J. Inst. Metals 80, 11, 577 (1952).

[2] A. Taylor and R. W. Floyd, "The constitution of nickel-rich alloys of the nickel-titanium-aluminum system," J. Inst. Metals 81, 1, 25 (1952).

[3] A. Taylor and R. W. Floyd, "The constitution of nickel-rich alloys of the nickel-chromium-aluminum system," J. Inst. Metals 81, 9, 451 (1953).

[4] A. Taylor, "Constitution of nickel-rich quaternary alloys of the Ni-Cr-Ti-Al system," J. Metals 8, 10 Sec. 2, 1356 (1956).

[5] F. Laves and H. J. Wallbaum, "Die Kristallstructur von Ni_3Ti and Si_2Ti (zwei neue Typen)," Z. Krist. 101, 78 (1939).

[6] Iu. A. Bagariatskii and Iu. D. Tiapkin, "Peculiarities of the structure of alloys in the process of dissociation of a supersaturated solid solution of aluminum in nickel," Doklady Akad. Nauk SSSR 108, 3, 451 (1956).

[7] C. B. Walker, J. Blin and A. Guinier, "Mise en evidence des heterogeneites d'une solution solid en equilibre," Compt. rend. Paris 235, 3, 254 (1952).

[8] J. Manenc, "Evolution de la structure d'un alliage type nickelchrome 80-20 apte au durcissement structural, etudiee aux rayons X," Ibid 238, 18, 1817 (1954).

[9] J. Manenc, "Sur l'evolution de la structure d'un alliage type Ni-Cr 80/20 modifie tenace a chaud," Ibid 240, 25, 2413 (1953).

[10] J. Manenc, "Sur l'evolution de la precipitation de nickelure d'aluminium dans un alliage a 7.8% d'aluminium," Ibid 242, 19, 2344 (1956).

[11] V. Daniel and H. Lipson, "An x-ray study of the dissociation of an alloy of copper, iron and nickel," Proc. Roy. Soc. 181, 987, 368 (1943).

[12] M. E. Hargreaves, "Modulated structures in some copper-nickel-iron alloys," Acta Cryst. 4, 4, 301 (1951).

[13] F. R. N. Nabarro, "The influence of elastic strain on shape of particles segregating in an alloy," Proc. Phys. Soc. 52, 289, 90 (1940).

[14] Iu. A. Bagariatskii, "Calculation of the intensity of the x-ray background for different degrees of order in the distribution of defects in crystals," Doklady Akad. Nauk SSSR 92, 6, 1157 (1953).

[15] Iu. A. Bagariatskii and Iu. D. Tiapkin, "X-ray study of the aging of nickel base alloys," Fifth Coll. Proc. Institute of Metallography and the Physics of Metals (TsNIIChM)* Problems of Metallography and the Physics of Metals [in Russian] (in press, 1957).

[16] M. L. Bernstein, Steels and Alloys for Work at High Temperatures [in Russian] (1956) p. 171.

Institute of Metallography and the Physics of Metals
TsNIIChERMET

Received February 22, 1957

---

* Central Scientific Research Institute of Ferrous Metallurgy.

ON THE FORMATION OF SPHERULITES

A.V. Shubnikov

In the paper it is shown that under certain conditions the formation of a crystalline element in the form of a spherulite, formed entirely by faces with the greatest specific surface energy, can be more advantageous energetically than its formation in acicular or laminar form.

It is known that the normal rate of growth v_i of any face of a crystal forming from a melt can be described to a first approximation by the formula

$$v_i = a_i (T_i - T_K),$$

where T_i is the equilibrium temperature between the medium and a face of the i-th simple form, T_K is the temperature of the medium at the surface of the crystal, a_i is a constant.

For simplicity we assume that the temperature T_K is the same at every given moment of time on all faces of the crystal. Let

$$T_1 > T_2 > T_3 \ldots$$

Experiment shows that under actual conditions faces of a very limited number of simple forms can grow on the crystal; for example, on crystals of alum grown from a pure water solution, faces of not more than three simple forms are observed.

If for the crystal under study all the values of a_i, T_i are known, then a general graph of the dependence of the rate of growth on the temperature T_K can be plotted, and according to this graph the form of the crystal for any temperature T_K can in its turn be reproduced, if the angles between the normals to the faces are known.

We shall consider the formation of a crystal in a viscous medium, when the heat exchange between the crystal and the medium is accomplished only by means of thermal conduction, with convection excluded.

We consider how a tetragonal crystal having only prism $\{100\}$ and basal $\{001\}$ faces will grow. It is assumed that the faces of all other simple forms have a considerably greater rate of growth and therefore cannot develop on the crystal under experimental conditions.

If the rate of growth v_1 of the basal faces is greater than the rate of growth v_2 of the prism faces, the crystal will have an acicular habit. With the inverse ratio of rates it will have a laminar habit. We shall consider both of these cases together, but for concreteness we shall consider that $v_1 > v_2$. This means that the straight line

$$v_1 = a_1 (T_1 - T_K)$$

lies entirely above the curve

$$v_2 = a_2 (T_2 - T_K),$$

within the observed temperature range as is shown in Fig. 1.

We assume that the crystal developed, as often happens, during a considerable supercooling of the melt, i.e., with the temperature of the lower-melting $\{100\}$ faces. Evidently in this case the form of the crystal being produced, i.e., the ratio of its width x to its height z will equal the ratio v_1/v_2:

$$\frac{x}{z} = \frac{v_1}{v_2}.$$

With further growth of the crystal its temperature, which we regard as equal (or approximately equal) to the temperature of the medium in the vicinity of the crystal, may rise owing to the liberation of heat of crystallization. As a result a certain fixed temperature T_K^* can be established at which the crystallization will proceed to its natural completion. The less the heat of fusion, the higher the temperature will be.

In Fig. 1 it is apparent that at T_K^* very close to temperature T_2, the ratio v_1/v_2 can become very large and in the limit, at $T_K = T_2$, even infinitely large. This means that in similar cases the growth of the prism faces can be practically completely arrested, in consequence of which the crystal will acquire a more and more elongated form. With the inverse ratio of rates, i.e., with $v_1 < v_2$, the crystal evidently will under analogous conditions assume a more and more compressed form.

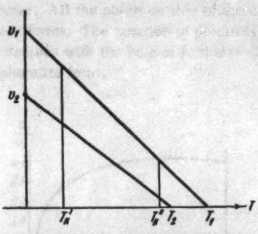

Fig. 1. Dependence of normal rates v_1 and v_2 of the basal and prism faces of a tetragonal acicular crystal on temperature T.

Such forms from the energy standpoint (the stipulation of a minimum of free surface energy for a given volume of the crystal) may prove to be less advantageous than a form of spherulite which develops as a result of the cleavage of an acicular crystal along the z axis and of a laminar crystal along the basal plane, i.e., less advantageous than a form of spherulite entirely covered by small quickly growing faces having higher specific surface energy than the slowly growing faces.

It is pertinent to note here that the form of a sphere covered by small faces of the crystal which have the least of possible values of specific surface energy is from the energy standpoint always more advantageous than any polyhedral form. However, inasmuch as the conversion of a single crystal into a spherulite can be accomplished, in our opinion, only by means of the cleavage of the crystal at the time of its growth, but the splitting itself can occur only along the planes of the best cleavability of the crystal, and such planes are those having the least specific surface energy, then the spherulite ought to be covered precisely by such planes as possess the greatest specific surface energy.

We now show by means of calculation that there can exist conditions under which the crystalline element can be the same from the energy standpoint, whether it have the form of a polyhedron with faces $\{100\}$ and $\{001\}$, or a spherulite, continuously covered either by faces $\{001\}$ if the crystal has an acicular habit, or faces $\{100\}$ if it has a laminar habit.

It is easy to see that for a crystal having the form of a polyhedron formed by the faces $\{100\}$ and $\{001\}$, the following relations are correct:

$$v_k = x^2 z, \tag{1}$$

where v_K is the volume of the crystal, x is the width of the crystal in the direction of axis X ⊥ (100), z is the height of the crystal along axis Z ⊥ (001);

$$\sum_K = 2x^2 + 4xz, \tag{2}$$

where Σ_K is the total surface of the crystal;

$$E_K = 2x^2\sigma_1 + 4xz\sigma_2, \tag{3}$$

where E_K is the overall surface energy of the crystal, σ_1 is the specific surface energy of the faces $\{001\}$, σ_2 is the specific surface energy of the faces $\{100\}$.

For a spherulite continuously covered by the faces $\{001\}$, i.e., for a spherulite which originates by means of cleavage of an acicular crystal and for the case of equality of the volume of the crystal v_K and the volume of the spherulite v_S, the following relations occur:

$$\sigma_1 > \sigma_2; \tag{4}$$

$$\sum_S = 4\pi R^2 = 4.8\sqrt[3]{x^4 z^2}, \tag{5}$$

where Σ_S is the surface of the spherulite, R is its radius;

$$E'_S = 4.8\cdot\sigma_1\sqrt[3]{x^4 z^2}, \tag{6}$$

where E'_S is the surface energy of the spherulite.

The crystalline element can be the same whether it have acicular or spherical form on the condition that

$$E_K = E_S, \tag{7}$$

i.e., if

$$2x^2\sigma_1 + 4xz\sigma_2 = 4.8\,\sigma_1\sqrt[3]{x^4 z^2}.$$

Hence finally

$$\frac{\sigma_2}{\sigma_1} = 1.2\sqrt[3]{\frac{x}{z}} - 0.5\,\frac{x}{z}. \tag{8}$$

For a spherulite which has formed by means of cleavage of a laminar crystal along the faces $\{001\}$, i.e., for a spherulite continuously covered by the faces $\{100\}$, instead of the relations (4) and (6) there occur the relations

$$\sigma_1 < \sigma_2, \tag{9}$$

$$E_S'' = 4.8 \cdot \sigma_2 \sqrt[3]{x^4 z^2}, \qquad (10)$$

where E_S'' is the surface energy of a spherulite which has formed from a laminar crystal.

In this case, when $E_S'' = E_K$,

$$2x^2 \sigma_1 + 4xz\,\sigma_2 = 4.8\,\sigma_2 \sqrt[3]{x^4 z^2},$$

and finally

$$\frac{\sigma_1}{\sigma_2} = 1.2 \sqrt[3]{\frac{z^2}{x^2} - \frac{z}{x}}. \qquad (11)$$

Equation (8) can be represented graphically (Fig. 2) if the value of x/z is plotted along the horizontal axis and the value of σ_2 / σ_1 along the vertical. The very possibility of constructing this graph indicates the possibility of the existence of conditions under which the crystalline element can be the same, whether it have an acicular form or the form of a spherulite. This state of "sameness" is characterized by the points lying on the curve. All the points outside of the curve denote a state in which the crystalline element should favor one of these forms. The question of precisely which of the two indicated forms is favored with the given x, z, σ_1, σ_2 is decided with the help of formulas (3) and (6): when $E_S' > E_K$ the acicular form is favored, when $E_S' < E_K$, the spherulite form.

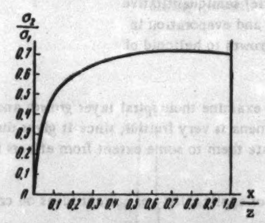

Fig. 2. Graph of dependence of σ_2 / σ_1 on x / z for a crystalline element for which the acicular form and the spherulite form are equally probable.

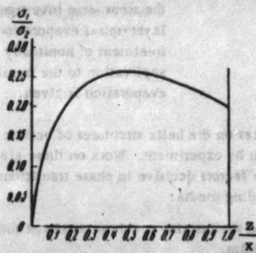

Fig. 3. Graph of dependence of σ_1 / σ_2 on z /x for a crystalline element for which the laminar form and the spherulite form are equally probable.

The conclusions drawn can be extended also to the laminar form.

The indifferent relation of the crystalline element to the laminar form and to the spherulite form is described by formula (11) and by the corresponding graph (Fig. 3). The question of the greater or the lesser favorableness of the laminar form over the spherulite form is decided simultaneously by application of formulas (3) and (10). When $E_S'' > E_K$ the laminar form is more stable, when $E_S'' < E_K$, the spherulite form.

We have discussed the influence of only two factors v_1 and σ_1 on the form of the crystalline element. It does not follow that these factors are the most important and that other factors, possibly more significant, cannot influence the formation of crystals.

Institute of Crystallography
Academy of Sciences, USSR

Received February 22, 1957

THE DYNAMICS OF CERTAIN ELEMENTARY CRYSTAL GROWTH AND EVAPORATION PROCESSES

G.G. Lemmlein, E.D. Dukova and A.A. Chernov

The results of our researches on the formation of the screw dislocations and mutual approach and cancelling of two dislocations with opposite signs by means of microcinemafilming are described and discussed. The step movement velocity dependence on the thickness of the corresponding layer was determined and interpreted. The melt drops behavior on the crystal surface and their interaction with the steps were investigated. Some results of the observation on the layer-spiral evaporation are described. The brief semiquantitative treatment of nonsteady processes of the growth and evaporation in application to the transition from helicoid of growth to helicoid of evaporation is given.

Studies on the helix structures of certain crystals [1-3] led us to examine their spiral layer growth and evaporation by experiment. Work on these elementary surface phenomena is very fruitful, since it gives direct data on the factors decisive in phase transitions and enables us to isolate them to some extent from effects in the surrounding media.

These studies also enable us to check the correctness and range of applicability of current ideas on crystal growth kinetics.

1. The Formation of Dislocation Growth Centers

We used the growth of volatile organics from the vapor phase at low supersaturations in our studies on the spiral growth of thin crystals (10μ) [4]. Suitable conditions were produced in a hollow glass cylinder with a heater sealed into the bottom. A miniature oven (evaporator) containing a small crucible filled with the material was fitted within the vessel. The bottom heater was used to regulate the general temperature in the chamber. The evaporator produced a temperature gradient along the cover of the chamber. Both heaters were rheostat-regulated. Copper-constantan thermocouples measured the temperature near the surface of the crystals. The chamber was placed on a microscope stage. The main disadvantage was that the supersaturation could not be measured precisely.

We used p-toluidine, naphthalene, diphenyl, diphenylamine and other organics on which we had found spiral growth. The p-toluidine was the most convenient. The crystals belong to the orthorhombic system and have layered structures; the unit cell contains 8 molecules (two layers of four each) and has a large value of C ($c = 23.5$ A). The birefringence along this direction is high; $n_g - n_p = 0.22$. It was therefore possible to make observations at 400 X on the (001) face in ordinary and in polarized light, and to detect steps one unit cell high.

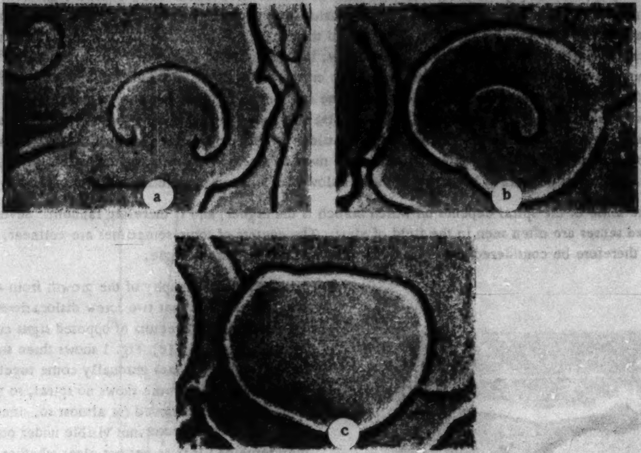

Fig. 1. Approach of two dislocation centers of opposed signs during growth.

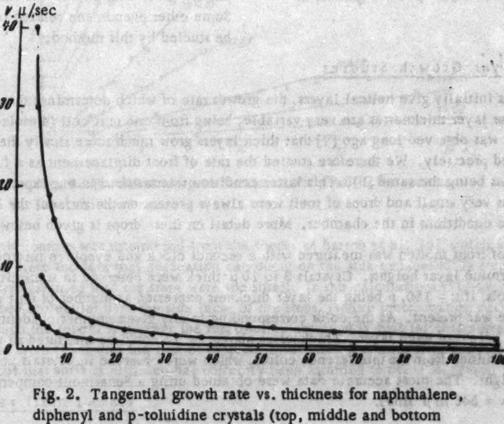

Fig. 2. Tangential growth rate vs. thickness for naphthalene, diphenyl and p-toluidine crystals (top, middle and bottom curves respectively).

Growth along face-normals occurred by tangential layer spread. The fronts could clearly be seen advancing. The layer sources were almost always structural defects which were screw dislocations.

We studied the early growth stages of the thinnest crystals to establish how these defects (and the associated spiral layers) formed [5]. The crystals were rarely found to have true isometric forms right at the start, but grew as more or less branched dendrites. A screw dislocation began to form when two branches of a dendrite from one crystal came into contact and one overlaid the other for some reason. The gap between the branches soon became covered over and remained as a hollow, visible as a thin line under the microscope. The resulting dislocation had its Buergers vector normal to the crystal surface; the surface itself showed a step. When the length of the step reached a certain critical value the step began to move, and a new helical layer was formed. This mechanism implies that one branch of the crystal lies above the other, and that the growth rate near the roots of the branches is reduced. The second we consider to be a consequence of the first. If one branch is raised above another the point where the roots meet must be a region of stress concentration; in such regions the saturation vapor pressure is higher, so growth is slowed or stopped completely.

The sense of the spiral depends on which branch is the higher, and is therefore random. Several spirals of opposed senses are often seen in the field of view. The centers of some sometimes are colinear, and the line can therefore be considered as the trace of an overgrown re-entrant angle.

Cinemicrography of the growth from existing dislocations showed that two screw dislocations of equal (or almost equal) vectors of opposed signs could overlap and cancel out [6]. Fig. 1 shows three successive frames. The two axes gradually come together during growth. The last frame shows no spiral, so the dislocations have been removed (or almost so, since a spiral of small Buergers vector, not visible under our conditions, may remain). It is as yet not clear whether this effect indicates that dislocation lines can actually move, or whether it occurs simply because the lines are not precisely normal to the crystal surface. In the latter case we would get one arc-shaped line when two fuse.

In dislocation formation and cancellation the layer pattern gives data on how the screw dislocations behave. Some other phenomena related to dislocations can also be studied by this method.

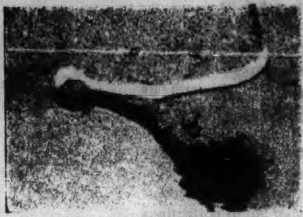

Fig. 3. Protuberance on the surface of a silicon carbide crystal. (The black spot is a granule of graphite).

2. Spiral-Layer Growth Studies

Dislocations initially give helical layers, the growth rate of which determines the crystal growth rate along face-normals. The layer thicknesses are very variable, being from one unit cell (4 molecules) thick to several thousand such. It was observed long ago [7] that thick layers grow much more slowly than thin, but the rates were not compared precisely. We therefore studied the rate of front displacement as a function of thickness, all other conditions being the same [8]. This latter condition was satisfied in our experiments because the area of crystal used was very small and drops of melt were always present on the surface; the behavior of these latter is very sensitive to conditions in the chamber. More detail on these drops is given below.

The rate v of front motion was measured with a seconds clock and eyepiece micrometer. Three methods were used to determine layer heights. Crystals 3 to 10 μ thick were observed in transmitted polarized light between crossed nicols; if n = 150, n being the layer thickness expressed as number of unit cells, a sensitive second-order color change was present. As the color corresponding to any given number of identical layers was known we could find the height of each layer. Thicknesses above n = 15 could be measured in this way. Heights down to n = 1 were determined from the interference colors, which were observed in crystals up to 1 μ thick in reflected ordinary light. The most accurate data were obtained using a Senarmont compensator (the light source was the mercury λ = 546 m μ line).

Figure 2 shows the results. The points fall into separate groups in the (v, n) plane; these correspond to layers of different thicknesses, which indicates that the measurements were precise and that the conditions were very similar in the various experiments. The layer heights were always multiples of the cell parameter.

The curve is well described (for $n \geq 3$) by

$$v = A + \frac{B}{n}, \tag{1}$$

where A and B are constants. Deviations from (1) exceeding the experimental error occur at lower $\underline{n}$. At $n = 1$ the observed rate is about half that given by (1).

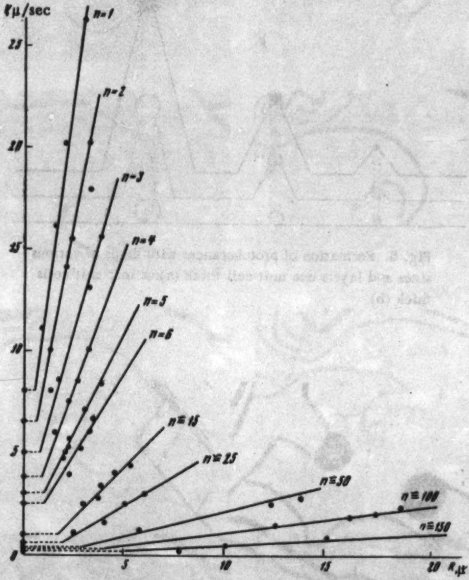

Fig. 4. Protuberance growth rate vs. drop radius for various layer thicknesses.

The observed relationship was interpreted from the theory of Barton et al., [9], which we have applied to steps of any height. Here the fact that nucleation can occur on the side surfaces of the steps [10] was either neglected, or else it was assumed that the steps were too small. In our calculations [11] we have allowed for the diffusion of adsorbed molecules over the side faces of the steps, (where incorporation occurs) as well as over the flats. Although the model is inexact the relationship obtained is qualitatively correct. The physical cause of the deviations from (1) is that the flux of incident molecules decreases with the step height. This effect is a further proof that surface diffusion has correctly been assumed to occur in crystal growth.

3. Protuberances from Layers

Morphologic studies on silicon carbide crystal faces showed that the spiral layer structures sometimes had projections with circular bodies at the ends reminiscent of pendant drops (Fig. 3). Observations on growth from the gas phase were used to study and record the rate of this process. Drops of liquid appeared on the surfaces of the crystals when the temperature was 3-4° below the m. p. When the crystal was growing, the drops were mobile; as equilibrium was approached they moved less, and at equilibrium they were localized and merely oscillated.

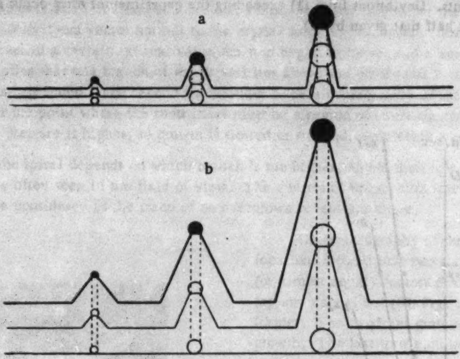

Fig. 5. Formation of protuberances with drops of various sizes and layers one unit cell thick (a) or four unit cells thick (b).

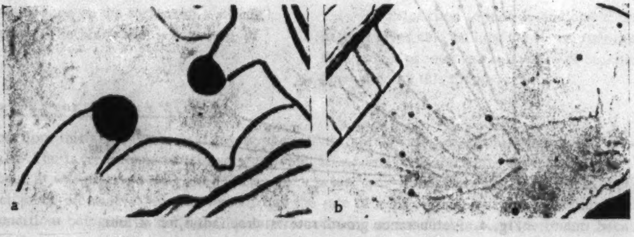

Fig. 6. Protuberances from thick (a) and thin (b) layers.

The spherical shape and high mobility of the drops indicates that they do not wet the surface. This supports the idea that there is a gas layer between drop and crystal.

The freely moving drops sometimes adhered to the fronts of growing layers. We then observed an effect which may be described as follows. The drops adhered because they wetted some small area of a side face, usually rather smaller than the drop. A part of the crystal surface was then in direct contact with the melt, and at a point where the transition to the solid state is easiest. The crystal then grew rapidly from the melt at this point. Elsewhere the step grew from the gas phase and at the same rate as before, i.e , more slowly. The smooth front then gave way to one with a protuberance, which pushed the drop feeding it on in front. Kowarski [12] first observed these protuberances. No appreciable change in drop size occurred while the protuberance was growing. The protuberance had the shape of a truncated equilateral triangle, with the drop at the upper truncated vertex. The area of crystal growing directly from the melt formed a rectangle, one side being of length equal to that of the protuberance and the other of length equal to the length of contact between drop and layer.

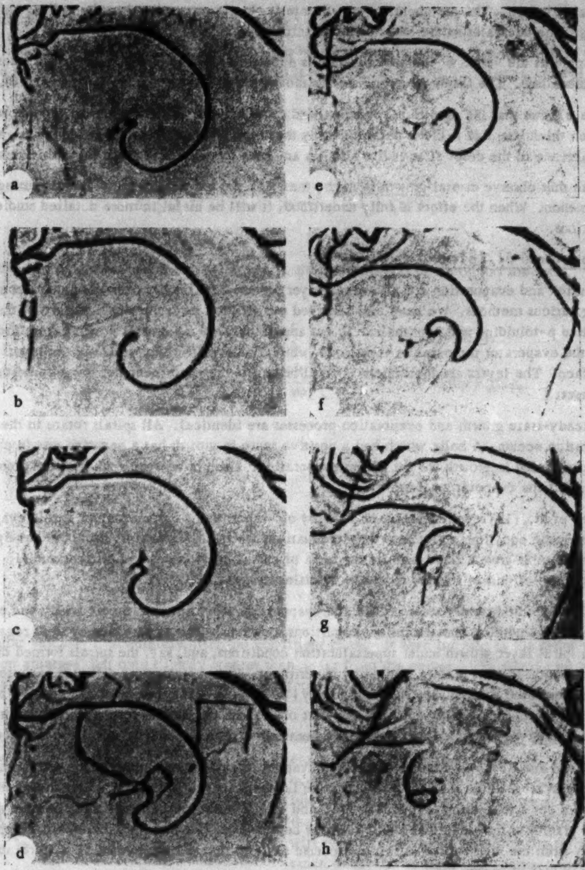

Fig. 7. Transformation of growth spirals into evaporation ones. Frames from a film. Intervals between frames: a and b, 4 min; b and c, 27 sec; c and d, 20 sec; d and e, 60 sec; e and f, 62 sec; f and g, 57 sec; g and h, 84 sec.

If the crystal is in equilibrium with its vapor near the m. p., a drop placed in this way gives no protuberance, but gradually flows over the step. Because of contact angle hysteresis, the drop can not completely wet the step; or in other words, as soon as the drop begins to wet the step, the crystal begins to grow and push the drop away.

Studies on the course of this effect involve measuring drop size, layer growth rate, protuberance growth rate, etc., simultaneously. This was done by cinemicrography. For a layer of given height the protuberance growth rate was found to depend on the radius of the adhering drop. Figure 4 shows how the effect varies with radius and layer height. The protuberance growth rate is clearly proportional to the radius, while the slope of the straight line decreases as the layer becomes thicker.

The angle at the vertex of the protuberance is determined by the ratio of the growth rates of the layer and the protuberance. The faster the protuberance moves the smaller the angle (Figs. 5 and 6).

Figure 4 shows that the drop radius must exceed some limiting value for a protuberance to form with a layer of given thickness; this value is determined by the slope of the appropriate straight line and the growth rate in the absence of the drop. The radius also has an upper limit for any given layer thickness.

We can thus observe crystal growth from the melt and the gas phase simultaneously, using the protuberance phenomenon. When the effect is fully understood, it will be useful in more detailed studies of these phase transitions.

4. Evaporation of Spiral Layers

Dissolution and evaporation are also spiral-layer processes. This has been concluded from studies on etch figures using various methods. We have also observed evaporation from the whole surface of the crystal. As before, we used p-toluidine and naphthalene in our apparatus. When a crystal growing from the gas phase is observed as the evaporator temperature is reduced (which reduces the vapor pressure) the layers cease to spread over the surface. The layers are motionless at equilibrium; if the vapor becomes unsaturated the direction of motion reverses.

The steady-state growth and evaporation processes are identical. All spirals rotate in the reverse sense when evaporation occurs. A helix which had a positive sense in growth has a negative one in evaporation; if outgrowths are formed in growth we get pits in evaporation. Deep holes soon appear at the points where dislocations occur if the evaporation is rapid.

Cabrera et al., [13] recently proposed a theory of evaporation. Spiral rotation during evaporation is described by the same equations as for growth; the equations are invariant against simultaneous sign reversal for the linear and angular growth rates, and for the radii of curvature of layers and critical nuclei. The difference only appears in the effects of stresses produced by dislocations.

Many have studied steady-state growth and evaporation processes both theoretically and experimentally. These studies tell us nothing about transient conditions, however. This is particularly so as regards the transition between spiral layer growth under supersaturation conditions, and, say, the spirals formed during evaporation. This transition is most readily studied by experiment. Visual studies are difficult because the rates are low. We therefore used time-lapse cinemicrography (300 ×, one frame per second). Figure 7 shows some frames from the film. The type of spiral at the start of evaporation clearly results from two simultaneous processes; general layer retraction and uneven evaporation at rates dependent on the curvature of the layer.

Figure 7, c and d, shows that the most rapid evaporation occurs at the top of the spiral where the dislocation emerges, i.e., where the radius of curvature is least. As this part of the spiral moves more rapidly than the rest we get a projecting tongue (Fig. 7, d and e). The tongue becomes more pointed as evaporation proceeds and gradually moves further away from the center (Fig. 7, e and f). The end of the spiral begins to move away from the dislocation, but in the reverse sense to that during growth. The spiral unwinds in a sense reverse to that of growth.

To derive an accurate formula for the behavior of the spiral we should have to solve the equation for the nonsteady state. Some qualitative deductions can, however, be made if we only know the distribution of angular velocities along the spiral at the time when conditions change sharply.

Suppose we have a spiral which derives from a nucleus of critical radius ρ_c with rate of displacement for a front of zero curvature v_θ and an angular velocity ω.

The shape is defined by

$$\omega = \frac{v_0}{r}\left(1 - \frac{\rho_c}{\rho}\right)\sqrt{1 + (r\theta')^2}\,. \tag{2}$$

Here r and θ are polar coordinates for a point on the spiral.

Suppose now that the vapor pressure suddenly falls below the equilibrium value at t = 0, so that the critical radius of an evaporation nucleus (pit in the surface) is $-\rho_c$ and the layer velocity v_0. Let us find how $\frac{d\theta}{dt}\Big|_{t=0}$ varies along the layer. Equation (2) shows that

$$\frac{\partial\theta}{\partial t}\bigg|_{t=0} = -\frac{v_0}{r}\left(1 + \frac{\rho_c}{\rho}\right)\sqrt{1 + (r\theta')^2},$$

where on the RHS we must substitute the solution to (2), the first integral of which has the form

$$\arctan r\,\frac{\partial\theta}{\partial r} = \frac{1}{2}\,\frac{r}{\rho_c} - \frac{\omega\rho_c}{3v_0}\left(\frac{r}{\rho_c}\right)^3 + \cdots \quad \text{when} \quad r \ll \rho_c,$$

$$\arctan\, r\,\frac{\partial\theta}{\partial r} = \frac{\pi}{2} - \frac{v_0}{\omega\rho_c}\left(\frac{\rho_c}{r}\right) + \frac{v_0}{\omega\rho_c}\left(\frac{\rho_c}{r}\right)^2 + \cdots \quad \text{when } r \gg \rho_c.$$

It is then readily shown that

$$\frac{\partial\theta}{\partial t}\bigg|_{t=0} = -\frac{2v_0}{r} \quad \text{when} \quad r \ll \rho_c,$$

$$\frac{\partial\theta}{\partial t}\bigg|_{t=0} = -\omega\left(1 + 2\frac{\rho_c}{r}\right) \quad \text{when} \quad r \gg \rho_c. \tag{3}$$

The angular velocity immediately after the conditions change is then infinite at the point where the screw dislocation emerges, but only slightly greater than ω far from the center. The spiral thus begins to uncoil rapidly at the center; the central area takes the form shown in Fig. 8.

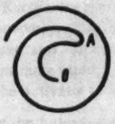

Fig. 8. How a growth spiral is transformed into an evaporation one.

It might be thought that the tongue A (Fig. 8) would move on and alter the sign of the curvature all along the spiral (reverse the spiral). If this were to occur, we should have to have ω at OA greater in absolute magnitude than in the area outside A. However, the second equation in (3) shows that this is not so. A will therefore not move on along the spiral. The distance between the turns will increase with time and the angle at the top of the growth cone will tend toward π. A then propagates rapidly along the spiral, and we get an evaporation pit instead of the outgrowth.

The type of figure shown in Fig. 8 was actually observed in our first experiments; it was found that in times large compared with 1/ω, point A did not get farther away than twice the distance between turns.

Precisely the same arguments can be applied to the transition between two spirals corresponding to different supersaturations.

Our qualitative arguments as to the transient processes do not, of course, give us the final picture; further development and refinement is required.

LITERATURE CITED

[1] G. G. Lemmlein, "The structure of the fine relief on a crystal face," Vestnik AN USSR 4, 119 (1945).

[2] G. G. Lemmlein, "Growing crystal face layers surround obstacles,' Doklady Akad. Nauk USSR 84, 6, 1167-1169 (1952).

[3] G. G. Lemmlein and N. V. Gliki, "A new method of detecting hyperfine relief on crystal faces," Doklady Akad. Nauk USSR 94, 3, 473-475 (1954).

[4] G. G. Lemmlein and E. D. Dukova, "Spiral growth in p-toluidine crystals," Doklady Akad. Nauk USSR 102, 77-79 (1955).

[5] G. G. Lemmlein and E. D. Dukova, "Screw dislocation formation during crystal growths," Kristallografiia 1, 3, 351-5 (1956).

[6] G. G. Lemmlein, "Approach of two centers of spirals of opposed senses during crystal growth," Kristallografiia 1, 4, 477-8 (1956).

[7] M. Volmer, Kinetik der Phasenbildung (Dresden, 1939).

[8] G. G. Lemmlein and E. D. Dukova, "The tangential growth rates of elementary layers on p-toluidine crystals," Kristallografiia 1, 1, 112-8 (1956).

[9] W. K. Burton, N. Cabrera and F. C. Frank, "The growth of crystals and the equilibrium structure of their surfaces," Phil. Trans. Roy. Soc. 243, 866, 299-358 (1951).

[10] N. Cabrera, "Macroscopic spirals and the dislocation theory of crystal growth," J. Chem. Phys. 21, 1111 (1953).

[11] A. A. Chernov, "The tangential growth rates of elementary layers on crystal surfaces," Kristallografiia 1, 1, 119-122 (1956).

[12] L. Kowarski, "Sur la croissance des cristaux tres minces," J. chim. phys. 32, 5, 303-331 (1935).

[13] N. Cabrera and M. Levine, "On the dislocation theory of evaporation of crystals," Phil. Mag. 1, 5, 450-458 (1956).

Institute of Crystallography
Academy of Sciences of the USSR

Received February 22, 1957

ACTIVATOR DISTRIBUTIONS IN ALKALI HALIDE CRYSTALS STUDIED WITH RADIOACTIVE TRACERS

L.M. Beliaev, V.A. Perl'shtein and V.P. Panova

The distribution of activators is studied by the radioactive isotope method in the crystals: potassium iodide, sodium iodide, cesium iodide.

The process of nonuniform distribution of crystal activator in crystals grown by Kyropoulos and Obreimov – Shubnikov methods is established.

Heavy-metal activators are used in alkali-halide crystals for scintillation counters. The light yield and decay times depend on the activator concentration [1]. The light yield becomes almost independent of activator content at $3\text{-}4 \cdot 10^{-4}$ moles Tl/mole NaI. The activator present in the charge only partially enters the crystal, however, and even then is unevenly distributed. This effect is partly due to the physicochemical properties of the components and partly to the processes occurring during growth. We may, therefore, expect that crystals grown in different ways will show different types of nonuniformity. The nonuniformity may be very marked, and may be as much as 20-40% per cm length of crystal even in the best specimens. Nonuniformities of this order disturb the proportionality between light yield and energy absorbed from the radiation and make the crystal unsuitable for use in spectrometry. We have used radioactive tracer methods to study growth processes and the laws of activator incorporation [2].

Both the Kyropoulos and Obreimov-Shubnikov methods were used to grow potassium, sodium and cesium iodide crystals. The activators (thallium iodide; silver chloride) contained the radioactive isotopes Tl^{204} and Ag^{110}.

In the Kyropoulos method [3] the crystals are grown in an open crucible which is charged with base material simultaneously. The differing melting points and vapor pressures of the components result in their evaporating at different rates. In our case the thallium iodide has the lower melting point and higher vapor pressure, and so escapes more rapidly. The TlI content of the melt therefore decreases during growth; this may be one reason why the activator is unevenly distributed in the crystal.

We did the following experiment to check this. An open crucible containing a melt with 99% KI and 1% $Tl^{204}I$ was sampled at equal time intervals and the thallium concentration determined. The Tl^{204} β-activity (E = 0.783 Mev) was also measured with a G-M counter, using a standard type B setup [5]. Equal weights of the material to be analyzed were first ground up in a mortar and then evenly spread between two paper strips, one of which was lightly smeared with glue. The strip could then conveniently be wrapped around a cylindrical G-M counter. This gave identical geometry (2π) in all cases, so no additional corrections were required. The $Tl^{204}I$ content in the melt was found to decrease with time according to the experimental law

$$K_{t_n} = K_{t_0} \cdot e^{-1.15(t_n - t_0)},$$

K_{t_0} being the initial activator concentration, and K_{t_n} that at some given instant. Figure 1 shows this graphically (Curve 1).

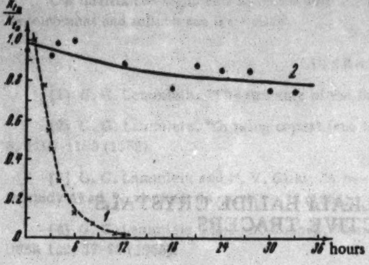

Fig. 1.

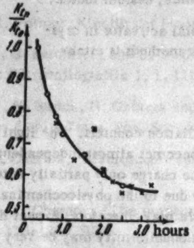

Fig. 2.

The free surface, and hence the evaporation loss, was reduced when a seed was introduced into the crucible to start the growth. The changes in $Tl^{204}I$ concentration caused the activator content in the crystal to vary. This was demonstrated by sampling during growth and by determining the thallium concentration in the corresponding area of the crystal. Figure 2 shows the relationship in graphical form.

The activator concentration was also determined from the relative radioactivity. Here the G-M counter was fitted with an Al diaphragm 2.5 mm thick having a 2 × 3 mm hole. The crystals grown by the Kyropoulos method were sawn up in directions normal to the growth layers, while those grown by the Obreimov-Shubnikov method were sawn up lengthwise. The flat cut faces were placed with the area to be studied over the hole in the diaphragm. No self-absorption corrections were then required.

For Ag^{110} activated crystals grown by the Obreimov-Shubnikov method, we used a scintillation counter with a NaI(Tl) crystal and FEU-19 photomultiplier. The crystals were sawn up into disks 1-1.5 mm thick. The disk size and position relative to the counter were the same in any one series. The statistical error of the measurements never exceeded 3%.

Figure 3 shows how the activator was distributed in the crystals grown by the Kyropoulos method. Figure 3 makes it clear that the activator is present in layered form. The layers formed later contain less activator, because some has been lost by evaporation. There is a marked tendency for the concentration to increase outward from the center, with a slight drop at the edges. This reflects the shape of the isothermal growth surfaces in the Kyropoulos method. The initial shape can be taken as hemispherical. The center of the hemisphere lies at the seed, which is attached to the cooled chuck. The growth rate at the center falls as the crystal grows larger because the thermal conductivity is low, whereas the diameter increases because the surface of the melt cools (in practice because the furnace temperature is reduced). The lower concentration at the center is thus caused by the self-purification resulting from the lower growth rate. The higher peripheral concentration is caused by the greater growth rate produced there by surface cooling. The effect is also caused by the evaporating activator passing over the growing crystal, which, as it were, corresponds to increasing the activator concentration in the melt. The edge contains less activator because it grows latest, when the melt has become depleted (the crystal is here grown without being lifted).

It was therefore natural to try to alter the Kyropoulos method in such a way as to reduce the evaporation.* A special furnace fitted with a lid containing a window (for observing the crystal) was constructed. This reduced the activator loss considerably. Curve 2 of Fig. 1 shows how the activator concentration in the melt changed with time in the sealed furnace. Curve 1 shows the same for an open furnace. It is clear that almost all the activator is lost in 12-15 hours with the open crucible, but that the fall is only 20% in 32 hours with the sealed furnace.

---

* The loss can be compensated by adding activator during growth, but this makes the technique very complicated. It is also difficult to get uniform crystals if sufficient activator to give the optimal concentration at the end is introduced into the initial charge.

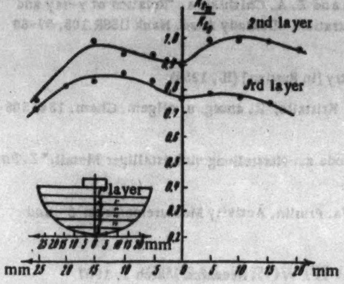

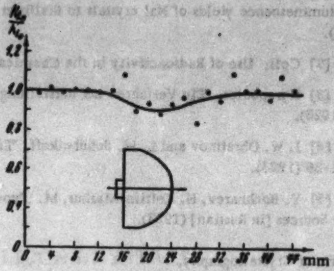

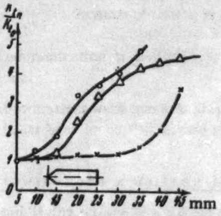

Fig. 5.

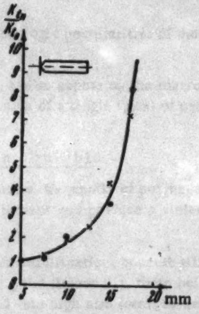

Fig. 6.

Several crystals of more uniform activator distribution were grown in the sealed furnace (see Fig. 4). Using longer times larger crystals were grown successfully (80 mm diameter and 50 mm high), which had very good spectral characteristics (resolution for Cs^{137} 8-10%).

Since a radioactive activator was used we could follow the diffusive redistribution on annealing the crystals. A KI crystal was heated to 600° for 7 days and then slowly cooled. The scatter in the concentration was reduced but not eliminated.

The Obreimov-Shubnikov method [4] was used with sealed ampules, so no evaporation of the activator occurred. It was, however, found that the activator was again unevenly distributed. The differences could be as much as 30-40% in a cm length of crystal. Figure 5 shows how the $Tl^{204}I$ was distributed in KI, NaI and CsI crystals grown at identical rates (35 mm/day) and with identical activator concentrations. The activator is clearly forced into the upper parts of the crystal, and the percent incorporation differs between crystals. Studies on KI crystals grown at equal rates from melts with differing $Ag^{110}Cl$ contents showed that the same fraction of the activator was incorporated in each case (Fig. 6).

LITERATURE CITED

[1] L. M. Beliaev, M. D. Galanin, Z. L. Morgenshtern and Z. A. Chizhikova, "Relation of γ-ray and photoluminescence yields of NaI crystals to thallium concentration," Doklady Akad. Nauk USSR 105, 57-60 (1955).

[2] Coll: Use of Radioactivity in the Chemical Industry [in Russian] (IL, 1954).

[3] Kyropoulos, "Ein Verfahren zur herstellung grosser Kristalle," Z. anorg. u. allgem. Chem. 154, 308-313 (1926).

[4] J. W. Obreimov and L. W. Schubnikoff, "Eine Metode zur Herstellung einkristalliger Metall." Z. Phys. 25, 31-36 (1924).

[5] V. Bochkarev, N. Keirim-Markus, M. L'vova and Ia. Pruslin, Activity Measurements on β- and γ-ray Sources [in Russian] (1953).

Institute of Crystallography,
Academy of Sciences of the USSR

Received March 1, 1957

SPIRAL GROWTH OF SILICON CRYSTALS

N.A. Shamba and N.N. Sheftal'

The important role of spiral forms of growth during the crystallization of silicon from the melt is stated. The spiral structure of the needle crystals of silicon is revealed.

This communication is preliminary, and deals with certain morphologic peculiarities of the growth of silicon crystals.

Spiral formations were found to play a large part in the growth, and to appear on the macrocrystals. In particular, it has been found that silicon needles 6-7 cm long may consist of a single spiral of pyramidal section.*

Spiral Growth when a Silicon Melt Crystallizes in a Crucible

The solidifying surface of a silicon melt gives rise to convex bodies, frequently of polyhedral shape (Fig. 1). These appear suddenly during slow cooling of the crucible in the furnace and produce a violent disturbance in the solidifying surface.

The free surface of a silicon melt normally shows a hillock after solidification, because silicon expands on solidifying. We sometimes (though rarely) find two hillocks forming simultaneously, these being some distance apart. A saddle-point forms in between. Polyhedral projections $\sim$ 0.1 mm high also form, as well as convex figures of well-developed dendritic form. Each of them belongs to an individual crystal (grain). The projections take the shape of hexagonal stepped pyramids with a mirror-like face at the top (Fig. 1). This projection only occurs in the saddle-point areas. They occur because there is a zone of comparatively quiescent crystallization between two hillocks, which latter, being polycrystalline, take up the main stresses occurring on expansion; the melt is largely withdrawn toward the hillocks. The side-faces of the pyramids are stepped (Fig. 2). The steps are not closed, but join onto one another, giving a clearly developed spiral structure. The topmost turn starts at the point where there is a scratch on the top face, which is evidently a macrodislocation (Fig. 3).

As Fig. 2 is only two-dimensional, it cannot give a complete picture of what is seen under the microscope. Figure 4 is therefore given as a schematic diagram of a pyramid. The steps seen in Fig. 2 are about 10 μ high.

The mirror-flat face forms on the upper surface of the melt at the start of crystallization, being the top surface of a very thin plate-like nucleus. Such nuclei can be produced in isolation by cooling a melt of spectroscopically pure silicon very slowly. They may cover the entire surface as an ideally smooth face. The nuclei are extremely thin, as is indicated by their extraordinary mobility on the surface of the melt.

---

* We have found no data on macrospirals, or on spiral growth in silicon in any form, in the literature.

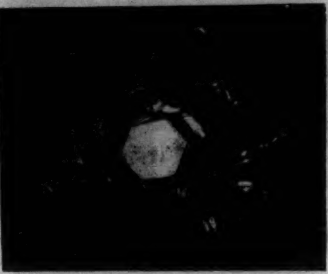

Fig. 1. Polyhedral formations on the solidifying surface of a silicon melt (× 16).

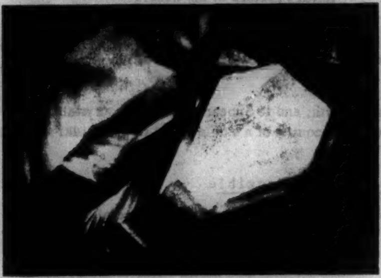

Fig. 2. Stepped structure of the side faces of a pyramid (× 37.5).

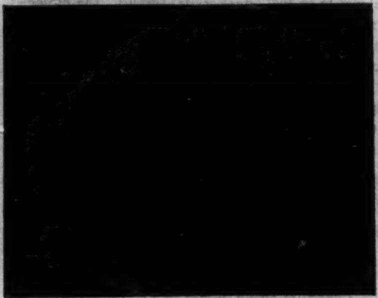

Fig. 3. Topmost turn of a spiral at the edge of a face (× 75).

In the case described the nuclei grew as the melt became more supercooled. The ultimate result of this is that impurities (or holes) are incorporated at the vertices, which in turn results in large-scale dislocations and spiral growth into the body of the melt. The nuclei simultaneously increase in diameter, thus giving rise to the final truncated pyramidal form.

The top (111) face often shows lines directed from the center to the vertices (Fig. 5). These lines continue as the edges of the pyramid. The periphery is broken up by these lines into areas which project somewhat from the plane. We may suppose that if the crystallization had not been instantaneous, these lines would have resulted in a six-fold spiral.

Pyramids which are not truncated are also sometimes found; these are distorted at the top. These pyramids have six curved faces which intersect to give curved edges (Fig. 6). The steps are larger in the lower parts of the pyramid and also have curved surfaces.

Nacken [1] has made a thorough study of this effect, and has shown that the curvilinear upper part occurs when insufficient material is available for the true polyhedral surface, which is energetically the most favorable, to form.

Monocrystal pyramids having top (111) faces of complex outline, like a flower with six petals, are sometimes found (Fig. 7). This form arises in conjunction with the curves and stepped pyramid shape described above. Figure 8 is a schematic drawing of such a face.

The steps form a spiral, and at points where the edges of steps occur the level of a "petal" drops. This occurs because the energetically most favored parts of the crystal (i.e., the rectilinear edges and the crystallographic plane of the "petals") compete for an inadequate supply of material.

Single-crystal formations are also found which have mirror-smooth top faces, lines to the vertices and a geometrically defined pit in the center (Fig. 5).

Comparison of all the above forms leads us to suppose that they are successive stages in macrospiral growth in a single crystal under conditions of gradually increasing strain produced by the expansion of the rapidly cooling melt.

When crystallization is slowest we get pyramids topped by mirror-flat faces. The peripheral areas are highly supercooled. The melt withdrawal produced by the hillocks leads to the face taking a flower-like form. If the withdrawal is very marked at the early stages of development the upper part of the pyramid develops curved faces. The polyhedral recesses are caused by the melt being withdrawn from within the growing pyramid.

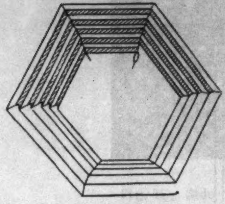

Fig. 4. Diagram of spiral structure of pyramid shown in Figures 1, 2 and 3.

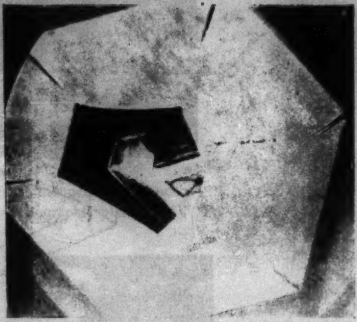

Fig. 5. Lines on the top (111) face. There is a polyhedral hollow on the face.

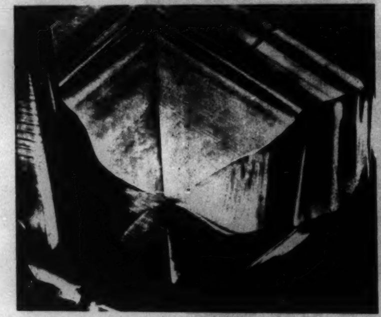

Fig. 6. Curved upper faces of a pyramid.

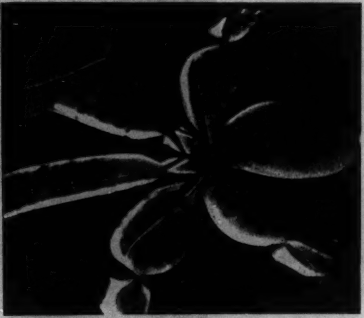

Fig. 7. (111) face of complex six-leaf form on a pyramid.

Spiral Growth of Monocrystals on Withdrawal from the Melt

The withdrawal was done at 1 mm/min, the crucible rotating at 2 rev/min in one direction and the seed at 2 rev/min in the other. A cylindrical rod-shaped seed with its (111) axis along the length was used. The seed was initially fused somewhat, after which the melt temperature was slightly reduced.

If the seed was polycrystalline a glistening aureole appeared around it when the temperature was reduced sufficiently. If it was monocrystalline glistening areas appeared (point B, Fig. 9). Then the diameter began to increase and the radially growing crystal took on a hexagonal outline with the vertices of the hexagon at the glistening areas (Fig. 9; A is the seed). The spiral growth proceeded by the formation of more and more steps, before the withdrawal had even begun.

On withdrawal at 1 mm/min the appearance changed, only edges and mirror-smooth crystallographic planes remaining (Fig. 10; a is such a plane). The surface took on a screw thread appearance, since this form

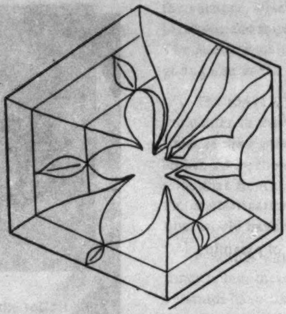

Fig. 8. Diagram of pyramid with face (111), having a six-leaf form.

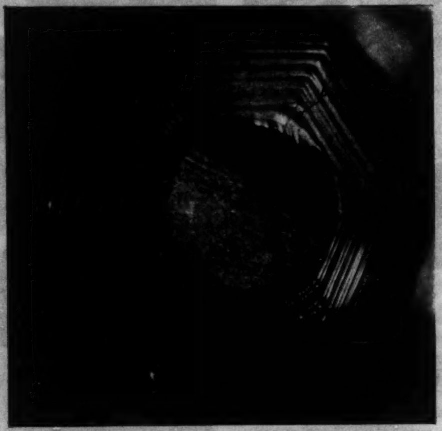

Fig. 9. Spiral expansion of a cylindrical monocrystal silicon seed. A) Seed, B) glistening area. Part of the spiral and one glistening area (B) are traversed by lines.

would appear to favor the same growth mechanism as occurs in the spiral growth when withdrawal is not used (Fig. 10).

Spiral Growth on Crystallization from the Gas Phase

Needle-like single crystals (Fig. 11) with clearly developed steps on the lateral faces are produced when silicon tetrachloride is reduced with zinc. The needles were up to 6-7 cm long, of area 4 mm^2 at the base.

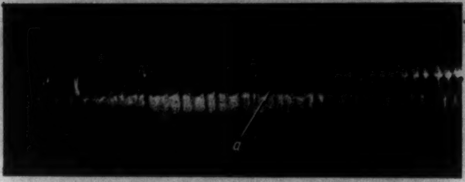

Fig. 10. Side-face structure in a silicon monocrystal grown by withdrawal from the melt [a is a crystallographic plane (×1)].

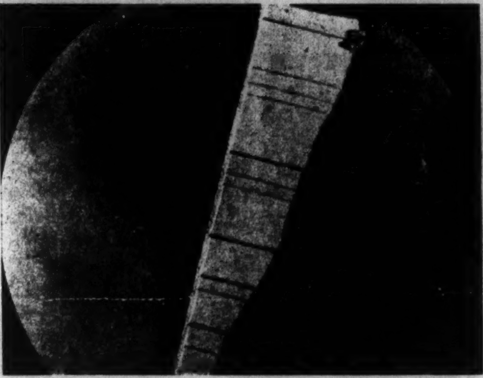

Fig. 11. Side surface of a needle-like silicon monocrystal (× 100).

If the layer or step sequence is followed in such a monocrystal which is grown without rotation it is found that the steps are not closed, but form a spiral.

We thus again have macrospiral growth form.

In conclusion we wish to thank B. P. Mitrenina for valuable assistance in the experimental work, B. I. Khachishvili for presenting us with the silicon crystals grown from the gas phase, and Dr. E. E. Rekser, who assisted us in carrying out this work.

LITERATURE CITED

[1] R. Nacken, "Uber das Wachsen von Kristallpolyedern in ihrem Schmelzfluss Neues Jahrb. Miner. II, 133 (1915).

Received October 23, 1956

SOVIET PHYSICS — CRYSTALLOGRAPHY VOL. 2, No. 3 MAY-JUNE, 1957

(Translation of the journal "Crystallography" of the USSR, Vol. 2,
No. 3, published by the American Institute of Physics, November, 1958)

CONTENTS

	Page	Russ. page
Shubnikov Groups. N. V. Belov, N. N. Neronova and T. S. Smirnova	311	315
Development of the Study of Crystal Forms. I. I. Shafranovskii	323	326
Symmetry of Homogeneous, Continuous Isotropic Media in Tensor, Vector and Scalar Fields. I. S. Zheludev	330	334
Intensity of Electron Diffraction Pattern Reflections (General Case) B. K. Vainshtein	334	340
The Theory of the Relation Between Structure Amplitudes and Methods of Direct Analysis of Crystal Structures. A. I. Kitaigorodskii	346	352
The Automatic Synthesis of a Two-Dimensional Representation of Atomic Structures. V. I. Vlasenko and G. S. Zhdanov	353	358
New Silicate Structures. N. V. Belov	361	366
The Atomic Crystal Structures of Complex Acid-Amine Nickel Compounds. M. A. Porai-Koshits, E. K. Iukhno, A. S. Antsishkina and L. M. Dikareva	366	371
x-Ray Investigation of Crystals of Some Ferrocene Derivatives. Iu. T. Struchkov and T. L. Khotsianova	376	382
The Crystal Structures of Diphenyl Halogen Compounds. T. L. Khotsianova and Iu. T. Struchkov	378	384
Electron Diffraction Study of Nitrides and Carbides of Transition Metals. Z. G. Pinsker and S. V. Kaverin	380	386
Determination of the Structure of Celadonite by Electron Diffraction. B. B. Zviagin	388	393
Crystallochemistry of Complex Divalent Platinum Compounds (The Effect of Transinfluence in Crystalline Substances). G. B. Bokii and G. A. Kukina	395	400
A Crystallochemical Investigation of the Structure of some Complex Compounds. Z. V. Zvonkova	403	408
Distortions of the Crystal Lattice in Solid Solutions. V. I. Iveronova, A. P. Zviagina and A. A. Katsnel'son	408	414
The Mechanism of Structure Transformations in Agehardening Alloys Based on Nickel. Iu. A. Bagariatskii and Iu. D. Tiapkin	414	419
On the Formation of Spherulites. A. V. Shubnikov	422	424
The Dynamics of Certain Elementary Crystal Growth and Evaporation Processes. G. G. Lemmlein, E. D. Dukova and A. A. Chernov	426	428
Activator Distributions in Alkali Halide Crystals Studied with Radioactive Tracers. L. M. Beliaev, V. A. Perl'shtein and V. P. Panova	435	437
Spiral Growth of Silicon Crystals. N. A. Shamba and N. N. Sheftal'	439	441

SIGNIFICANCE OF ABBREVIATIONS MOST FREQUENTLY ENCOUNTERED IN SOVIET CRYSTALLOGRAPHY LITERATURE

AN SSSR	*Academy of Sciences, USSR*
FIAN	*Physics Institute, Academy of Sciences USSR*
GITI	*State Scientific and Technical Press*
GITTL	*State Press for Technical and Theoretical Literature*
GOI	*State Optical Institute*
GONTI	*State United Scientific and Technical Press*
Gosfizkhimizdat	*State Physical Chemistry Press*
Gozkhimizdat	*State Chemistry Press*
GOST	*All-Union State Standard*
Goztekhizdat	*State Technical Press*
GTTI	*State Technical and Theoretical Press*
GUPIAE	*State Office for Utilization of Atomic Energy*
IF KhI	*Institute of Physical Chemistry Research*
IFP	*Institute of Physical Problems*
IK	*Institute of Crystallography*
IL	*Foreign Literature Press*
IPF	*Institute of Applied Physics*
IPM	*Institute of Applied Mathematics*
IREA	*Institute of Chemical Reagents*
ISN (Izd. Sov. Nauk)	*Soviet Science Press*
IIaP	*Institute of Nuclear Studies*
Izd	*Press (publishing house)*
KISO	*Solar Research Commission*
LETI	*Leningrad Electrotechnical Institute*
LFTI	*Leningrad Institute of Physics and Technology*
LIM	*Leningrad Institute of Metals*
LITMiO	*Leningrad Institute of Precision Instruments and Optics*
MATI	*Moscow Aviation Technology Institute*
MGU	*Moscow State University*
Metallurgizdat	*Metallurgy Press*
MOPI	*Moscow Regional Pedagogical Institute*
NIAFIZ	*Scientific Research Association for Physics*
NIFI	*Scientific Research Institute of Physics*
NIIMM	*Scientific Research Institute of Mathematics and Mechanics*
NII ZVUKSZAPIOI	*Scientific Research Institute of Sound Recording*
NIKFI	*Scientific Institute of Motion Picture Photography*
OIIaI	*Joint Institute of Nuclear Studies*
ONTI	*United Scientific and Technical Press*
OTI	*Division of Technical Information*
OTN	*Division of Technical Science*
RIAN	*Radium Institute, Academy of Sciences of the USSR*
SPB	*All-Union Special Planning Office*
Stroiizdat	*Construction Press*
TsNIIChERMET	*Central Scientific Research Institute for Ferrous Metallurgy*
URALFTI	*Ural Institute of Physics and Technology*

NOTE: Abbreviations not on this list and not explained in the translation have been transliterated, no further information about their significance being available to us.—*Publisher.*

The expanded program of the American Institute of Physics comprises translation of six leading Soviet physics journals, as listed below. These translations, by competent, qualified scientists, provide all research laboratories and libraries with accurate and up-to-date information of the results of research in the U.S.S.R.

Soviet Physics—Technical Physics

A translation of the "Journal of Technical Physics" of the Academy of Sciences of the U.S.S.R. The translation began with the 1956 issues. Twelve issues per year, approximately 3,000 Russian pages. Annually $75.00 domestic, $79.00 foreign. Libraries* $35.00 domestic, $39.00 foreign. Back numbers, all issues $8.00.

Soviet Physics—Acoustics

A translation of the "Journal of Acoustics" of the Academy of Sciences of the U.S.S.R. The translation began with the 1955 issues. Four issues per year, approximately 400 Russian pages. Annually $12.00 domestic, $14.00 foreign. (No library discounts.) Back numbers, all issues $4.00.

Soviet Physics—Doklady

A translation of all of the "Physics Sections" of the Proceedings of the Academy of Sciences of the U.S.S.R. The translation began with the 1956 issues. Six issues per year, approximately 1,500 Russian pages. Annually $35.00 domestic, $38.00 foreign. Libraries* $15.00 domestic, $18.00 foreign. Back numbers for Volumes 1 and 2, $5.00 per issue; Volume 3 and subsequent, $7.00 per issue.

Soviet Physics—JETP

A translation of the "Journal of Experimental and Theoretical Physics" of the Academy of Sciences of the U.S.S.R. The translation began with the 1955 issues. Twelve issues per year, approximately 4,000 Russian pages. Annually $75.00 domestic, $79.00 foreign. Libraries* $35.00 domestic, $39.00 foreign. Back numbers, all issues $8.00.

Soviet Physics—Crystallography

A translation of the journal "Crystallography" of the Academy of Sciences of the U.S.S.R. The translation began with the 1957 issues. Six issues per year, approximately 1,000 Russian pages. Annually $25.00 domestic, $27.00 foreign. Libraries* $10.00 domestic, $12.00 foreign. Back numbers, all issues $5.00.

Soviet Astronomy—AJ

A translation of the "Astronomical Journal" of the Academy of Sciences of the U.S.S.R. The translation began with the 1957 issues. Six issues per year, approximately 1,100 Russian pages. Annually $25.00 domestic, $27.00 foreign. Libraries* $10.00 domestic, $12.00 foreign. Back numbers, all issues $5.00.

Subscriptions should be addressed to the American Institute of Physics, 335 East 45th Street, New York 17, N. Y.

---

* For libraries of non-profit academic institutions.